BEILSTEIN JOURNAL OF ORGANIC CHEMISTRY

Spatial effects in polymer chemistry

Edited by Helmut Ritter

Imprint

Beilstein Journal of Organic Chemistry
www.bjoc.org
ISSN 1860-5397
Email: journals-support@beilstein-institut.de

The *Beilstein Journal of Organic Chemistry* is published by the Beilstein-Institut zur Förderung der Chemischen Wissenschaften.

Beilstein-Institut zur Förderung der Chemischen Wissenschaften
Trakehner Straße 7–9
60487 Frankfurt am Main
Germany
www.beilstein-institut.de

BEILSTEIN JOURNAL OF ORGANIC CHEMISTRY

Spatial effects in polymer chemistry

Helmut Ritter

Editorial

Open Access

Address:
Institute of Organic Chemistry and Macromolecular Chemistry, Heinrich-Heine-University, Universitätsstraße 1, 40225 Düsseldorf, Germany

Email:
Helmut Ritter - h.ritter@hhu.de

Keywords:
polymer; spatial effects

Beilstein J. Org. Chem. **2017,** *13,* 2015–2016.
doi:10.3762/bjoc.13.198

Received: 19 July 2017
Accepted: 01 August 2017
Published: 27 September 2017

This article is part of the Thematic Series "Spatial effects in polymer chemistry".

Guest Editor: H. Ritter

Our modern life is no longer conceivable without macromolecular materials. Important developments in materials science, for example in the field of medical technology, electronic communication, transport and energy technology, became only possible thanks to the extensive development in the field of polymer chemistry. Although a large number of polymeric materials have already taken their place in the market, there is still a great need to develop novel materials for specific purposes and corresponding practical applications. Consequently, the synthesis and modification of macromolecules remain high priorities in scientific research.

Neighboring group effects and cross over space effects play a crucial role for the chain growth and chemical conversion of polymers in many cases. Among the spatial effects are H-bonds, van der Waals interactions, ionic forces, dipolar interactions, self-ordering effects and steric influences.

Through IR-spectroscopic studies we have recently found that the carbonyl group of, e.g., poly(acrylates) show different IR signals when positioned side by side. If, for example, they are separated by styryl units, these carbonyl signals are clearly shifted. Such effects also play an important role in the reactivity of, e.g., ester-side groups.

For example, the tacticity of a polymeric chain is a result of spatial interactions between the active growing chain end and the free monomer or a monomer–metal complex. Moreover, the preferred head-to-tail chain growth of vinyl monomers can be a result of such spatial effects. The spatial arrangement of polymer chains in the solid phase is not only influenced by external forces, for example, during extrusion, but is often also a result of chain mobility and strong intermolecular interactions. It should also be mentioned that the solubility of polymer chains is a spatial interplay between the solvent molecules and the polymer chains. Here, the LCST effects fit into the dynamic, space-spreading strength model.

I am convinced that this systematic approach provides the insights to allow a targeted and rapid development of new materials and methods. Findings concerned with spatial effects can be further explored by modern spectroscopic methods and model tests. The latter can often be carried out in a result-oriented manner, which accelerates the gain of knowledge.

Some of these points are emphasized in the present Thematic Series and may offer different perspectives for developments – right now and in the near future.

Helmut Ritter

Düsseldorf, July 2017

BEILSTEIN JOURNAL OF ORGANIC CHEMISTRY

Methylenelactide: vinyl polymerization and spatial reactivity effects

Judita Britner and Helmut Ritter*

Full Research Paper

Open Access

Address:
Institute of Organic Chemistry and Macromolecular Chemistry, Heinrich-Heine-University, Universitätsstraße 1, 40225 Düsseldorf, Germany

Email:
Helmut Ritter* - h.ritter@hhu.de

* Corresponding author

Keywords:
copolymerization; kinetic study of the radical homopolymerization; push–pull monomer; reversible addition fragmentation chain transfer (RAFT)

Beilstein J. Org. Chem. **2016,** *12,* 2378–2389.
doi:10.3762/bjoc.12.232

Received: 31 August 2016
Accepted: 26 October 2016
Published: 14 November 2016

This article is part of the Thematic Series "Spatial effects in polymer chemistry".

Associate Editor: P. J. Skabara

Abstract

The first detailed study on free-radical polymerization, copolymerization and controlled radical polymerization of the cyclic push–pull-type monomer methylenelactide in comparison to the non-cyclic monomer α-acetoxyacrylate is described. The experimental results revealed that methylenelactide undergoes a self-initiated polymerization. The copolymerization parameters of methylenelactide and styrene as well as methyl methacrylate were determined. To predict the copolymerization behavior with other classes of monomers, *Q* and *e* values were calculated. Further, reversible addition fragmentation chain transfer (RAFT)-controlled homopolymerization of methylenelactide and copolymerization with *N*,*N*-dimethylacrylamide was performed at 70 °C in 1,4-dioxane using AIBN as initiator and 2-(((ethylthio)carbonothioyl)thio)-2-methylpropanoic acid as a transfer agent.

Introduction

Methylenelactide (MLA) with the IUPAC name (6*S*)-3-methylene-6-methyl-1,4-dioxane-2,5-dione is a radically polymerizable vinyl-lactide derivative. The molecule's quaternary carbon atom located at the double bond is substituted with an electron withdrawing ("pulling") carbonyl group and an electron donating ("pushing") oxygen atom. Monomers with such substitution patterns are defined as captodative or push–pull monomers [1]. MLA was first synthesized in 1969 by Scheibelhoffer et al. through a bromination of L-lactide followed by a basic HBr elimination [2]. In 2008, the first Diels–Alder reaction employing MLA as dienophile was described [3-6]. In a recent NMR study we demonstrated that, poly(MLA) prepared via free radical polymerization contains mainly isotactic units. Furthermore, we found that the polymer attached lactide rings react like activated esters and thus readily undergo quantitative amidation reactions with aliphatic primary amines under mild conditions [7]. In the underlying study, we focused on spatial effects with respect to interactions between neighboring lactide rings. Based on these findings, polymer analogous reactions of poly(MLA) with different alcohols were recently investigated [8]. Up to now, it was not possible to polymerize MLA via ring opening [9]. Only indirectly, unsaturated polylactide carrying

vinyl side groups can be obtained through a copolymerization of chlorolactide with L-lactide followed by subsequent dehydrochlorination [10]. Recently, thiol-Michael additions on MLA were reported [11,12].

In this paper, we wish to present a kinetic study of free radical and controlled/living radical polymerization of MLA. The latter reactions were conducted via a reversible addition fragmentation chain transfer (RAFT) mechanism. We also investigated the copolymerization of MLA with styrene and methyl methacrylate, respectively. The results were compared to the well-known push–pull type monomer α-acetoxyacrylate.

Results and Discussion

Free-radical polymerization of methylenelactide MLA

The push–pull type monomer MLA contains an electron-deficient vinyl group which is structurally related to acrylate monomers. Electron-rich vinyl groups are structurally related to vinyl ester monomers. However, the free-radical polymerization of MLA proceeds smoothly at elevated temperature without ring-opening side reactions (see Figure S1 in Supporting Information File 1). To evaluate the free-radical polymerization of MLA, we compared the behavior to non-cyclic, pull-type methyl methacrylate (MMA), non-cyclic, push–pull-type methyl α-acetoxyacrylate (MAA) and ethyl α-acetoxyacrylate (EAA), respectively and cyclic pull-type α-methylene-δ-valerolactone (MVL, see Figure 1).

Since the polymerization kinetics are mainly controlled by steric effects and the polarity of the double bonds, we evaluated the electronic structure of the different monomers via ^{1}H nuclear magnetic resonance (NMR) spectroscopy. As expected, the double bond protons of MLA at 5.77 and 5.56 ppm clearly differ from the double bond protons of MAA (6.02 and 5.65 ppm) and EAA (5.99 and 5.62 ppm). Surprisingly, their chemical shifts are very similar to the double bond protons of MMA (6.03 and 5.66 ppm). This suggests that the electron-withdrawing substituent has a stronger influence on the electron density of the vinyl protons than the electron-pushing substituent (Table S1, Figures S2 and S3, Supporting Information File 1). We further employed ^{13}C NMR spectroscopy to provide a better view on the electron density of the double bond. It turned out that the quaternary carbon atoms of the double bond of EAA (144.31 ppm), MAA (144.04 ppm) and MLA (143.69 ppm) experience a stronger impact through the electron-withdrawing substituent than the corresponding carbon atoms of MMA (135.77 ppm) and MVL (134.09 ppm). The electron-pushing substituent influences preferentially the methylene carbon atom. This methylene carbon atom shows a relatively high electron density in case of MLA (108.31 ppm), MAA (114.67 ppm,) and EAA (114.32 ppm) compared to the lower electron density in MMA (125.59 ppm) and MVL (127.74 ppm) (Table S1 and Figure S3, Supporting Information File 1).

The homopolymerization reactions were carried out in presence of 1 mol % of AIBN at 70 °C. The conversion after different reaction times was determined via ^{1}H NMR spectroscopy (Figure 1). The molecular weights and dispersities ($Đ$) of the obtained polymers are summarized in Table S2 (Supporting Information File 1).

Interestingly, the polymerization kinetics of MLA are similar to these of MMA. In contrast, the non-cyclic push–pull type monomers MAA and EAA are both less reactive. This indicates that in addition to steric hindrance, the mobility of the substituents plays an important role in the spatially controlled

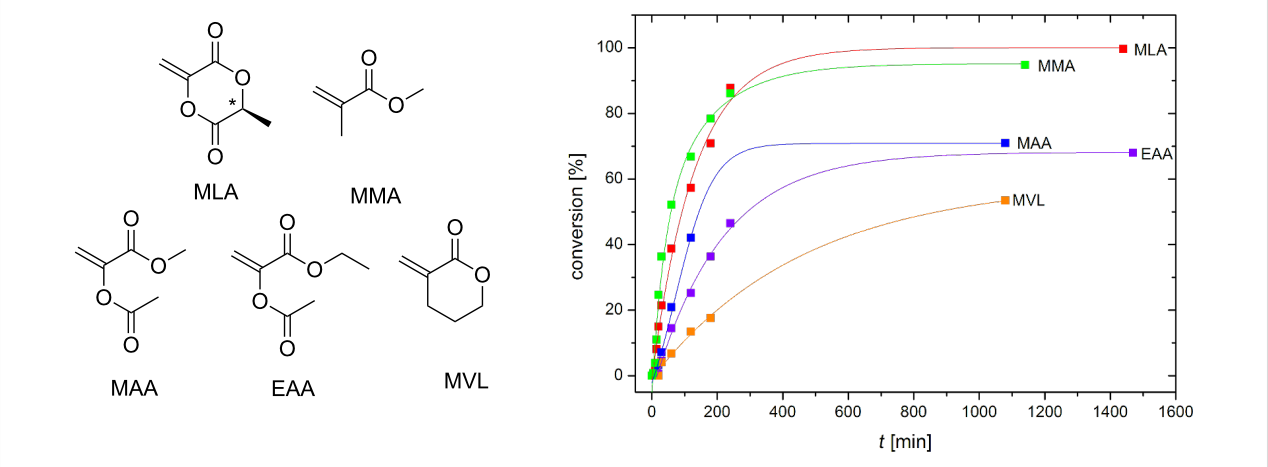

Figure 1: Structures of used monomers and the time-conversion plot of the corresponding free-radical polymerization reactions (80 wt % DMF, 1 mol % AIBN, 70 °C).

chain growth reactions. The molecular weights (M_n) are 21 600 g mol^{-1} for poly(MAA) and 31 600 g mol^{-1} for poly(EAA) with narrow dispersities ($Đ$) between 1.5 and 1.7, indicating that chain termination mainly occurs through recombination of polymer radicals [13].

The moderate conversion of MVL is presumably a result of the relatively low ceiling-temperature of the corresponding polymer (at 81 °C) [14]. This means that under the applied reaction conditions the rate of the polymerization reaction is only slightly higher than the depolymerization rate, which results in slow polymer growth. The obtained data also indicates that the electron densities of the vinyl groups of the used monomers play a minor role with respect to the polymerization kinetics. The higher mobility of the free substituents of the non-cyclic push–pull type monomers MAA and EAA causes a reduced polymerization rate (Figure 1) compared to that of the stiff cyclic molecule MLA.

Stereochemistry of poly(MLA)

As we reported recently, MLA polymerizes via free-radical polymerization to yield predominantly isotactic polymer structures (Figure S4, Supporting Information File 1). Similar findings were reported by Tanaka et al. who investigated the polymerization of methylene dioxolanone derivatives yielding predominantly isotactic polymers [15]. Our recently reported spatial dipole–dipole interactions between neighboring lactide units were supported by IR spectroscopy, as the interactions causes two separate carbonyl stretching vibrations. This effect may also play a crucial role in the isotactic propagation steps during MLA polymerization [7]. In contrast, the polymer of non-cyclic MAA shows a preferred syndiotactic (*rr*) conformation caused by steric control of the free substituents as indicated by ^{13}C NMR spectroscopy (Figure S5, Supporting Information File 1). Scheme 1 shows the different potential propagation steps of MLA.

Deviation of classical polymerization kinetics of MLA

Usually, the rate of polymerization is proportional to the square root of initiator concentration [In] and the degree of polymerization (P_n) is inversely proportional to the square root of [In]. To investigate the polymerization behavior of MLA at 70 °C, different molar amounts of AIBN were used. The polymerization reactions were evaluated after ca. 2 minutes at low conversions up to 10% as determined by ^{1}H NMR spectroscopy. The precipitated polymers were analyzed by size exclusion chromatography (SEC) in DMF (Table 1). The logarithmic plot

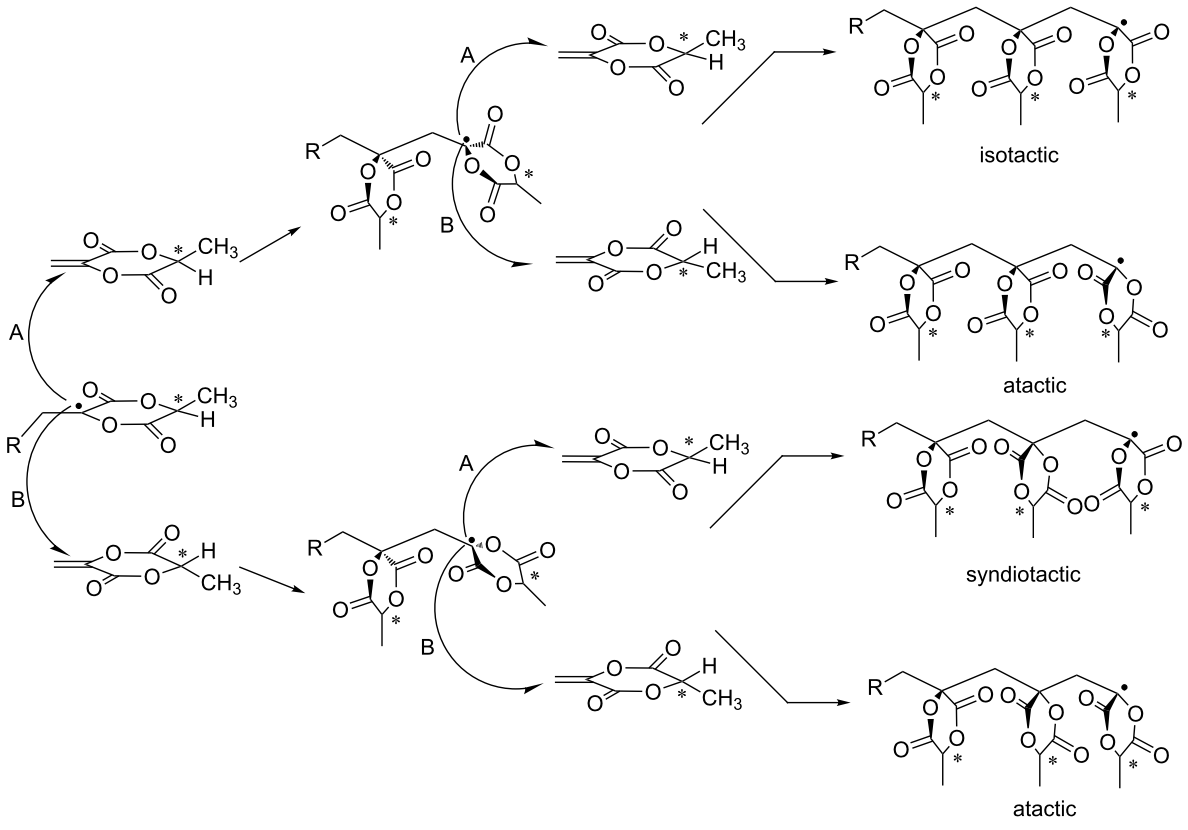

Scheme 1: Stereospecific propagation of chiral MLA illustrating the triade formation [15].

Table 1: SEC data from the polymerization of MLA with different amounts of AIBN ($c_{(MLA)}$ = 1.812 mol L^{-1}in 1,4-dioxane, 15–1 mol % AIBN, 70 °C, polymerization time 2 minutes).

sample	1	2	3	4	5	6	7
$\frac{[AIBN]}{mol\ \%}$	15	12.5	10	7.5	5	2.5	1
$\frac{M_n}{g/mol}$	35 600	46 800	47 600	62 200	85 400	158 800	358 200
Đ	1.8	5.7	4.6	3.4	5	2.7	2.4

displayed in Figure 2 shows the correlation between the degree of polymerization and the initiator concentration. The slope was determined to be −0.84, which significantly deviated from the expected value of 0.5. This observation indicates some self-initiation beside AIBN initiation.

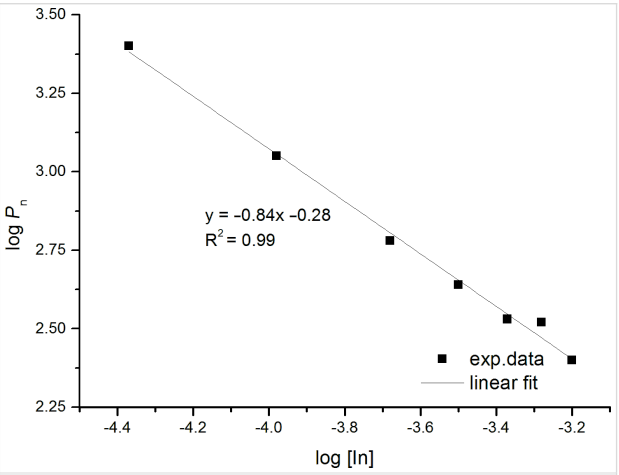

Figure 2: Plot of log P_n versus log [In] of the polymerization of MLA with different mol % AIBN.

Self-initiation of MLA

The self-initiation of some non-cyclic push–pull monomers is already known [1]. However, up to now, the free radical self-initiation of cyclic MLA has not been described in the literature. Thus, we herewith show our postulated mechanism for the self-initiation of MLA in Scheme 2. We propose that a homolytically H–C cleavage takes place in a first step yielding two radicals. This process is accompanied by a change of hybridization from a tetrahedral sp^3 structure of the chiral center to a trigonal planar sp^2 structure of the resulting radical. Scheme 2 also shows additional postulated radical reactions including the formation of a bicyclic lactide radical to initiate the main polymerization. Since the spontaneous homolytically C–H cleavage may represent the first step in the reaction cascade, theoretical calculations on a DFT level were conducted. The above mentioned hybridization change as driving force for C–H cleavage is verified in the reduced bond length of the C–CH_3 bond from 1.542 Å (MLA) to 1.479 Å for the corresponding radical. This clearly indicates a stabilization of this C–C bond after C–H cleavage (Figure 3).

Since only soluble polymers were obtained, the C–H bonds in the linear MLA-polymer units must be more stable than in the monomeric MLA. Otherwise, crosslinking should take place via spontaneous C–H cleavage and chain recombination. This important point could be verified by IR spectroscopy and also by theoretical calculations of the force constants of the C–H bonds on a DFT level.

The C–H stretching vibrations $\nu_{(C\text{-}H)}$ = 2948 cm^{-1} of poly(MLA) determined via IR spectroscopy correlate well with the force constant of k = 473 N m^{-1} (calculations see Figure S6, Supporting Information File 1). In contrast, the monomer MLA ($\nu_{(C\text{-}H)}$ = 2938 cm^{-1}) has a significantly lower force constant of k = 467 N m^{-1}. This also gives a strong hint on the postulated relatively easy C–H homolytical cleavage from MLA as described in Scheme 2. This measured IR values correspond nicely to the DFT calculations (poly(MLA) $\nu_{(C\text{-}H)}$ = 2922 cm^{-1}, MLA $\nu_{(C\text{-}H)}$ = 2914 cm^{-1}). Figure 4 shows the IR spectra of MLA and of the obtained poly(MLA).

To evaluate some kinetic solvent effects of the discussed self-initiated polymerization reactions of MLA, the kinetics of the AIBN-initiated and initiator-free radical polymerizations of MLA were repeated in less polar 1,4-dioxane and dipolar DMF as solvents (Figure 5). Surprisingly, the yields of self-initiated polymerization in 1,4-dioxane are very similar to the yields of AIBN-initiated polymerization. In contrast, the self-initiation polymerization of MLA is much more retarded in DMF solution than in 1,4-dioxane. Taking our postulated radical formation process into account, the dipolar solvent DMF stabilizes the polar educt MLA more than the less polar 1,4-dioxane. Since the formed radical is planar and less polar, the activation energy to this radical formation must be higher in DMF than in 1,4-dioxane [16]. Interestingly, the self-initiated poly(MLA) has a relatively high molecular weight of M_n = 180 000 g mol^{-1} (*Đ* = 2.5) compared to the AIBN initiated poly(MLA)

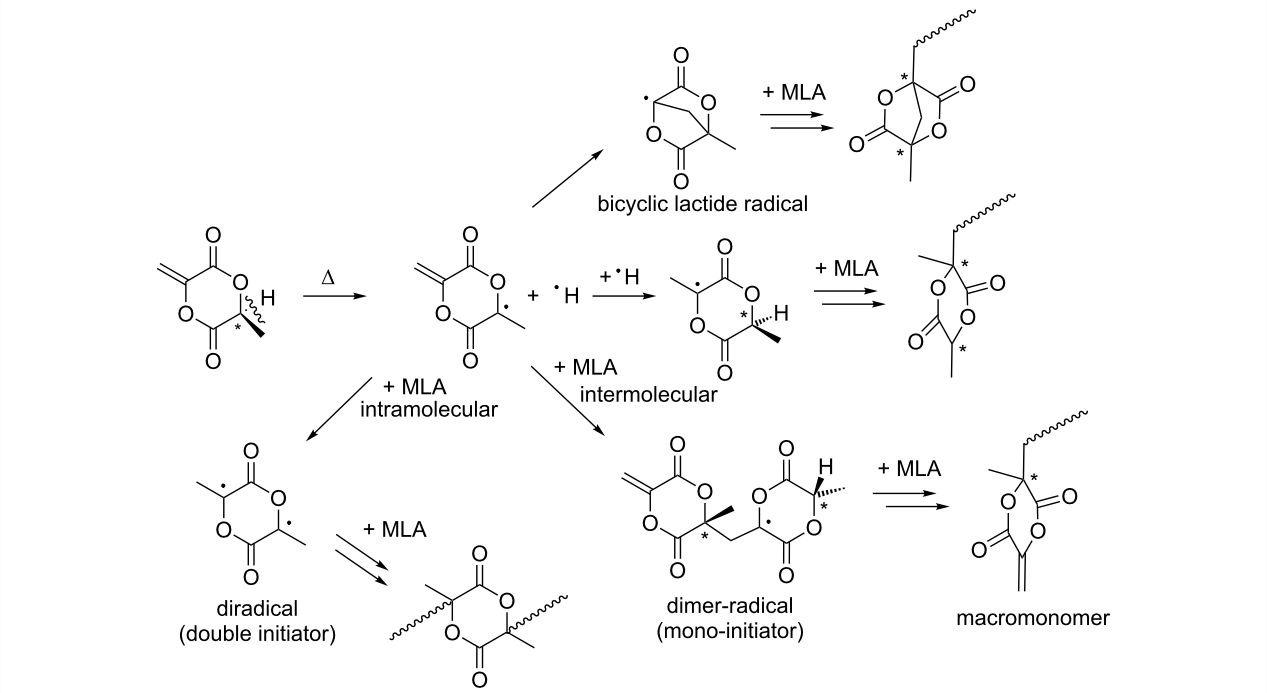

Scheme 2: Postulated mechanism of the self-initiation of MLA.

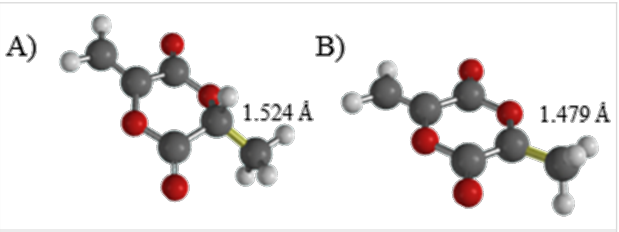

Figure 3: DFT-calculated C–C binding length (yellow) of (A) MLA and (B) the corresponding radical.

(M_n = 73 000 g mol^{-1}, $Đ$ = 2.6). A self-initiated poly(MLA) obtained at 30 °C yields with a reduced molar mass of M_n = 28 600 g mol^{-1}, $Đ$ = 1.9 (Figure S7, Supporting Information File 1). Poly(MLA) polymerized in DMF could not be analyzed by SEC because of some unknown side products (Figure S8, Supporting Information File 1).

For comparison, the non-cyclic MAA shows even in bulk only a very low yield of ca. 10 mol % of self-initiated polymer at 60 °C [13,17]. Thus, the ring shaped MLA is much more reactive in respect to the self-initiated polymerization.

Calculated initial rate for the self-initiated polymerization of MLA by the use of DPPH

As discussed above, the formation of free radicals is a key step for spontaneous polymerization of MLA. Accordingly, spontaneously formed radicals can be proved by the use of the strongly colored 1,1-diphenyl-2-picrylhydrazyl radical (DPPH) which reacts with H radicals under decolorization. The consumption of DPPH-radicals can be followed by the naked eye. Figure 6 shows the UV–vis absorption spectra of DPPH from the beginning of the self-initiated polymerization at 70 °C and after 15 h.

The concentration of DPPH plotted against the time at 70 °C and 30 °C gives a straight line indicating that the reaction follows pseudo zero-order kinetics (Figures S10 and S11, Supporting Information File 1). The slope of this plot corresponds to the reaction rate. The reaction rate of disappearance of DPPH (R_{DPPH}) is equal to the value of the rate of MLA self-initiation (R_i). Accordingly, at 70 °C the self-initiated polymerization with a rate of 2.4 × 10^{-4} mM s^{-1} is 5 times higher than at 30 °C with a rate of 4.42 × 10^{-5} mM s^{-1} (Figure S12, Supporting Information File 1). The actual polymerization reaction takes place after DPPH was consumed, since the molecule acts as an inhibitor. In a control experiment performed in absence of MLA, the DPPH concentrations remained stable.

Free radical copolymerization behavior of MLA

The copolymerization parameters of MLA with styrene and MMA, respectively were evaluated through the method of Kelen and Tüdös [18]. For this, the residual monomer ratio was determined by high performance liquid chromatography (see execution, characterization methods and Figures S14 and S15 in Supporting Information File 1).

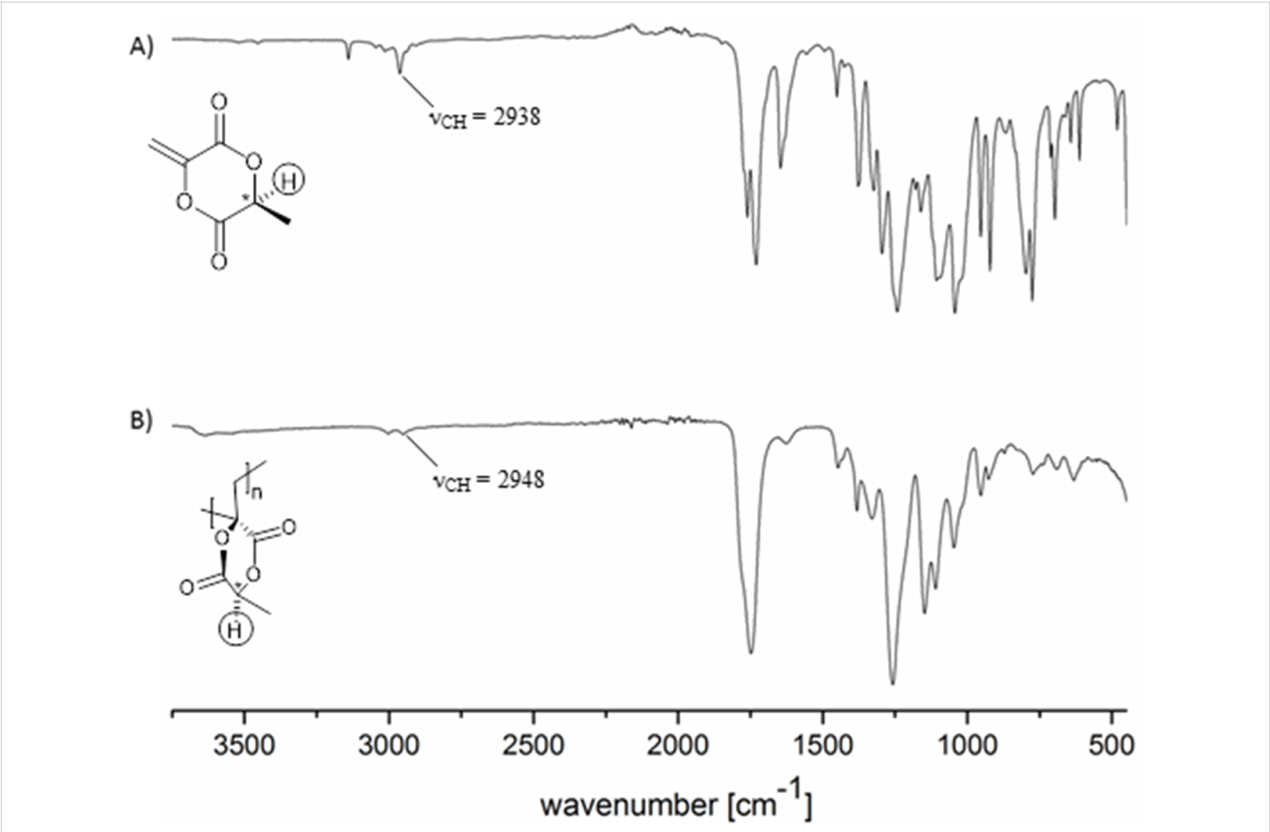

Figure 4: IR spectra of (A) MLA and of (B) poly(MLA) prepared by the self-initiated polymerization at 70 °C.

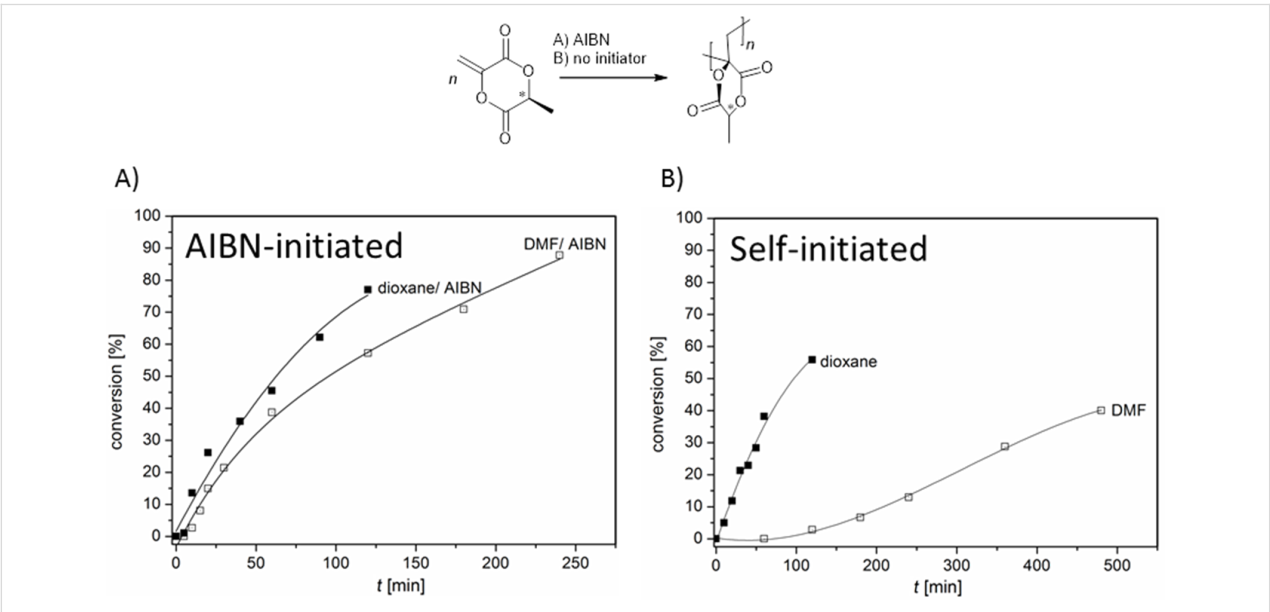

Figure 5: Conversion plot of the polymerization of MLA in 1,4-dioxane and DMF (c_{MLA} = 1.8 mol L^{-1}, c_{AIBN} = 1.8 × 10^{-2} mol L^{-1}, 70 °C) with AIBN (A) and without initiator (B).

The copolymerization parameters obtained from the MLA and styrene system were r_1 = 0.8 (MLA) and r_2 = 0.7 (styrene) which indicates that the copolymerization process proceeds partially alternating. The Alfrey–Price Q and e values were also calculated from the experimental data. The values for MLA are Q = 0.79 and e = 0.015 (see Figure S16 for Q and e value calcu-

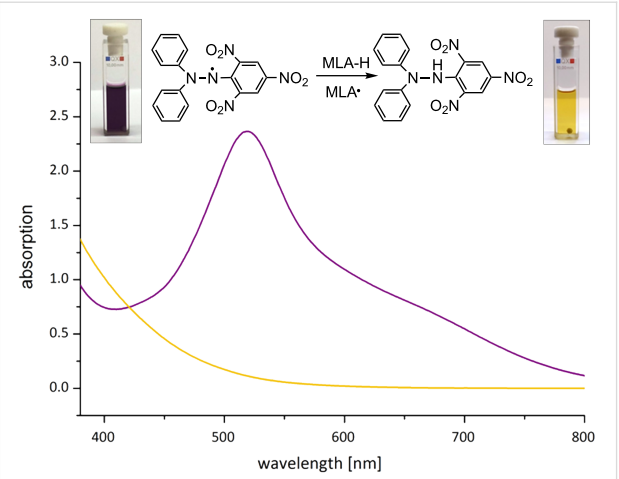

Figure 6: UV–vis spectra of the reaction mixture with DPPH radical at the beginning (violet line, 0.23 mM) of the self-initiated polymerization of MLA and after 15 h (yellow line) in a range from 380–800 nm (c_{MLA} = 1.8 mol L^{-1}, 70 °C).

lation, Supporting Information File 1) [19]. The constant *Q* reflects the resonance stabilization of the growing radical. Large *Q* values (>0.5) indicate stabilized monomers. The constant *e* reflects the polarity of the double bond and of the growing radical. For instance positive *e* values point to an electrophilic character while negative *e* values point to a nucleophilic character.

In contrast, the non-cyclic monomers MAA and EAA show higher positive *e* values and are thus highly influenced by the pull substituents. These higher *e* values are also indicated in the ^{13}C NMR data described above and by higher dipole moments in MAA (3.79 Debye) and EAA (2.26 Debye) compared to MMA (4.10 Debye) and MLA (2.09 Debye) (refer to Table S1, Supporting Information File 1).The *Q* and *e* values of various monomers are summarized in Table 2 [20-22].

Table 2: Alfrey–Price *Q* and *e* values of various monomers with styrene as reference system.

Monomer	*Q*	*e*
styrene	1	−0.8
MLA	0.79	0.015
MMA	0.78	0.40
MAA	1.65	0.57
EAA	0.52	0.77
vinyl acetate	0.026	−0.88
N,N-dimethylacrylamide (DMAa)	0.55	−0.56

The copolymerization parameters obtained from MLA and MMA were r_1 = 1.1 (MLA) and r_2 = 1.2 (MMA) which indicate an almost statistical process, with a slight tendency to homoadditon. Figure 7 illustrates the obtained copolymer composition curves for the systems of MLA with styrene and MMA, respectively.

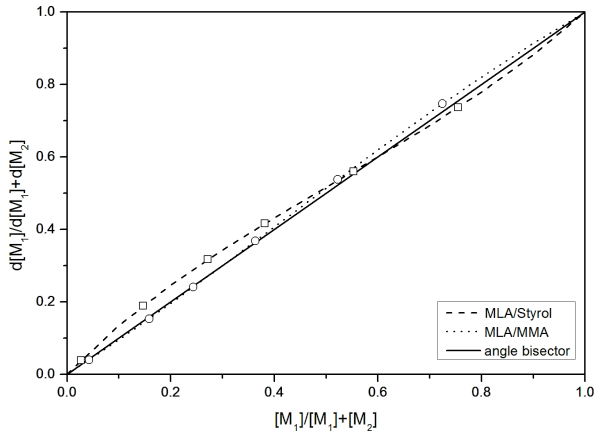

Figure 7: Copolymer composition curves for the systems MLA with styrene and MMA.

Chain-transfer agents for free-radical polymerization

Attempts to reduce the molecular weight during the MLA polymerization by the use of classical chain-transfer agents such as mercaptoethanol, mostly failed (Figure S17 and Table S7, Supporting Information File 1). A preferred nucleophilic attack of the thiol takes place**.** This can be clearly seen in the ^1H NMR spectra (Figures S18 and S19, Supporting Information File 1).

Thioacetic acid was used as a potential chain-transfer agent due to its lower nucleophilicity. However, a complete thiol-Michael addition can be seen in Figure 8 (not full conversion of MLA due to the impurities of thioacetic acid like disulfide and acetic acid). In this context, the iodine catalyzed thiol-Michael addition was investigated [11].

Controlled radical polymerization of MLA via RAFT

Since MLA acts as a vinyl monomer, it was also interesting to evaluate the controlled RAFT mechanism. Recently, the MADIX (macromolecular design via the interchange of xanthates) technique was found to be unsuccessful for the controlled radical homopolymerization of the non-cyclic monomer EAA. Only in the presence of acrylic monomers copolymerization of EAA under MADIX conditions was possible [23]. For MLA polymerization under controlled radical conditions, we evaluated a similar type of polymerization, the RAFT mechanism as shown in Scheme 3. The reversible series of addition and fragmentation between dormant and active chain ensure uniform growth of all chains with narrow dispersity (*Đ*).

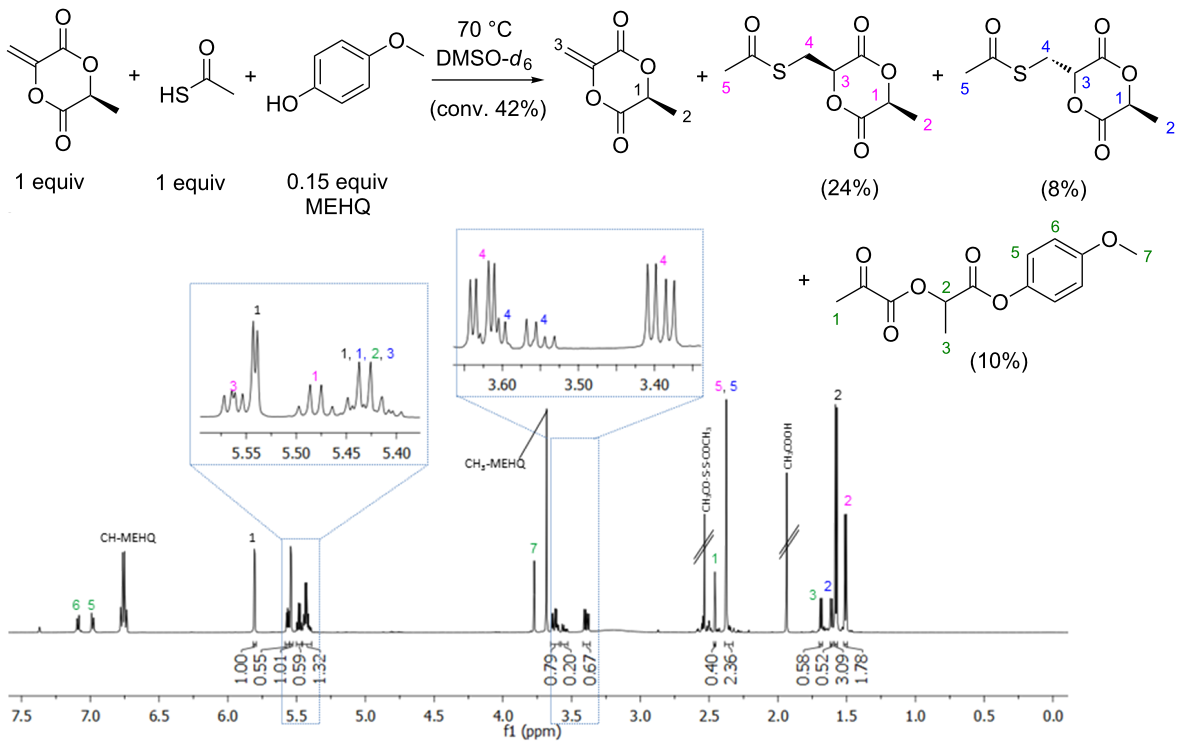

Figure 8: ^{1}H NMR spectrum of MLA with 1 equiv of thioacetic acid and 0.15 equivalents of an inhibitor 4-methoxyphenol (MEHQ) measured after 30 min at 70 °C in a NMR spectrometer (600 MHz, DMSO-d_6, 70 °C, $c_{MLA} = c_{Thioacetic\ acid}$ 0.5 mol·L^{-1}).

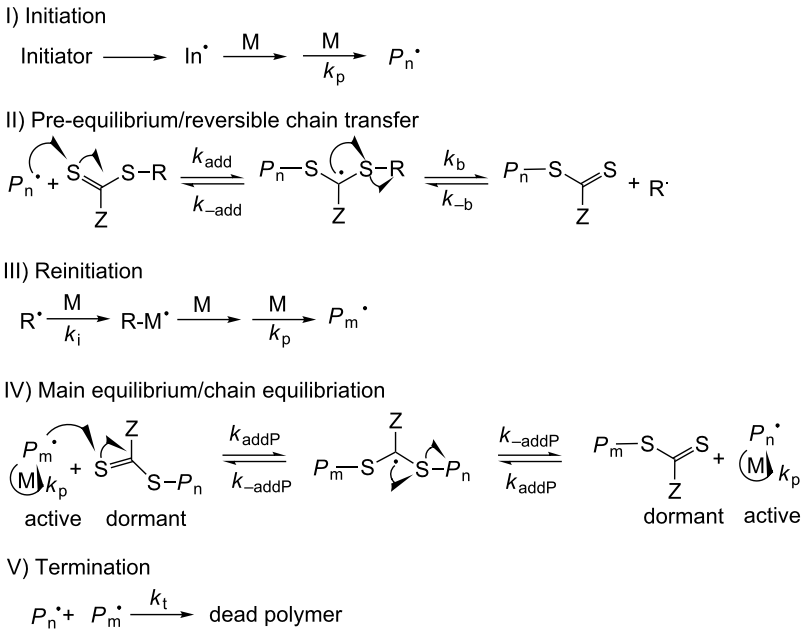

Scheme 3: Mechanism of RAFT polymerization [24].

The general structures of the RAFT agents contain a thiocarbonylthio group with reactive C–S double bond and attached R- and Z-group, whereas MADIX only refers to xanthates. Four RAFT agents with different polarities based on trithiocarbonate were examined in the RAFT homopolymerization of MLA (Figure 9).

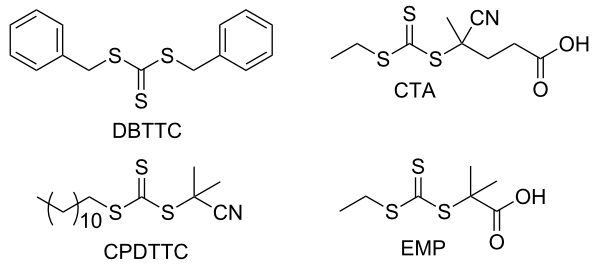

Figure 9: Structures of used RAFT agents examined in the polymerization of MLA.

The data of the RAFT homopolymerization of MLA are summarized in Table 3. Only in the presence of the more polar 4-cyano-4-(((ethylthio)carbonothioyl)thio)pentanoic acid (CTA) and 2-(((ethylthio)carbonothioyl)thio)-2-methylpropanoic acid (EMP) a polymerization took place. However only with EMP narrow dispersity was achieved ($Đ$ = 1.6). This dispersity of 1.6 illustrates the upper limit for a successful RAFT process. Beside the good dispersity, the M_n in comparison to the theoretical value $M_{n\ theo.}$ is much higher due to the known parallel running process of self-initiation. For this reason, the polymerization with EMP was further examined.

Upon further experiments with EMP (Table 4), the self-initiation becomes evident. Run 6 show the extent of the self-initiation with M_n of 17 200 g mol^{-1} and $Đ$ = 2. A reduced amount of MLA result in bimolecular M_n (run 7, Table 4) and a doubling of the amount of MLA in much higher M_n (runs 8 and 9, Table 4), by the dominant part of self-initiation. The runs in dry DMF seem to be better in terms of M_n, but in terms of dispersity, too high for the RAFT process (runs 10 and 11, Table 4). The isotacticity of the MLA polymers obtained in the RAFT polymerization was identical to those measured in the free-radical polymerization (Figure S20, Supporting Information File 1). The RAFT copolymerization with *N*,*N*-dimethylacrylamide (DMA) was investigated to reduce the self-initiated part [23].

RAFT-Copolymerization of MLA with *N*,*N*-dimethylacrylamide (DMA)

Copolymerization of MLA with DMA was conducted aiming for copolymers with a molecular weight of M_n of 20 000 g mol^{-1}. The results of the RAFT copolymerization are summarized in Table 5 (see SEC traces Figure S21, Supporting Information File 1).

As expected, the M_n values come closer to the theoretical values, the more DMA is used (Figure S21, Supporting Information File 1). At runs 12, 14 and 16 (Table 5) the MLA

Table 3: RAFT polymerization of MLA with different RAFT agents in a ratio of 98.87:1:0.125 ([MLA]/[RAFT]/[AIBN]) (80 wt % 1,4-dioxane, at 70 °C).

run	[1]/RAFT/[AIBN] [mol %]	Time [h]	Conversion [%]	$M_{n\ theo}$[a] [g/mol]	$M_{n\ SEC}$[b] [g/mol]	$Đ$
1	98.87/**DBTTC**/0.125	16	2.7	–	–	–
2	98.87/**CPDTTC**/0.125	16	4.2	–	–	–
3	98.87/**CTA**/0.125	18	87	12 500	55 400	2.3
4	98.87/**EMP**/0.125	16	>99	14 30	43 000	1.6

[a]Calculated theoretical molecular weights see characterization method in Supporting Information File 1. [b]Determined by PS-calibrated SEC.

Table 4: RAFT homopolymerization of MLA with EMP (80 wt % 1,4-dioxane at 70 °C).

run	[MLA]/[EMP]/[AIBN] [mol %]	Time [h]	Conversion [%]	$M_{n\ theo}$[a] [g/mol]	$M_{n\ SEC}$[b] [g/mol]	$Đ$
4	98.87/1/0.125	16	>99	14 300	43 000	1.6
5	98.87/0/0.125	17	>99	79 100	35 800	2.3
6	98.87/0/0	16	100	–	17 200	2.0
7	49.44/1/0.125	16	97	7 000	16 600	1.5
8	197.74/1/0.125	18	>99	28 300	191 300	2.4
9[c]	197.74/1/0.125	18	58	16 400	80 900	1.9
10[d]	197.74/1/0.125	20	92	26 200	18 500	1.9
11[d]	98.87/1/0.125	18	70	10 000	50 000	2.2

[a]Calculated theoretical molecular weights (see characterization methods in Supporting Information File 1). [b]Determined by PS-calibrated SEC. [c]180 wt % of 1,4-dioxane. [d]80 wt % dry DMF as solvent.

Table 5: RAFT copolymerization of MLA with DMA (0.5 mol % EMP and 0.0625 mol % AIBN, 80 wt % 1,4-dioxane, 70 °C).

run	[DMA]/[MLA] [mol %] [a)]	Time [h]	Conversion [%][a)]	$M_{n\ theo}$[a] [g/mol]	$M_{n\ SEC}$[b] [g/mol]	$Đ$	T_g [°C]
12	50/50	18	43/91	17 400	31 200	1.6	193
13	75/25	18	100/100	22 200	29 300	1.3	149
14	85/15	18	72/100	16 600	22 300	1.3	139
15	90/10	18	100/100	20 900	28 800	1.2	131
16	95/5	18	63/100	13 400	22 200	1.3	127.
17	100/0	18	100	19 900	20 400	1.2	121

[a]Calculated theoretical molecular weights (see characterization methods in Supporting Information File 1). [b]Determined by PS-calibrated SEC.

revenues were not quantitative with a slightly lower dispersity may be due to a longer induction period, but this also occurred in the repetition in other runs.

To investigate the process of the RAFT copolymerization of DMA with MLA the semi-logarithmic plot of conversion against time of run 15 (ratio 90/10, Table 5) was conducted which shows linearity for both monomers after a very short induction period (Figure 10A). This linearity confirmed a constant radical concentration during the copolymerization. MLA was converted quite rapidly in comparison to DMA. Therefore, the copolymerization trend seems to follow a gradient copolymer. This copolymerization process can be also identified in Figure 10B in which the highest value of the dispersity ($Đ$ = 1.35) corresponds to a quantitative conversion of MLA but to approximately 20% of the total revenue. After this point, the dispersity reduces until 1.23, corresponding to a dominant DMA part. An evidence for the gradient copolymerization can be found in the ^{1}H NMR spectrum by two separate lactide CH signals for the part of MLA and the copolymer part with DMA (Figure S22, Supporting Information File 1). In addition, at low conversion a rapid increase of the molecular weight of M_n = 4 000 g mol^{-1} ($M_{n\ theo}$ = 1 300 g mol^{-1}) can be observed (Figure S23 and Table S8, Supporting Information File 1). This observation has already been described in the literature and termed "hydrid behavior". It is characterized by a rapid increase in molecular weight in the initial stage due to deviation from the ideal kinetic behavior, leading to a mixed form of free radical and controlled radical polymerization followed by a controlled increase in molecular weight up to high monomer conversions which is responsible for the poor matches to the theoretical M_n values.

The semi-logarithmic plot of conversion against time of run 13 (ratios 75/25, Table 5) refer to Figure S24 show almost linearity for MLA, but with low conversion compared to the known rapid polymerization behavior. However, from the beginning until 8 h no conversion of DMA was observed, the

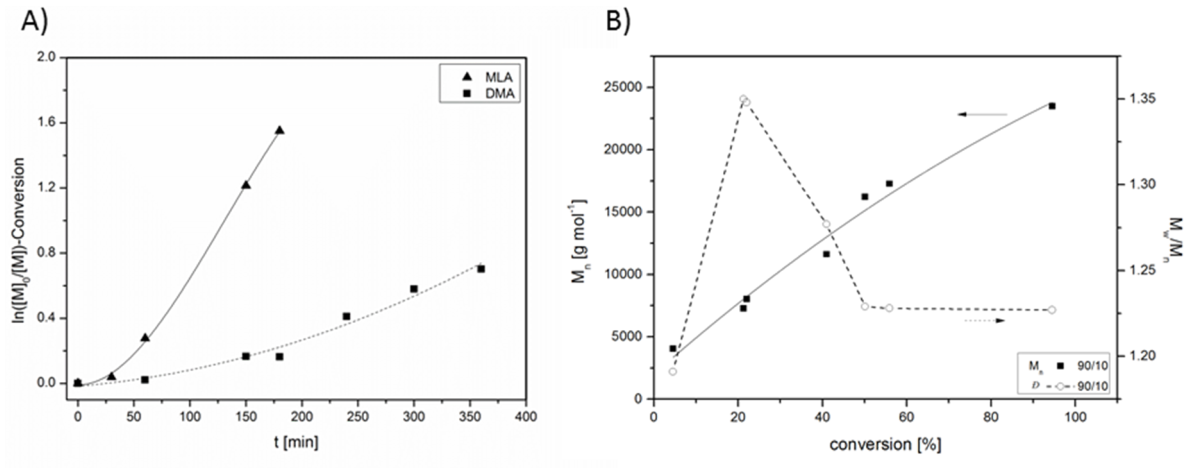

Figure 10: A) Kinetic plot for the RAFT copolymerization of MLA and DMA for the ratio 90/10 employing EMP. B) The evolution of M_n (full symbols) and $Đ$ (empty symbols) with conversion of the copolymerization.

finally 55% conversion of DMA were achieved afterwards until 22 h. The evolution of M_n and $Đ$ with conversion could not be evaluated due to overlapping signals in the SEC with the solvent DMF. Only at the end of the kinetic at 22 h the copolymer shows a useful value of M_n = 10 700 g mol^{-1} and $Đ$ = 1.6 with incorporated ratio of DMA/MLA of 60/40 determined by ^{1}H NMR spectroscopy. The theoretical molecular weight $M_{n\ theo}$ = 14 000 g mol^{-1} is higher than the achieved M_n which is a sign for the occurrence of transfer reactions. However, in the repetition of the kinetic of run 13 (Table 5) the conversion started with linearity for both monomers after an induction period (refer to Figure S24, Supporting Information File 1) with otherwise the same results (conv. MLA completely and DMA 65%, at 24 h M_n = 13 400 g mol^{-1} with $Đ$ =1.6 ($M_{n\ theo}$ of 17 000 g mol^{-1})).

These findings support the thesis that the copolymerization process of DMA and MLA is based on gradient copolymerization. The low conversion of MLA could be based on a slowly occurring sequence of addition and fragmentation between dormant and active chains because of the radical stabilized by the push–pull substituents. However, with this result it has been shown that the RAFT polymerization is a successful technique for MLA to achieve (co)polymers with narrow dispersities and with almost low molecular weight.

Conclusion

This first detailed study on the radical polymerization behavior of the cyclic push–pull-type monomer methylenelactide has been conducted. This was performed in comparision to the analogous non-cyclic push–pull-type monomers methyl α-acetoxyacrylate (MAA), ethyl α-acetoxyacrylate, (EAA) and pull-type methyl methacrylate (MMA) and cyclic pull-type α-methylene-δ-valerolactone (MVL).

A deviation from classical free-radical polymerization kinetics was found and correlated with significant self-initiation. A mechanism for the radical formation was proposed and supported by theoretical calculations. With the help of a strongly colored 1,1-diphenyl-2-picrylhydrazyl radical (DPPH) the spontaneous radical formation could also be observed by the naked eye. Furthermore, the copolymerization parameters of MLA with styrene and MMA were obtained and the Q and e values calculated. The latter allows the prediction of the copolymerization process with further monomers. Finally, this work reports on the first controlled polymerization of methylenelactide and controlled copolymerization with *N*,*N*-dimethylacrylamide via RAFT technique. From the above presented results it can be summarized that MLA represents a highly reactive monomer with a potential for many practical applications and further investigations.

Supporting Information

Full experimental section containing the description of the materials, characterization methods and syntheses of the obtained polymers, spectroscopic data (^{1}H, ^{13}C and IR), ^{1}H NMR kinetics, UV–vis measurements, polymerization analytics to determine the chain transfer constant, SEC curves of the RAFT initiated (co)polymers, the determination of the copolymerization parameters Q and e values and force constant.

Supporting Information File 1

Experimental part.
[http://www.beilstein-journals.org/bjoc/content/supplementary/1860-5397-12-232-S1.pdf]

References

1. Viehe, H. G.; Janousek, Z.; Merenyi, R.; Stella, L. *Acc. Chem. Res.* **1985,** *18,* 148–154. doi:10.1021/ar00113a004
2. Scheibelhoffer, A. S.; Blose, W. A.; Harwood, H. J. *Polym. Prepr. (Am. Chem. Soc., Div. Polym. Chem.)* **1969,** *10,* 1375–1380.
3. Jing, F.; Hillmyer, M. A. *J. Am. Chem. Soc.* **2008,** *130,* 13826–13827. doi:10.1021/ja804357u
4. Fiore, G. L.; Jing, F.; Young, V. G., Jr.; Cramer, C. J.; Hillmyer, M. A. *Polym. Chem.* **2010,** *1,* 870–877. doi:10.1039/c0py00029a
5. Barker, I. A.; Hall, D. J.; Hansell, C. F.; Du Prez, F. E.; O'Reilly, R. K.; Dove, A. P. *Macromol. Rapid Commun.* **2011,** *32,* 1362–1366. doi:10.1002/marc.201100324
6. Castillo, J. A.; Borchmann, D. E.; Cheng, A. Y.; Wang, Y.; Hu, C.; García, A. J.; Weck, M. *Macromolecules* **2012,** *45,* 62–69. doi:10.1021/ma2016387
7. Britner, J.; Ritter, H. *Macromolecules* **2015,** *48,* 3516–3522. doi:10.1021/acs.macromol.5b00040
8. Mauldin, T. C.; Wertz, J. T.; Boday, D. J. *ACS Macro Lett.* **2016,** *5,* 544–546. doi:10.1021/acsmacrolett.6b00023
9. Miyake, G. M.; Zhang, Y.; Chen, E. Y.-X. *J. Polym. Sci., Part A: Polym. Chem.* **2015,** *3,* 1523–1532. doi:10.1002/pola.27629
10. Kalelkar, P. P.; Alas, G. R.; Collard, D. M. *Macromolecules* **2016,** *49,* 2609–2617. doi:10.1021/acs.macromol.5b02431
11. Long, T. R.; Wongrakpanich, A.; Do, A.-V.; Salem, A. K.; Bowden, N. B. *Polym. Chem.* **2015,** *6,* 7188–7195. doi:10.1039/C5PY01059D
12. Fuoco, T.; Finne-Wistrand, A.; Pappalardo, D. *Biomacromolecules* **2016,** *17,* 1383–1394. doi:10.1021/acs.biomac.6b00005
13. Tanaka, H.; Kunouchi, Y.; Takeichi, T. *Macromolecules* **1997,** *30,* 4010–4012. doi:10.1021/ma9702253
14. Ueda, M.; Takahashi, M.; Imai, Y.; Pittman, C. U. *Macromolecules* **1983,** *16,* 1300–1305. doi:10.1021/ma00242a009
15. Tanaka, H.; Matsubara, Y.; Kusunoki, K.; Saito, N.; Kibayashi, T. *J. Polym. Sci., Part A: Polym. Chem.* **2015,** *53,* 2007–2016. doi:10.1002/pola.27649
16. Reichardt, C.; Welton, T. *Solvents and Solvent Effects in Organic Chemistry,* 4th ed.; Wiley-VCH: Weinheim, Germany, 2011. doi:10.1002/9783527632220

17. Tanaka, H.; Kameshima, T.; Sasai, K.; Sato, T.; Ota, T. *Makromol. Chem.* **1991,** *192,* 427–435. doi:10.1002/macp.1991.021920222
18. Kelen, T.; Tüdös, F. *J. Macromol. Sci., Chem.* **1975,** *9,* 1–27. doi:10.1080/00222337508068644
19. Alfrey, T., Jr.; Price, C. C. *J. Polym. Sci.* **1947,** *2,* 101–106. doi:10.1002/pol.1947.120020112
20. Unruh, C. C.; Laakso, T. M. *J. Polym. Sci.* **1958,** *33,* 87–94. doi:10.1002/pol.1958.1203312609
21. Greenley, R. Z. *J. Macromol. Sci., Chem.* **1975,** *9,* 505–516. doi:10.1080/00222337508065873
22. Hongo, T.; Yoshida, S.; Yamada, T.; Tanaka, H. *Polym. Int.* **1999,** *48,* 505–508. doi:10.1002/(SICI)1097-0126(199906)48:6<505::AID-PI182>3.0.CO;2-2
23. Batt-Coutrot, D.; Robin, J.-J.; Bzducha, W.; Destarac, M. *Macromol. Chem. Phys.* **2005,** *206,* 1709–1717. doi:10.1002/macp.200500065
24. Barner-Kowollik, C., Ed. *Handbook of RAFT Polymerization;* Wiley-VCH: Weinheim, Germany, 2008. doi:10.1002/9783527622757

License and Terms

BEILSTEIN JOURNAL OF ORGANIC CHEMISTRY

Highly reactive, liquid diacrylamides via synergistic combination of spatially arranged curing moieties

Maximilian Maier[1], Magnus S. Schmidt[2], Markus Ringwald[2] and Christoph P. Fik[*1]

Full Research Paper

Open Access

Address:
[1]Dentsply Sirona Restorative, De-Trey-Str. 1, 78467 Konstanz, Germany and [2]MCAT GmbH, Raiffeisenstr. 35, 78166 Donaueschingen, Germany

Email:
Christoph P. Fik[*] - christoph.fik@dentsplysirona.com

* Corresponding author

Keywords:
acrylamide; allyl; cyclopolymerization; photopolymerization; spatial effect

Beilstein J. Org. Chem. **2017,** *13,* 372–383.
doi:10.3762/bjoc.13.40

Received: 19 November 2016
Accepted: 02 February 2017
Published: 27 February 2017

This article is part of the Thematic Series "Spatial effects in polymer chemistry".

Guest Editor: H. Ritter

Abstract

Six polymerizable *N*,*N*'-diacylamides containing spatially arranged *N*-acryl, *N*-allyl and/or *N*-alkyl groups were prepared via two-step syntheses and characterized by $^{1}H/^{13}C$ NMR-spectra, refractive index (RI) and viscosity measurements. Photo DSC measurements on activated samples provided reactivity parameters ΔH_p, $R_{p,max}$ and t_{max}, while FTIR spectra before and after curing elucidated the underlying polymerization mechanism. Mechanical testing of the obtained polymers exhibited gradual differences in network densities, depending on the intramolecular arrangement and number of functional groups. Overall, a general building principle for highly reactive, liquid diacrylamides via synergistic combination of optimally arranged functional groups could be identified. The highest possible level of intramolecular synergism was found for low viscous *N*,*N*'-diacryloyl-*N*,*N*'-diallyl-1,4-but-2-enediamine.

Introduction

The selection of suitable monomers is a critical step for any free-radical polymerization approach. Particularly for (in situ) photo-induced polymerizations, monomers should comprise sufficient solubility in a given matrix, moderate viscosity, matching refractive indices as well as an optimized reactivity – the proper design of these features ensures continuous light transmittance, adequate propagation rates and, ultimately, thorough polymerization [1,2]. The number of applications for UV–vis curable monomer systems has greatly increased over the last decades [3]. At the same time, the selection of new monomers and crosslinkers remained limited [4].

Mono-, di-, tri- and multifunctional (meth)acrylates are among the first choices for photopolymerized mixtures as they exhibit a favorable balance between reactivity and thermal stability upon storage [5-7]. Moreover, they comprise compatibility with different matrices/solvents together with an adequate reactivity in a broad temperature range [8-10]. In general, acrylate monomers exhibit a higher reactivity than the respective methacrylates [11-13], but tend to be more sensitive to oxygen inhibition [14]. A major drawback of many (meth)acrylate-based compositions, however, is their susceptibility to premature hydrolysis when used in aqueous solutions, especially at pH values <2.5 [15,16].

One strategy to improve the hydrolytic stability is the oxygen-to-nitrogen substitution. The obtained class of (meth)acrylamides is of interest in the field of biomedical applications, e.g., for dental materials, artificial cornea, or drug-delivery systems, for which contact with body fluids is inevitable [17,18]. Whilst some of the resulting secondary di(meth)acrylamides end up being solids, tertiary di(meth)acrylamides can be obtained as relatively low viscous, highly soluble/compatible liquids [19]. Furthermore, acrylamides are generally more reactive than the respective methacrylamides. Regarding the substitution pattern, N-monosubstituted acrylamides tend to homopolymerize more readily than their N,N-disubstituted analogues [20]. Yet, acrylamides are particularly affected by the solvent regarding propagation reaction in free radical polymerization, even more so, if water is present [21].

Factors such as hydrogen bonding, hydrogen abstraction and the overall electronic characteristics are crucial in the design of improved monomer structures [22]. In this sense, Bowman et al. demonstrated increased photo-polymerization rates for monoacrylates equipped with secondary functionalities, yet limiting discussion to oxygen-based (meth)acrylate derivatives [23].

In this study, we present the synthesis and characterization of tailor-made, liquid *N*,*N*'-diacyl diacrylamides with enhanced reactivity through synergistic combination of spatially arranged curing moieties. The obtained structures were investigated in terms of underlying building principle, chemical and physical properties as well as polymerization behavior upon photoinitiation.

Results and Discussion

As stated earlier [24] we strive to investigate the unique physical properties and reactivity of tertiary *N*,*N*'-diallyl-diacrylamides. Closely related to this class of crosslinkers are bifunctional *N*-alkyl-*N*-allylacrylamides, which are known to undergo radical cyclopolymerization due to their adjacent double-bond functionalities [25-27]. The propagation reaction of these structures proceeds intramolecularly between acryl and allyl groups and intermolecularly (mostly) between polymer-radical and acrylamide groups. Cyclo- is preferred over linear polymerization due to the preformed five or six-membered lactams and gets even more predominant with increasing chain length of *N*-alkyl groups [28]. Expanding this concept in view of an optimized spatial layout, we synthesized molecules with additional "internal" (at the molecules' center), symmetrical allyl functions, connecting two *N*-allylacrylamide groups, thus adding a two-way, intramolecular reaction site. In order to individually assess the effect of "internal" and "external" (at the molecules' periphery) *N*-allylic functions on the physical/polymerization properties, a systematic variation of the molecular structure has been realized. When allyl- and acrylamide functionalities were spatially adjacent, a "synergistic potential" beneficial in radical polymerization was expected (Scheme 1).

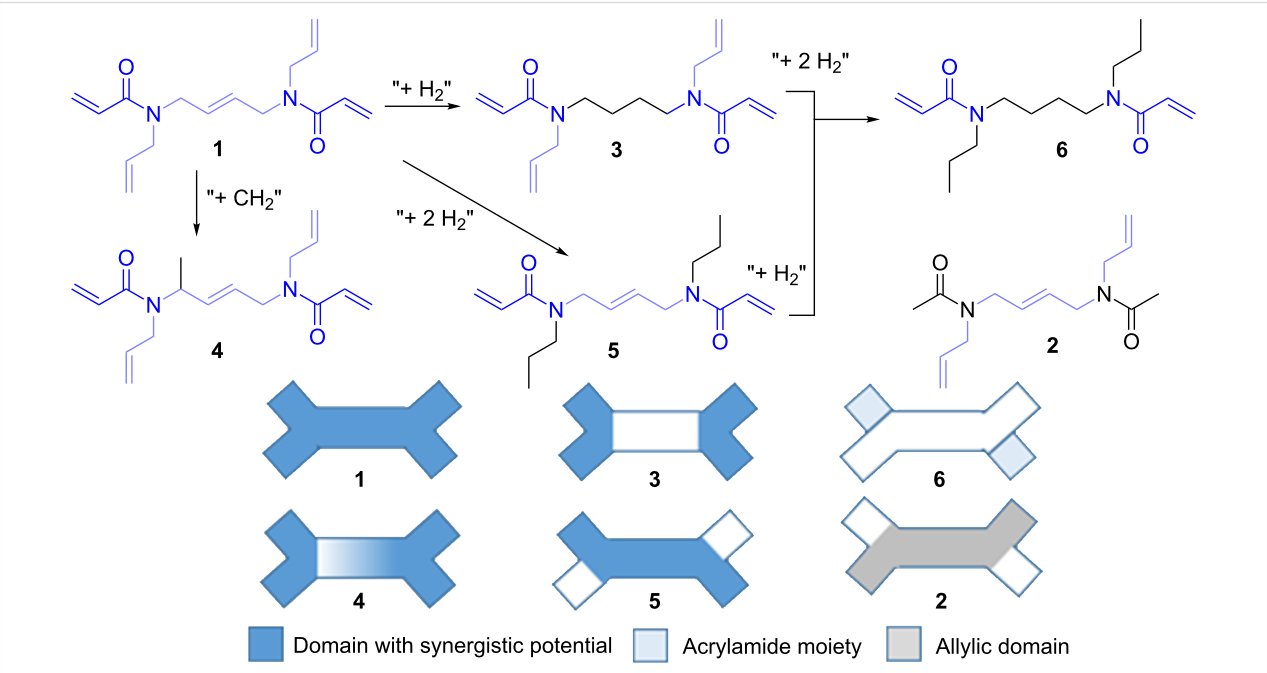

Scheme 1: Top: Overview of the synthesized crosslinkers **1–6** and their correlation to each other via formal reactions. Bottom: Schematic of **1–6** in terms of their structural synergistic potential due to adjacent acrylamide and allyl functions.

Synthesis

Six derivatives of highly functionalized crosslinkers **1**–**6** were synthesized as outlined in Scheme 2. We started from dibromide **7** to gain access to the corresponding compounds **1**, **2** and **5**. In case of the alpha-methyl compound **4**, we started from *trans*-1,3-pentadiene (**14**) and synthesized the dibromide **15** ac-

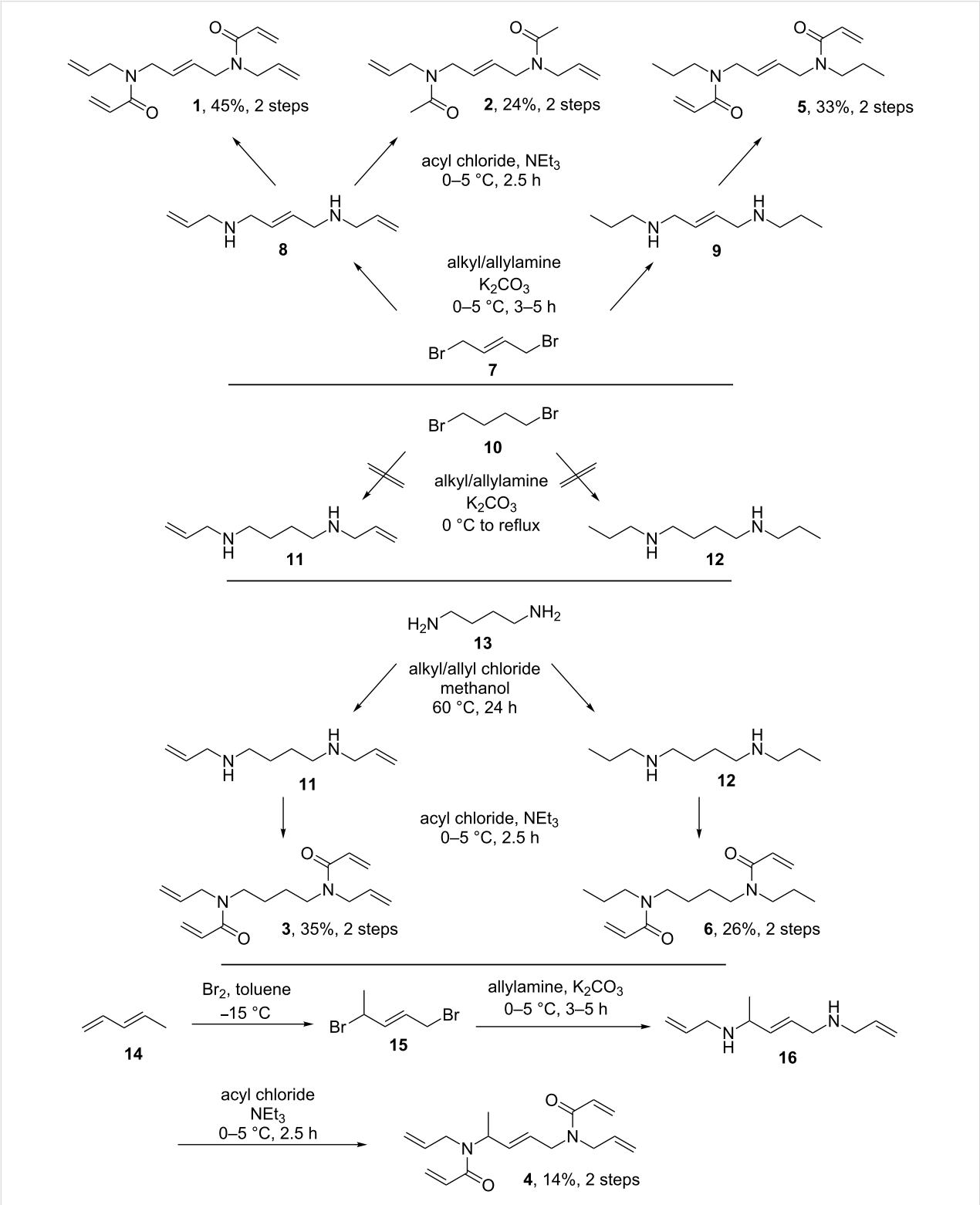

Scheme 2: Synthetic pathways to structurally related compounds **1**–**6**.

cording to the work of Heasley et al. [29]. Intermediates like compound **8** have already been synthesized in the 1990s by Havis et al. through the dropwise addition of **7** in chloroform to a solution of primary amines such as aminocyclohexane at room temperature [30]. After stirring for 24 hours the resulting diamino hydrobromide was isolated in moderate yield. To avoid quenching/scavenging of the hydrobromide in the later stages, we decided to use a procedure which would allow the isolation of the free diamine. Therefore, we used a substantial excess of the alkylamine without any other/further solvent and potassium carbonate as scavenger base for the hydrobromide (leading to insoluble potassium bromide). After work-up, we could isolate crude diamines **8** and **9**, containing significant amounts (10–15%) of the tertiary amines **8a** and **9a** (Scheme 3) or diamine **16**, respectively; each could be used without further purification. Classical acylation with acetyl chloride or acryloyl chloride in the presence of triethylamine led to the corresponding diallyl diacylamides **1**, **2** and **5** in 24–45% yields or, in the case of the alpha-methyl-substituted system, to compound **4**, in 14% yield. In all systems, we were able to remove acylated by-products of **8a** and **9a** by washing the organic solutions several times with 2 N HCl after which the compounds could be used without further purification. The synthesis of diamines **11** and **12** on the other hand was not possible by reacting 1,4-dibromobutane (**10**) with the corresponding alkyl or allylamines due to the lower reactivity of **10** compared to the unsaturated dibromide **7**.

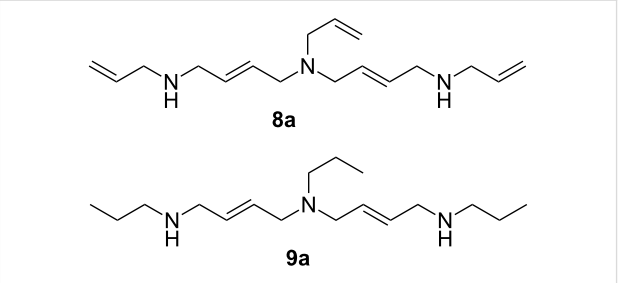

Scheme 3: Byproducts **8a** and **9a**.

Feuer et al. reported the synthesis of **12** and other similar derivatives through a multistep reaction with the final step comprising the treatment of *N*,*N*'-dipropylperhydropyridazine-3,6-dione with a borane solution in THF [31]. Considering the high reactivity of **7** and the assumption, that the allylic double bond to the halide is responsible for this effect, we decided to use 1,4-diaminobutane (**13**) and allyl chloride for the synthesis of diamine **11**. This also resulted in the positive side effect, that a formation of tertiary amines, comparable to compounds **8a** and **9a**, is not possible in this case. Interestingly, during the addition of allyl chloride to **13**, we could not observe any exothermic behavior or fast formation of the desired compound. So we decided to raise the temperature to 60 °C for 24 hours resulting in a significant increase of product formation. The subsequent direct acylation of the crude product **11** with acryloyl chloride afforded **3** in 35% yield. Based on this result, the analogous reaction of propyl chloride with 1,4-diaminobutane resulted in compound **6** in 26% yield.

In this context, attempts were made towards a cost-efficient synthesis of a possible *cis*-compound **19** (Scheme 4). For this, *cis*-dibromobut-2-ene (**18**) was synthesized from *cis*-but-2-ene-1,4-diol (**17**) using two different pathways; both reactions resulted in poor yields and product quality. Unfortunately, the reaction of **18** with allylamine did not result in the formation of **19**, but to the undesired cyclic compound **20**. The formation of the latter compound can only be explained by an intramolecular reaction of **21** (Scheme 4).

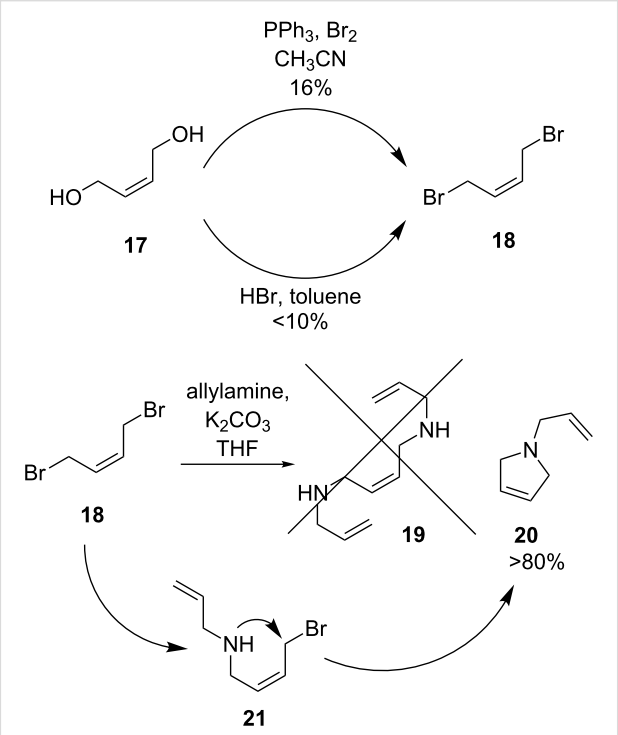

Scheme 4: Synthetic pathways towards the planned *cis*-intermediate **19**.

The NMR spectra of the final compounds show interesting aspects, reflecting the similar characteristic for this family of compounds (Scheme 5). Most importantly, all compounds exhibit line broadening (^{1}H NMR) or multiple signal sets (^{13}C NMR) for the possible *E*/*Z*-rotaisomers resulting in doubled signal sets in the ^{1}H and ^{13}C NMR spectra. The broader spectral field of the ^{13}C spectra as well as the used decoupled method provided generally high resolution, led to hardly any overlap of the signals and resulted in the observed

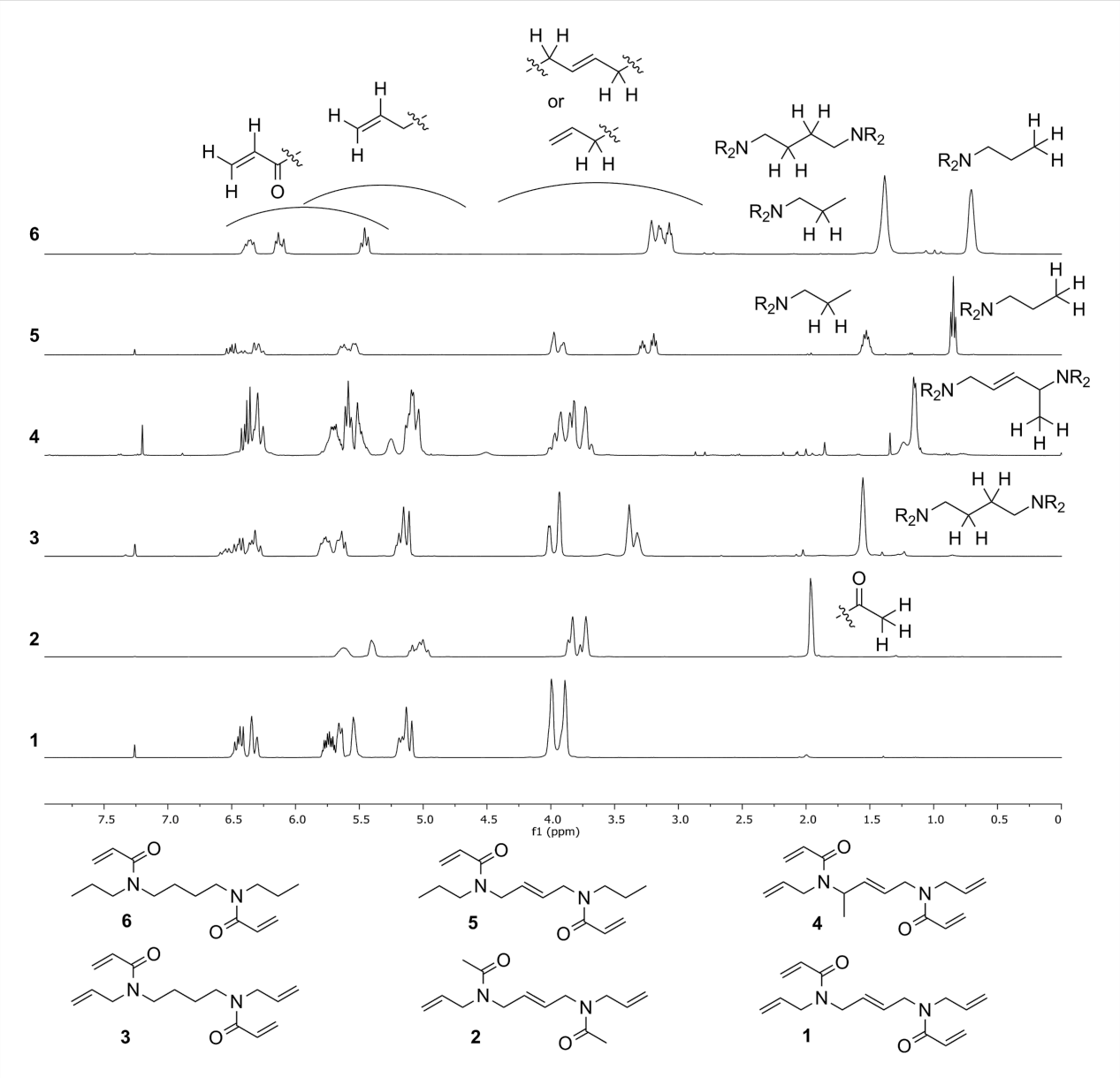

Scheme 5: Comparison of structural elements of **1–6** in the ^{1}H NMR spectra (400 MHz).

multiple signal sets. In the ^{1}H NMR spectra, however, the small differences of the chemical shifts for the different rotaisomers lead to a decrease of the resolution. This makes it quite demanding to read out any coupling constants, as broad multiplets for the many methylene and double bond protons are observed. Nevertheless, the ^{1}H NMR spectra (in combination with the two-dimensional methods COSY and HSQC) provided significant information for the classification of the compounds (Scheme 5).

Due to the increasing number of double bonds, refractive indices (RI) n^D_{20} ranged from 1.505 to remarkable 1.529. RIs of **1** and **4** are thus close to that of aromatic crosslinkers such as ethoxylated bisphenol-A dimethacrylate, EBPADMA (2 ethoxy groups, n^D_{20} 1.525, $\eta \approx 900$ mPa·s), but at a significantly lower viscosity and with the important difference, that all double bonds can take part in polymerization reactions. Compound **1** exhibits the most pronounced combination of a rather low viscosity and a high refractive index (Figure 1). Next, the solubility of the compounds **1–6** was tested in water, ethanol, isopropanol, acetone and methacrylic acid. Whereas all compounds **1–6** were highly soluble in acetone and methacrylic acid, no solubility in water was observed. A more differentiated analysis was possible using water/ethanol and water/isopropanol mixtures. By adding small amounts of alcohol to water (around 5% v/v), all compounds except **3** became fully

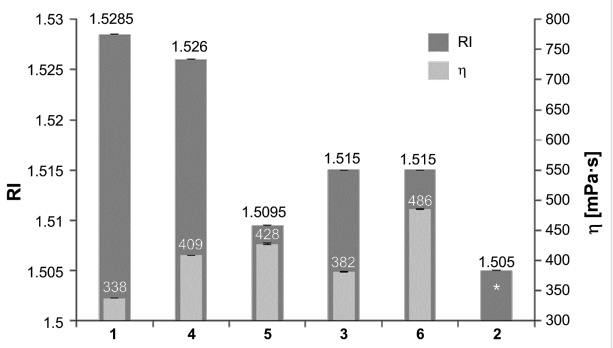

Figure 1: Refractive indices (RI) and viscosities (η) of crosslinkers **1–6** (* solid at room temperature).

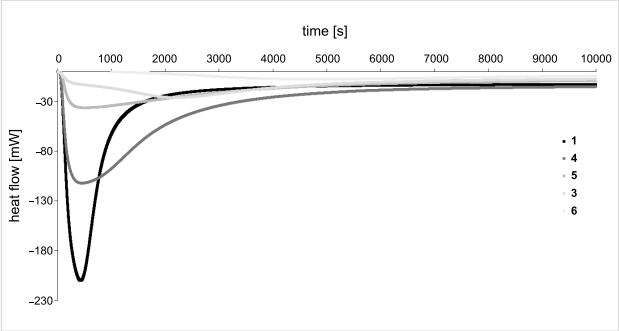

Figure 2: Exemplary photo-DSC plots for the curing of **1** and **3–6** at 37 °C.

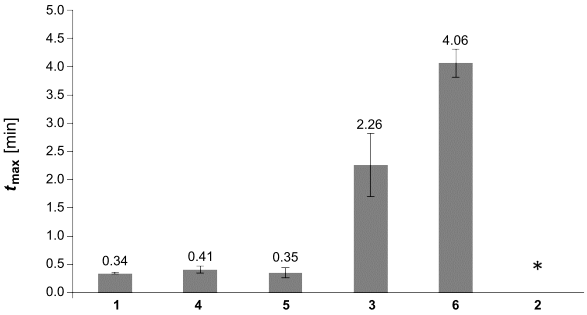

Figure 3: t_{max} for the curing of **1** and **3–6** at 37 °C (* no polymerization heat detected).

soluble. Interestingly, compound **3** remained insoluble – even in pure ethanol or isopropanol – in contrast to compounds **1**, **2** and **4–6**. Overall, a broad solubility spectrum was found (Table 1).

Polymerization behavior

Bulk homopolymerization of **1** and **3–6** was monitored by photo-DSC. Curing plots showed a rapid polymerization for **1**, **4** and **5** (t_{max} = 20 s, 24 s and 21 s, respectively), while curing of **3** (t_{max} = 1 min 58 s) and **6** (t_{max} = 4 min 15 s) was delayed to later stages (Figure 2, Figure 3). As expected, irradiation of activated samples of **2** did not lead to any detectable polymerization heat at all, most likely due to obstructed allylic homopolymerization. As a) linear copolymerization of acrylamido and allyl moieties heavily favors acrylamide homopolymerization [28,32] and b) the allyl group is known for its chain-transfer behavior, but still c) reaction is fastest for the highest (intramolecular) occurrence of acryl/allyl groups, a dominant, non-classical polymerization mechanism of molecules containing both acrylamido and allyl functions can be assumed. The theoretical value for ΔH_p of the well-studied acrylamide-double bonds is 19.8 kcal·mol^{-1} (82.8 kJ·mol^{-1}). For allyl double bonds, the disclosure is more complex. As mentioned, the tendency of allyl groups to homopolymerize is weak and in many cases, no polymerization can be observed at all. Therefore, we suggest a two-step estimation: In a best case, ΔH_p of allyl groups should be as high as that of 1-butene, which is 20.9 kcal·mol^{-1} (87.5 kJ·mol^{-1}) [33]. In a worst case, the reactivity of allyl groups is only half of 1-butene's reactivity, giving modest 10.5 kcal·mol^{-1} (43.7 kJ·mol^{-1}). The borderline case that allyl groups would show no reactivity at all was not reflected in our calculations (however, it would result in the highest maximum polymerization rates, $R_{p,max}$ values). Regarding $R_{p,max}$ of **1** it stands out with a value of 0.147/0.102 (Figure 4). In case of compound **5** (0.052/0.043) and **4** (0.045/0.031) the values were slightly higher as or comparable to the often used 2-hydroxyethyl methacrylate (HEMA), as measured

Table 1: Solubility parameters of compounds **1–6**.[a]

compound	water	ethanol	isopropanol	acetone	methacrylic acid
1	−	+	+	+	+
2	−	+	+	+	+
3	−	−	−	+	+
4	−	+	+	+	+
5	−	+	+	+	+
6	−	+	+	+	+

[a]+ soluble in the respective solvent, − insoluble in the respective solvent.

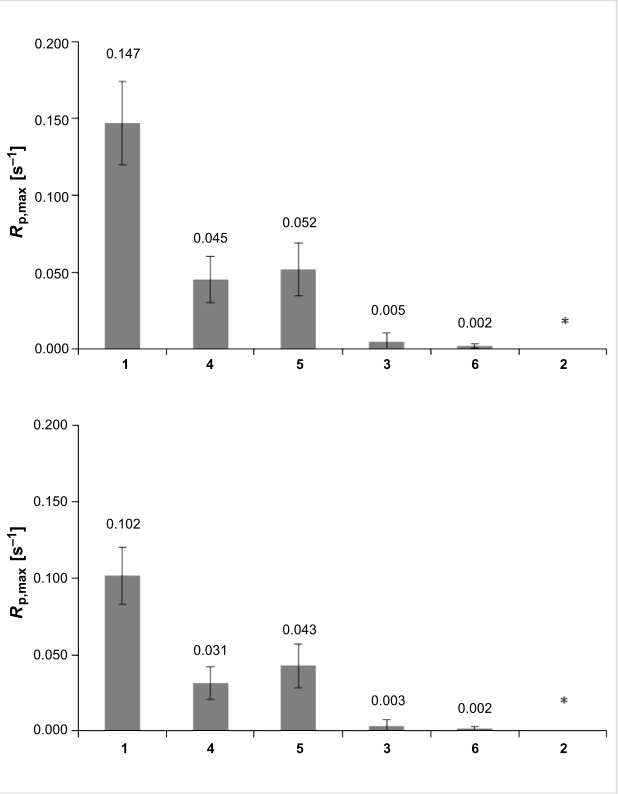

Figure 4: $R_{p,\,max}$ for the curing of **1–6** at 37 °C for a) top: ΔH_p of allyl groups = 87.5 kJ·mol^{-1} and b) bottom: ΔH_p of allyl groups = 43.7 kJ·mol^{-1} (*no polymerization heat detected).

by a different work group (0.032) [34]. Interestingly, equipping the amide α-carbon with a methyl group (1→4) led to a ~70% decrease of $R_{p,max}$ from 0.147/0.102 to 0.045/0.031, indicating the special role of the internal double bond. Also, when comparing **5** (0.052/0.043) and **3** (0.005/0.003), the internal allylic function contributes to a remarkable 10-fold higher $R_{p,max}$ than both external allyl functions.

The ΔH_p values ranged from ca. −35 to −153 kJ·mol^{-1} and, again, were highest for **1** (Figure 5). Notably, the ΔH_p of −153 kJ·mol^{-1} corresponds to almost two times the polymerization heat of primary acrylamide when fully converted (82.8 kJ·mol^{-1}) [35]. However, as incomplete conversion under the tested bulk conditions has to be expected, spatially adjacent allyl groups have to take part in the polymerization. Interestingly, the internal allylic function again seems to contribute to a much higher extent to the overall reactivity when compared to two external allyl functions (**5** vs **3**).

In order to verify an assumed, underlying cyclopolymerization mechanism, FTIR spectra of the crosslinkers were recorded before and after photopolymerization (Figure 6). All compounds containing both, acrylamido and allyl functions (**1**, **3**–**5**), showed two peaks for the acrylamide vibration at ≈1645 cm^{-1} and ≈1610 cm^{-1} before, and 3 peaks at ≈1645 cm^{-1}, ≈1610 cm^{-1} and ≈1680 cm^{-1} after the polymerization. Compound **6** showed only two peaks before and after polymerization, while the spectrum of **2** contains the typical acetamide peak at 1633 cm^{-1} before and after polymerization. In accordance with the FTIR data and literature [27,28], we propose that some of the possible intramolecular reaction products (intermolecular cyclization products are conceivable as well) start most likely from the formed acrylamide radical as depicted in Scheme 6. Upon subsequent cyclization, either 6-membered δ-lactams, or 5-membered γ-lactams can be formed. The

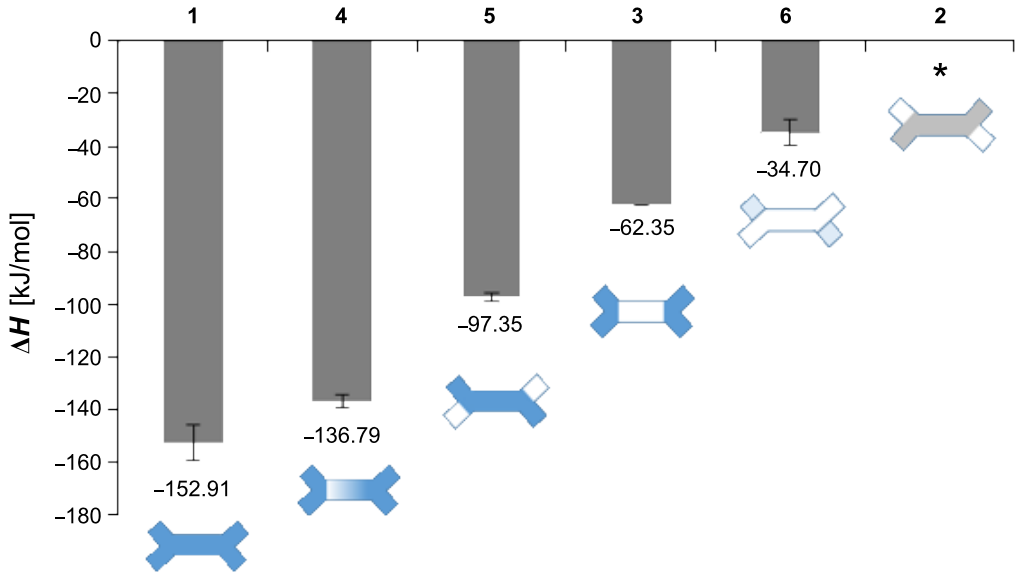

Figure 5: Polymerization heat, ΔH_p for the curing of **1–6** at 37 °C (* no polymerization heat detected).

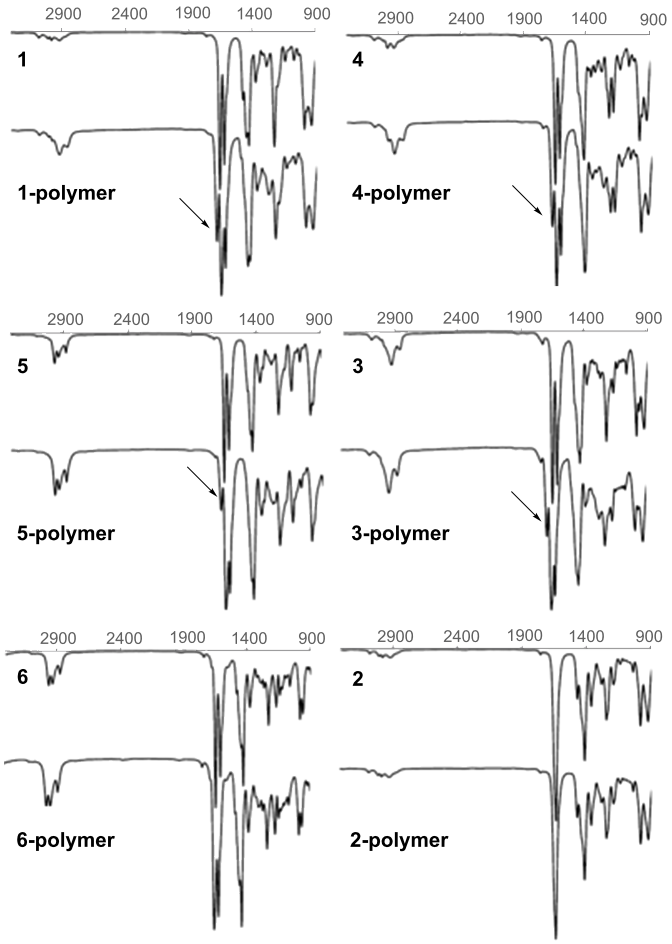

Figure 6: FTIR spectra of **1–6** before (top) and after (bottom) curing; the arrows indicate emerging, characteristic γ-lactam vibration at ~1680 cm^{-1} for polymers **1** and **3–5**.

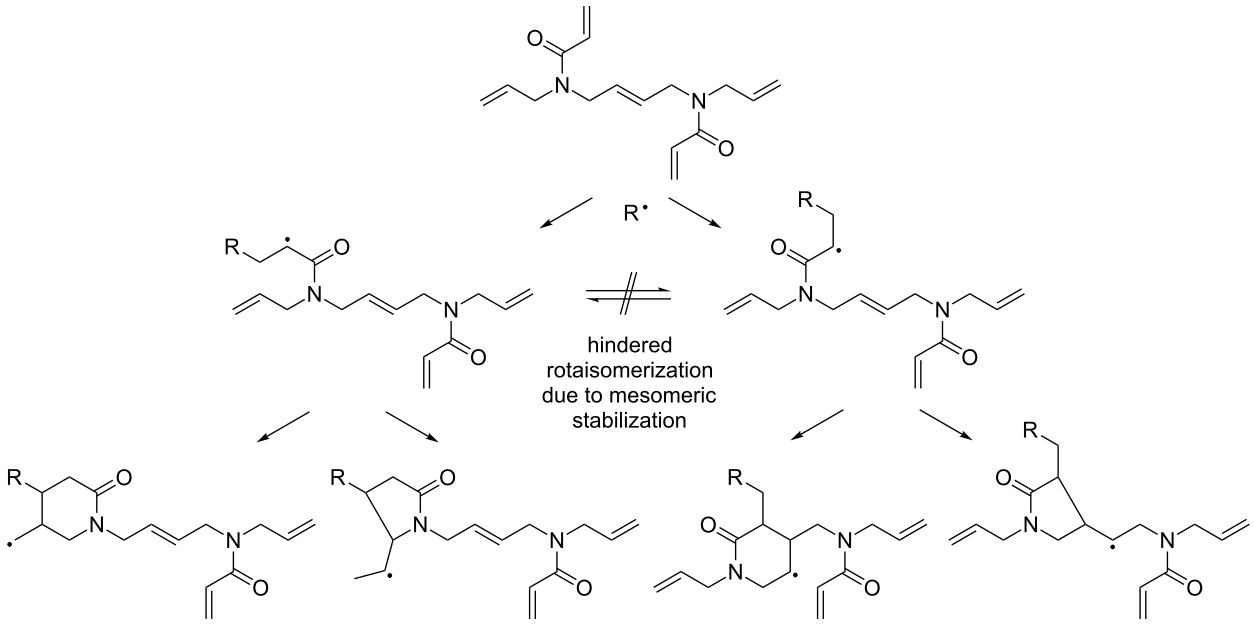

Scheme 6: Proposed reaction pathways for the intramolecular propagation within **1**.

emerging FTIR signal at ≈1680 cm^{-1} strongly indicates the formation of γ-lactams as it can be attributed to the stretching vibration of γ-lactam carbonyl groups [28]. However, the corresponding δ-lactam peak could be located below the amide peak at ≈1645 cm^{-1}. After one intramolecular ring is formed, there are three general options for a further radical reaction: a) Intermolecular radical propagation, b) intermolecular cyclization, and/or c) intramolecular cyclization. Assuming an incomplete conversion and judging from the remaining IR signals in the finger print regime, we can only assume that all three propagation pathways a), b) and c) take place simultaneously. Furthermore, taking in account FTIR and DSC data, we expect that ring formation significantly contributes to the overall reaction enthalpy. It is quite clear, that the combination of internal allylic and acrylamide functions is more favored than one of acrylamide functions with external allylic moieties. A reason for that might be the spatial arrangement of the rotationally obstructed double bond of the acrylamide group, which has two favorable out of three possible orientations to initiate the lactam formation with the internal butene group, whereas there is only one favorable orientation for the external allyl group.

Polymer network properties

To assess the influence of functionalities on the network densities of the obtained polymers, mechanical data of rod-like samples according to ISO 4049 3-point bending was collected. The photocured sample of **2** was gel-like and could not be tested whereas compound **6** led to brittle material. Concerning the other samples, flexural moduli (E-moduli) were statistically different. The polymer of **1** exhibited the highest flexural-modulus and thus highest apparent network density. This means that ring formation, which in principle should reduce the amount of covalent network points in the cured material, is superimposed by effects of conversion, entanglement and rigidity of the formed polymer. The decreasing trend of flexural modulus from **1**, **4**, **5** to **3** is in accordance with the data on reactivity obtained from photo-DSC measurements (Figure 7).

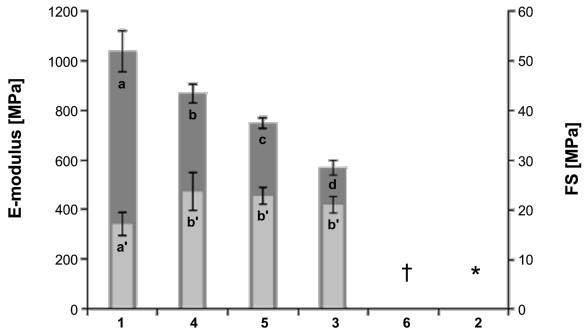

Figure 7: Flexural strength (FS) and E-modulus of cured crosslinkers **1–6**; letters refer to statistical groups (* gel-like polymer, pretest failure; † brittle polymer, pretest failure).

Conclusion

In this study, six polymerizable *N*,*N*'-diacylamides containing *N*-acryl, *N*-allyl and/or *N*-alkyl groups were synthesized in two steps. With the exception of the single solid *N*,*N*'-diacetyl-*N*,*N*'-diallyl-1,4-but-2-enediamine, all compounds were obtained as remarkably low-viscous liquids, characterized by high refractive indices above 1.500 and good solubilities in exemplary solvents. A significant increase in the polymerization reactivity and rate was achieved by systematic spatial intramolecular arrangement and the substitution with *N*-allyl, *N*-acyl and *N*-acrylamide functional groups. Surprisingly, the contribution of internal *N*-allyl groups was higher than that of external ones indicating a dominant, non-classical polymerization mechanism. The results support exothermic ring formation on the *N*,*N*'-diallyl-diacrylamide moieties being responsible for the considerable plus in reactivity. Due to the flexible character of the functional groups, intermolecular cyclization is also probable and thus, will contribute to the overall polymerization reactivity. A general building principle was found based on the synergistic combination of spatially adjacent functional groups. It allows a tremendous increase in the overall double-bond susceptibility in the studied molecules. The *N*,*N*'-diacryloyl-*N*,*N*'-diallyl-1,4-but-2-enediamine revealed the highest level of intramolecular synergism rendering this type of crosslinkers highly attractive for a broad range of free radical (photo)polymerization applications, for example in the constantly growing medical device sector.

Experimental

Materials. Chemicals and reagents were purchased from Acros, Carl Roth, ChemPUR, Sigma-Aldrich, TCI or ABCR or have been used from the MCAT company stock and were used without further purification.

Measurements. TLC was carried out on Silica Gel 60 F254 (Merck, layer thickness 0.2 mm) with detection by UV light (254 nm) and/or by charring with 15% sulfuric acid in ethanol. Flash column chromatography (FC) was performed on M&N Silica Gel 60 (0.063–0.200 mm). ^{1}H NMR and ^{13}C NMR spectra were recorded on a Bruker Avance II 400. Chemical shifts are reported in ppm relative to solvent signals ($CDCl_3$: δ_H = 7.26 ppm, δ_C = 77.0 ppm). Signals were assigned by first-order analysis and assignments were supported, where feasible, by two-dimensional $^{1}H,^{1}H$ and $^{1}H,^{13}C$ correlation spectroscopy. The polymerization enthalpies ΔH were measured with a photo-DSC 7/DPA 7 (Perkin-Elmer) having a light intensity in the visible portion of the spectrum of 108 mW/cm² in an isothermal mode at 37 °C. Each sample was activated with

0.3 wt % camphorquinone, 0.4 wt % ethyl 4-dimethylaminobenzoate and irradiated twice. After the first run a second run was made that was subtracted from the first one. The subtraction of these runs from one another removed the effect of sample heating by illumination. The DSC experiments were carried out twice and maximum rates of polymerization, $R_{p,max,}$ were calculated according to Equation 1.

$$R_{p,max} = ((Q / s \cdot M) / n \cdot \Delta H_p \cdot m) \quad (1)$$

With Q/s being the heat flow per second at the global minimum of the first deviation of the respective measurement (maximum Q/s), M the molar mass of the monomer, n the number of double bonds per monomer molecule, ΔH_p the heat released per mole of double bonds reacted, and m the mass of the monomer in the sample. Mechanical data was measured in the 3-point bending mode according to ISO 4049:2009 using a Zwick instrument. Sample activation was done by adding 0.3 wt % camphorquinone and 0.4 wt % ethyl 4-dimethylaminobenzoate. FTIR spectra were measured using an iS10 FTIR spectrometer (Thermo Scientific). Viscosity was measured on an Anton Paar Physica MCR 300 equipped with CP 50-1 plate–plate geometry at a shear stress τ of 5 Pa and 25 data points from 0.72 to 1450 rad were taken and averaged. Refractive indices (RI) were measured using an Anton Paar Abbemat 200 refractometer at 20 °C.

General procedure for the synthesis of *N*,*N*'-diacyl-*N*,*N*'-dialkyl-1,4-diamines **1–6**

Amination

a) Synthesis of 1,4-but-2-enediamine: Potassium carbonate (2.5 equiv) was added to the alkylamine (15 equiv) and cooled to 0–5 °C. The corresponding dibromide (1 equiv) was added in portions and the resulting mixture was stirred for 3–5 h at rt. Then the remaining amine was removed by distillation and the resulting residue was suspended in acetone. After removing the salts by filtration the acetone was evaporated.

b) Synthesis of the 1,4-butanediamine: The corresponding alkyl chloride (2.1 equiv) was added drop wise to a solution of 1,4-diaminobutane (1 equiv) in methanol at 50 °C. The resulting mixture was stirred at 60 °C for 24 h. Then methanol was removed by distillation and the residue was diluted with 2 M NaOH and extracted with DCM. The organic layer containing the crude product was dried (Na_2SO_4) and the solvent evaporated.

Acrylation

The resulting diamines were dissolved in THF and triethylamine (3.5 equiv) was added. Acryloyl chloride (2.2 equiv) was addeddrop wise at 0–5 °C after which the resulting mixture was stirred for 2.5 h at rt. Then, the THF was evaporated, ethyl acetate was added and the resulting mixture was washed 3 times with 2 N HCl and once with water. The organic layer was dried (Na_2SO_4), the solvent was evaporated and the residue was purified by flash chromatography.

***N*,*N*'-Diacryloyl-*N*,*N*'-diallyl-1,4-but-2-enediamine (1):** Yield: 45%; purity (^{1}H NMR) >98%; $\eta_{23°C}$ = 338 mPa·s; n^D_{20} = 1.529; ^{1}H NMR ($CDCl_3$) δ 6.50–6.43 (m, 2H, H_2CCHC(O)), 6.37–6.33 (m, 2H, H_2CCHC(O)), 5.81–5.72 (m, 2H, H_2CCHCH_2), 5.69–5.66 (m, 2H, $H_2CCHC(O)$), 5.59–5.56 (m, 2H, $H_2CHCCHCH_2$), 5.22–5.11 (m, 4H, H_2CCHCH_2), 4.02 (m, 4H, $H_2CHCCHCH_2$), 3.92 (m, H_2CCHCH_2); ^{13}C NMR ($CDCl_3$) δ 166.3, 166.1 ($C(O)CHCH_2$), 132.9, 132.8 (H_2CCHCH_2), 128.5–127.3 ($H_2CCHC(O)$, $H_2CHCCHCH_2$), 117.5-116.7 (H_2CCHCH_2), 49.3–48.1 (H_2CCHCH_2), 47.1 ($H_2CHCCHCH_2$); FTIR $\tilde{\nu}_{max}$ [cm^{-1}]: 3517, 3080, 3018, 2986, 2917, 1645, 1611, 1463, 1416, 1363, 1276, 1213, 1129, 1059, 975, 919, 794.

***N*,*N*'-Diacetyl-*N*,*N*'-diallyl-1,4-but-2-enediamine (2):** Yield: 24%; purity (^{1}H NMR) >97%; T_m = 32 °C; n^D_{20} = 1.505; ^{1}H NMR ($CDCl_3$) δ 5.69–5.61 (m, 2H, H_2CCHCH_2), 5.43 (m, 2H, $H_2CHCCHCH_2$), 5.12–4.98 (m, 4H, H_2CCHCH_2) 3.88–3.74 (m, 8H, $H_2CHCCHCH_2$, H_2CCHCH_2), 2.00 (s, 6H, $C(O)CH_3$); ^{13}C NMR ($CDCl_3$) δ 170.3–169.4 ($C(O)CH_3$), 132.9–132.3 (H_2CCHCH_2), 127.9–127.0 ($H_2CHCCHCH_2$), 116.7–116.2 (H_2CCHCH_2), 49.9–46.2 (H_2CCHCH_2, $H_2CHCCHCH_2$) 21.1–21.0 ($C(O)CH_3$); FTIR $\tilde{\nu}_{max}$ [cm^{-1}]: 3074, 3012, 2986, 2916, 1633, 1468, 1411, 1360, 1242, 1187, 1035, 978, 919.

***N*,*N*'-Diacryloyl-*N*,*N*'-diallyl-1,4-butanediamine (3):** Yield: 35%; purity (^{1}H NMR) >94%; $\eta_{23°C}$ = 382 mPa·s; n^D_{20} = 1.515; ^{1}H NMR ($CDCl_3$) δ 6.58–6.28 (m, 4H, H_2CCHC(O)), 5.80–5.71 (m, 2H, H_2CCHCH_2), 5.68–5.60 (m, 2H, $H_2CCHC(O)$), 5.21–5.10 (m, 4H, H_2CCHCH_2), 4.02–3.93 (m, 4H, H_2CCHCH_2), 3.41–3.40 (m, 4H, $H_2CH_2CCH_2CH_2$), 1.55 (m, 4H, $H_2CH_2CCH_2CH_2$); ^{13}C NMR ($CDCl_3$) δ 166.6, 166.0 ($C(O)CHCH_2$), 133.3, 133.0 (H_2CCHCH_2), 128.2–127.5 ($H_2CCHC(O)$), 117.1–116.7 (H_2CCHCH_2), 50.1–48.6 (H_2CCHCH_2), 46.9–45.9 ($H_2CH_2CCH_2CH_2$), 26.5–25.0 ($H_2CH_2CCH_2CH_2$); FTIR $\tilde{\nu}_{max}$ [cm^{-1}]: 3472, 3082, 2924, 1646, 1609, 1428, 1374, 1217, 1163, 1133, 1059, 978, 957, 918, 794.

***N*,*N*'-Diacryloyl-*N*,*N*'-diallyl-2,4-pent-2-enediamine (4):** Yield: 14%; purity (^{1}H NMR) >98%; $\eta_{23°C}$ = 409 mPa·s; n^D_{20} = 1.526; ^{1}H NMR ($CDCl_3$) δ 6.50–6.26 (m, 5H, 2x H_2CCHC(O)), 5.84–5.70 (m, 2H, H_2CCHCH_2), 5.68–5.60 (m, 2H, $H_2CCHC(O)$), 5.61–5.51 (m, 2H, $H_2CHCCHCH_2$), 5.31

(m, 1H, *H*C(CH$_3$)HCCHCH$_2$), 5.25–5.08 (m, 4H, *H*$_2$CCHCH$_2$), 4.06–3.71 (m, 6H, HC(CH$_3$)HCCHC*H*$_2$, 2× H$_2$CCHC*H*$_2$); ^{13}C NMR (CDCl$_3$) δ 166.4, 166.3, 166.1 (*C*(O)CHCH$_2$), 135.1–132.8 (H$_2$C*C*HCH$_2$), 128.5–126.5 (H$_2$*C*CHC(O), HC(CH$_3$)H*C*CHCH$_2$), 117.5–116.4 (H$_2$*C*CHCH$_2$), 50.0 (H*C*(CH$_3$)HCCHCH$_2$), 49.1–45.5 (H$_2$CCH*C*H$_2$, H$_2$*C*HCCHCH$_2$), 18.7, 17.1, 16.8 (HC(*C*H$_3$)HCCHCH$_2$); FTIR $\tilde{\nu}_{max}$ [cm^{-1}]: 3532, 3491, 3080, 2977, 2924, 1644, 1609, 1416, 1362, 1328 1276, 1217, 1184, 1129, 1059, 976, 919, 794.

_N_,_N_'-Diacryloyl-_N_,_N_'-dipropyl-1,4-but-2-enediamine (5): Yield: 33%; purity (^{1}H NMR) >97%; $\eta_{23°C}$ = 428 mPa·s; n^D_{20} = 1.5095; ^{1}H NMR (CDCl$_3$) δ 6.54–6.47 (m, 2H, *H*$_2$CCHC(O)), 6.33–6.25 (m, 2H, *H*$_2$CCHC(O)), 5.66–5.58 (m, 2H, H$_2$CC*H*C(O)), 5.56–5.51 (m, 2H, H$_2$C*H*CC*H*CH$_2$), 3.99–3.89 (m, 4H, *H*$_2$CHCCHC*H*$_2$), 3.30–3.18 (m, H$_3$CCH$_2$C*H*$_2$), 1.54 ('quint', 4H, H$_3$CC*H*$_2$CH$_2$), 0.85 (t, 6H, *H*$_3$CCH$_2$CH$_2$); ^{13}C NMR (CDCl$_3$) δ 166.1, 165.9 (*C*(O)CHCH$_2$), 128.1–127.3 (H$_2$*CC*HC(O), H$_2$CH*CC*HCH$_2$), 117.5–116.7 (H$_2$*C*CHCH$_2$), 49.1–47.4 (H$_3$CCH$_2$*C*H$_2$, H$_2$*C*HCCH*C*H$_2$), 22.5–20.9 (H$_2$CH$_2$*CC*H$_2$CH$_2$, H$_3$C*C*H$_2$CH$_2$), 11.2–11.0 (H$_3$*C*CH$_2$CH$_2$); FTIR $\tilde{\nu}_{max}$ [cm^{-1}]: 3525, 2963, 2932, 2875, 1645, 1609, 1442, 1426, 1368, 1279, 1224, 1123, 1059, 975, 888, 794.

_N_,_N_'-Diacryloyl-_N_,_N_'-dipropyl-1,4-butanediamine (6): Yield: 26%; purity (^{1}H NMR) >96%; $\eta_{23°C}$ = 486 mPa·s; n^D_{20} = 1.515; ^{1}H NMR (CDCl$_3$) δ 6.40–6.33 (m, 2H, *H*$_2$CCHC(O)), 6.16–6.09 (m, 2H, *H*$_2$CCHC(O)), 5.49–5.43 (m, 2H, H$_2$CC*H*C(O)), 3.21–3.05 (m, 8H, *H*$_2$CH$_2$CCH$_2$C*H*$_2$, H$_3$CCH$_2$C*H*$_2$), 1.38 (m, 8H, H$_3$CC*H*$_2$CH$_2$, H$_2$C*H*$_2$CC*H*$_2$CH$_2$), 0.70 (m, H$_3$CC*H*$_2$CH$_2$); ^{13}C NMR (CDCl$_3$) δ 165.5, 165.4 (*C*(O)CHCH$_2$), 127.5–126.9 (H$_2$*CC*HC(O)), 49.1–45.3 (H$_3$CCH$_2$*C*H$_2$, H$_2$*C*H$_2$CCH$_2$*C*H$_2$), 26.3–20.5 (H$_2$CH$_2$*CC*H$_2$CH$_2$, H$_3$C*C*H$_2$CH$_2$), 10.9–10.6 (H$_3$*C*CH$_2$CH$_2$); FTIR $\tilde{\nu}_{max}$ [cm^{-1}]: 3314, 2963, 2933, 2874, 1645, 1608, 1481, 1449, 1426, 1374, 1263, 1227, 1166, 1136, 1058, 978, 954, 794.

Acknowledgements

The authors thank Marina Stojiljkovic for sample preparation and Christine Regenscheit for viscosity measurements.

References

1. Decker, C. *Prog. Polym. Sci.* **1996,** *21,* 593–650. doi:10.1016/0079-6700(95)00027-5
2. Decker, C. *Mater. Sci. Technol.* **1997,** *18,* 615–657.
3. Yagci, Y.; Jockusch, S.; Turro, N. J. *Macromolecules* **2010,** *43,* 6245–6260. doi:10.1021/ma1007545
4. Andrzejewksa, E. *Prog. Polym. Sci.* **2001,** *26,* 605–665. doi:10.1016/S0079-6700(01)00004-1
5. Grassie, N.; Torrance, B. J. D.; Fortune, J. D.; Gemmell, J. D. *Polymer* **1965,** *6,* 653–658. doi:10.1016/0032-3861(65)90048-0
6. Roos, S. G.; Müller, A. H. E.; Matyjaszewski, K. *Macromolecules* **1999,** *32,* 8331–8335. doi:10.1021/ma9819337
7. Scorah, M. J.; Hua, H.; Dubé, M. A. *J. Appl. Polym. Sci.* **2001,** *82,* 1238–1255. doi:10.1002/app.1958
8. Hakim, M.; Verhoeven, V.; McManus, N. T.; Dubé, M. A.; Penlidis, A. *J. Appl. Polym. Sci.* **2000,** *77,* 602–609. doi:10.1002/(SICI)1097-4628(20000718)77:3<602::AID-APP15>3.0.CO;2-F
9. Ito, K.; Uchida, K.; Kitano, T.; Yamada, E.; Matsumoto, T. *Polym. J.* **1985,** *17,* 761–766. doi:10.1295/polymj.17.761
10. Fenrnández-García, M.; Torrado, M. F.; Martínez, G.; Sánchez-Chaves, M.; Madruga, E. L. *Polymer* **2000,** *41,* 8001–8008. doi:10.1016/S0032-3861(00)00167-1
11. Anseth, K. S.; Wang, C. M.; Bowman, C. N. *Polymer* **1994,** *35,* 3243–3250. doi:10.1016/0032-3861(94)90129-5
12. Park, C. J.; Kim, J. H. *J. Korean Fiber Soc.* **1999,** *36,* 680–686.
13. Yu, X.; Pfaendtner, J.; Broadbelt, L. J. *J. Phys. Chem. A* **2008,** *112,* 6772–6782. doi:10.1021/jp800643a
14. Lee, T. Y.; Guymon, C. A.; Jönsson, E. S.; Hoyle, C. E. *Polymer* **2004,** *45,* 6155–6162. doi:10.1016/j.polymer.2004.06.060
15. Salz, U.; Zimmermann, J.; Zeuner, F.; Moszner, N. *Polym. Prepr.* **2004,** *45,* 325–326.
16. Moszner, N.; Salz, U.; Zimmermann, J. *Dent. Mater.* **2005,** *21,* 895–910. doi:10.1016/j.dental.2005.05.001
17. Hartmann, L.; Watanabe, K.; Zheng, L. L.; Kim, C.-Y.; Beck, S. E.; Huie, P.; Noolandi, J.; Cochran, J. R.; Ta, C. N.; Frank, C. W. *J. Biomed. Mater. Res., Part B* **2011,** *98B,* 8–17. doi:10.1002/jbm.b.31806
18. Yang, T.-H. *Recent Pat. Mater. Sci.* **2008,** *1,* 29–40. doi:10.2174/1874464810801010029
19. Moszner, N.; Zeuner, F.; Angermann, J.; Fischer, U. K.; Rheinberger, V. *Macromol. Mater. Eng.* **2003,** *288,* 621–628. doi:10.1002/mame.200350003
20. Otsu, T.; Inoue, M.; Yamada, B.; Mori, T. *J. Polym. Sci., Polym. Lett. Ed.* **1975,** *13,* 505–510. doi:10.1002/pol.1975.130130811
21. De Sterck, B.; Vaneerdeweg, B.; Du Prez, F.; Waroquier, M.; Van Speybroeck, V. *Macromolecules* **2010,** *43,* 827–836. doi:10.1021/ma9018747
22. Berchtold, K. A.; Nie, J.; Stansbury, J. W.; Hacioglu, B.; Beckel, E. R.; Bowman, C. N. *Macromolecules* **2004,** *37,* 3165–3179. doi:10.1021/ma035862+
23. Kilambi, H.; Reddy, S. R.; Schneidewind, L.; Stansbury, J. W.; Bowman, C. N. *J. Polym. Sci., Part A: Polym. Chem.* **2009,** *47,* 4859–4870. doi:10.1002/pola.23503
24. Lampe, U.; Maier, M.; Klee, J. E.; Ritter, H. *Polym. Int.* **2016,** *65,* 1142–1149. doi:10.1002/pi.5179
25. Trossarelli, L.; Guaita, M.; Priola, A. *Macromol. Chem. Phys.* **1967,** *100,* 147–155. doi:10.1002/macp.1967.021000116
26. Kodaira, T.; Sumiya, Y. *Macromol. Chem. Phys.* **1986,** *187,* 933–942. doi:10.1002/macp.1986.021870422
27. Seno, M.; Ikezumi, T.; Sumie, T.; Masuda, Y.; Sato, T. *J. Polym. Sci., Part A: Polym. Chem.* **2000,** *38,* 2098–2105. doi:10.1002/(SICI)1099-0518(20000601)38:11<2098::AID-POLA190>3.0.CO;2-O
28. Fukuda, W.; Takahashi, H.; Takeneka, Y.; Kakiuchi, H. *Polym. J.* **1988,** *20,* 337–344. doi:10.1295/polymj.20.337
29. Heasley, V. L.; Heasley, G. E.; Taylor, S. K.; Frye, C. L. *J. Org. Chem.* **1970,** *35,* 2967–2970. doi:10.1021/jo00834a025

30. Havis, N. D.; Walters, D. R.; Martin, W. P.; Cook, F. M.; Robins, D. J. *Tests Agrochem. Cultiv.* **1994,** *15,* 14–15.
31. Feuer, H.; Brown, F. *J. Org. Chem.* **1970,** *35,* 1468–1471. doi:10.1021/jo00830a045
32. Abe, Z.; Tanaka, H.; Sumimoto, M. *J. Polym. Sci., Polym. Chem. Ed.* **1978,** *16,* 305–308. doi:10.1002/pol.1978.170160129
33. Roberts, D. E. *J. Res. Natl. Bur. Stand. (U. S.)* **1950,** *44,* 221–232. doi:10.6028/jres.044.021
34. Cinar, S. A.; De Proft, F.; Avci, D.; Aviyente, V.; De Vleeschouwer, F. *Macromol. Chem. Phys.* **2015,** *216,* 334–343. doi:10.1002/macp.201400484
35. Cheremisinoff, P., Ed. *Handbook of Engineering Polymeric Materials;* Marcel Dekker: New York, 1997.

BEILSTEIN JOURNAL OF ORGANIC CHEMISTRY

Interactions between shape-persistent macromolecules as probed by AFM

Johanna Blass[‡1,2], Jessica Brunke[‡3], Franziska Emmerich[1,2], Cédric Przybylski[4], Vasil M. Garamus[5], Artem Feoktystov[6], Roland Bennewitz[1,2], Gerhard Wenz[3] and Marcel Albrecht[*3]

Full Research Paper

Open Access

Address:
[1]INM-Leibniz-Institute for New Materials, Saarland University, Campus D 2.2, D-66123 Saarbrücken, Germany, [2]Physics Department, Saarland University, Campus D 2.2, D-66123 Saarbrücken, Germany, [3]Organic Macromolecular Chemistry, Saarland University, Campus C 4.2, D-66123 Saarbrücken, Germany, [4]UPMC, IPCM-CNRS UMR 8232, Sorbonne Universités, 75252 Paris Cedex 05, France, [5]Helmholtz-Zentrum Geesthacht (HZG), Centre for Materials and Costal Research, Max-Planck-Str. 1, 21502 Geesthacht, Germany and [6]Jülich Centre for Neutron Science (JCNS) at Heinz Maier-Leibnitz Zentrum (MLZ), Forschungszentrum Jülich GmbH, Lichtenbergstr. 1, 85748 Garching, Germany

Email:
Marcel Albrecht[*] - m.albrecht@mx.uni-saarland.de

* Corresponding author ‡ Equal contributors

Keywords:
AFM; cyclodextrin; inclusion complexes; molecular recognition; polyconjugated polymers; shape persistent polymers

Beilstein J. Org. Chem. **2017,** *13,* 938–951.
doi:10.3762/bjoc.13.95

Received: 23 October 2016
Accepted: 24 April 2017
Published: 18 May 2017

This article is part of the Thematic Series "Spatial effects in polymer chemistry". Dedicated to Gerhard Wegner and his work on shape-persistent polymers.

Guest Editor: H. Ritter

Abstract

Water-soluble shape-persistent cyclodextrin (CD) polymers with amino-functionalized end groups were prepared starting from diacetylene-modified cyclodextrin monomers by a combined Glaser coupling/click chemistry approach. Structural perfection of the neutral CD polymers and inclusion complex formation with ditopic and monotopic guest molecules were proven by MALDI–TOF and UV–vis measurements. Small-angle neutron and X-ray (SANS/SAXS) scattering experiments confirm the stiffness of the polymer chains with an apparent contour length of about 130 Å. Surface modification of planar silicon wafers as well as AFM tips was realized by covalent bound formation between the terminal amino groups of the CD polymer and a reactive isothiocyanate–silane monolayer. Atomic force measurements of CD polymer decorated surfaces show enhanced supramolecular interaction energies which can be attributed to multiple inclusion complexes based on the rigidity of the polymer backbone and the regular configuration of the CD moieties. Depending on the geometrical configuration of attachment anisotropic adhesion characteristics of the polymer system can be distinguished between a peeling and a shearing mechanism.

Introduction

Shape-persistence is an important key feature in self-organisation strategies of supramolecular building blocks resulting in high structural perfection of the obtained molecular assemblies [1], such as shape persistent macrocycles, cage compounds or rotaxanes [2-4]. Especially shape-persistent polymers are of significant scientific interest as their defined structural characteristics offer various applications as sensor materials, biomimetic filaments or organic electronics [5-7]. Furthermore, compared to polymers with flexible chains, shape persistent macromolecules with high structural rigidity are able to form stable aggregates based on multiple supramolecular interactions, which can be detected and quantified without the presence of side effects, such as self-passivation or coiling processes. Dendrimers, nanoparticles and shape-persistent polymers had been previously discussed as scaffolds for the design of multiple ligands of high affinity [8]. Nevertheless, well-defined model systems in which the influence of rigidity and regularity on cooperativity of binding was systematically investigated have not been reported so far.

Rigid linear polymers have been considered as suitable scaffolds for the design of supramolecular systems showing multiple interactions. A high rigidity of the macromolecule is maintained by rigid, linear repeat units, such as *trans*-ethenylene, ethynylene, or *p*-phenylene moieties. The observed persistence lengths of polyconjugated polymers ranged from 6 to 16 nm, depending on the side groups and the method of determination [9-11].

Among many supramolecular interactions, such as hydrogen bonding, π–π-interactions or hydrophobic host–guest interactions [12-16], the interactions of cyclodextrins (CDs) with hydrophobic guest molecules are of special interest, since CDs are readily available bio-based materials and interactions take place under physiological conditions [17]. CDs are ideal candidates for the investigation of multivalent interactions as they combine high affinities with a versatile integrability in macromolecular systems [18]. CDs have already been employed for the construction of supramolecular polymers [19-21], supramolecular hydrogels [22,23], molecular printboards [24,25] or multivalent interfaces [26-28] with tunable chemical and physical properties. Herein, for the first time, we present studies concerning the synthesis of shape-persistent CD polymers to investigate multivalent binding with ditopic guest molecules on the molecular level (Figure 1). The ditopic guest (shown in red colour) should act as a connector between opposing CD moieties.

Only a few examples of shape-persistent CD polymers have been reported so far, including CD-modified conjugated oligomers and polymers composed of rigid phenylene ethynylene (PPE) structure units which are able to form self-inclusion complexes with tunable electrochemical properties [29-35]. The synthesis of PPE, in which two β-CD rings were attached to every second phenylene group, was described by Ogoshi et al. [36] using a Sonogashira–Hagiwara coupling. We preferred a poly-phenylene-butadiynylene backbone, synthesized by a

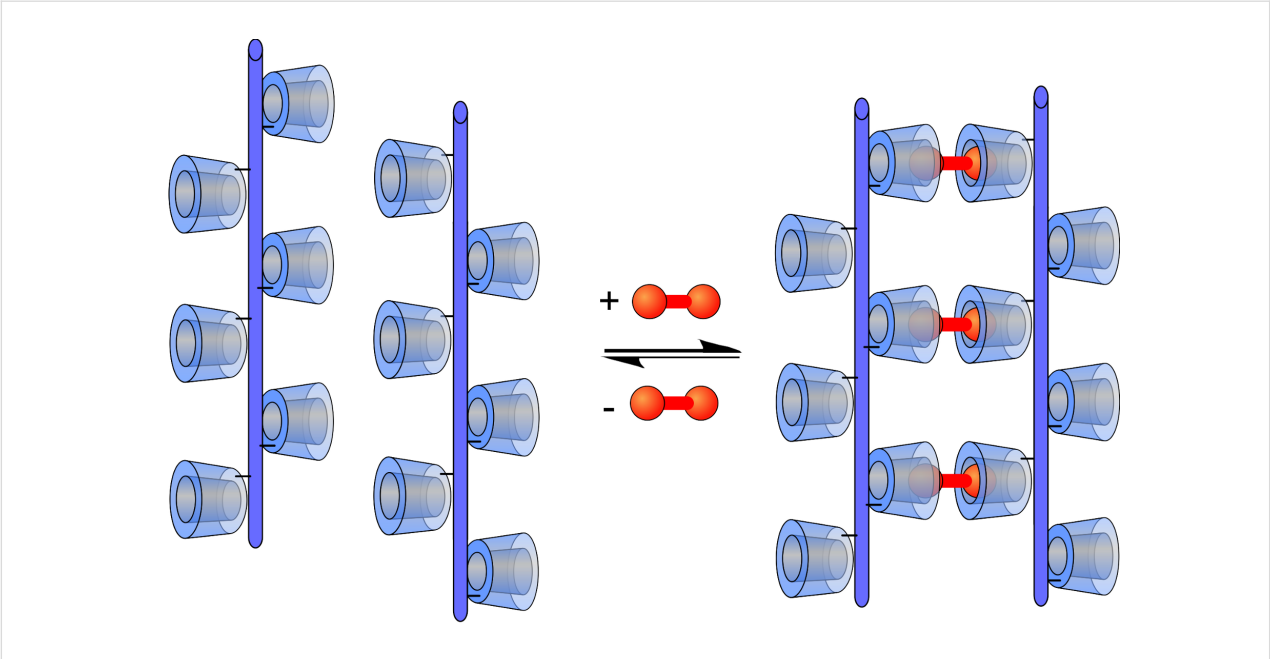

Figure 1: Interaction of a shape-persistent CD polymer with ditopic guests.

Glaser–Eglington coupling, since the repeating unit is long enough (l = 0.944 nm) to allow the connection of one CD moiety at each phenylene unit. Based on the stiffness of the polymer chain self-passivation of CD polymer modified surfaces is reduced to a minimum. Furthermore, the ethynyl end groups are easily functionalized by click chemistry.

Isothermal titration calorimetry (ITC), fluorescence spectroscopy, quartz crystal microbalance (QCM), surface plasmon resonance (SPR) and atomic force microscopy (AFM) have been employed to quantify the strength of the multivalent interactions [8]. Because binding affinities can be very high for multivalent supramolecular systems, the constituents are commonly used in low equilibrium concentrations. Since AFM even allows the investigation of single molecules, such as DNA [37,38] or molecular self-assembling based on "Dip-Pen" nanolithography [39], it was chosen as the most reliable technique to probe highly cooperative recognition processes.

The investigation of cooperativity of multiple host–guest interactions using AFM has been reported by several groups [40-45]. Huskens and co-workers measured the supramolecular interactions between a β-CD-modified planar surface and mono-, di- and trivalent adamantane guest molecules attached to an AFM tip and found enhancement factors up to 2, depending on the force loading rate [46]. We have previously explored the adhesion characteristics of dense CD layers on an AFM tip and a planar silicon surface connected by various ditopic linker molecules. In this system we were able to switch adhesion and friction by applying external stimuli onto the responsive ditopic linkers [47-49]. In contrast to previous work our molecular toolkit, based on ditopic connector molecules, allows the independent determination of unspecific interactions between CD polymers at tip and planar surface as well as the specific interactions to ditopic connector molecules. In the following, we describe the first example of multivalent interaction of ditopic guest molecules with shape-persistent CD polymers covalently attached to an AFM tip and a planar surface. Nano force measurements between CD and CD polymer, CD polymer and CD, and CD and CD at the tip and the planar surface, respectively, exerted by the adamantane ditopic connector molecules were systematically investigated. All four configurations are schematically depicted in Figure 2.

Results and Discussion

Synthesis of the shape-persistent CD polymer

Our synthetic approach for the preparation of modified poly(phenylene butadiynylene)s bearing one CD molecule per repeat unit started from 2,5-dibromo-4-methylbenzoic acid (**2**)

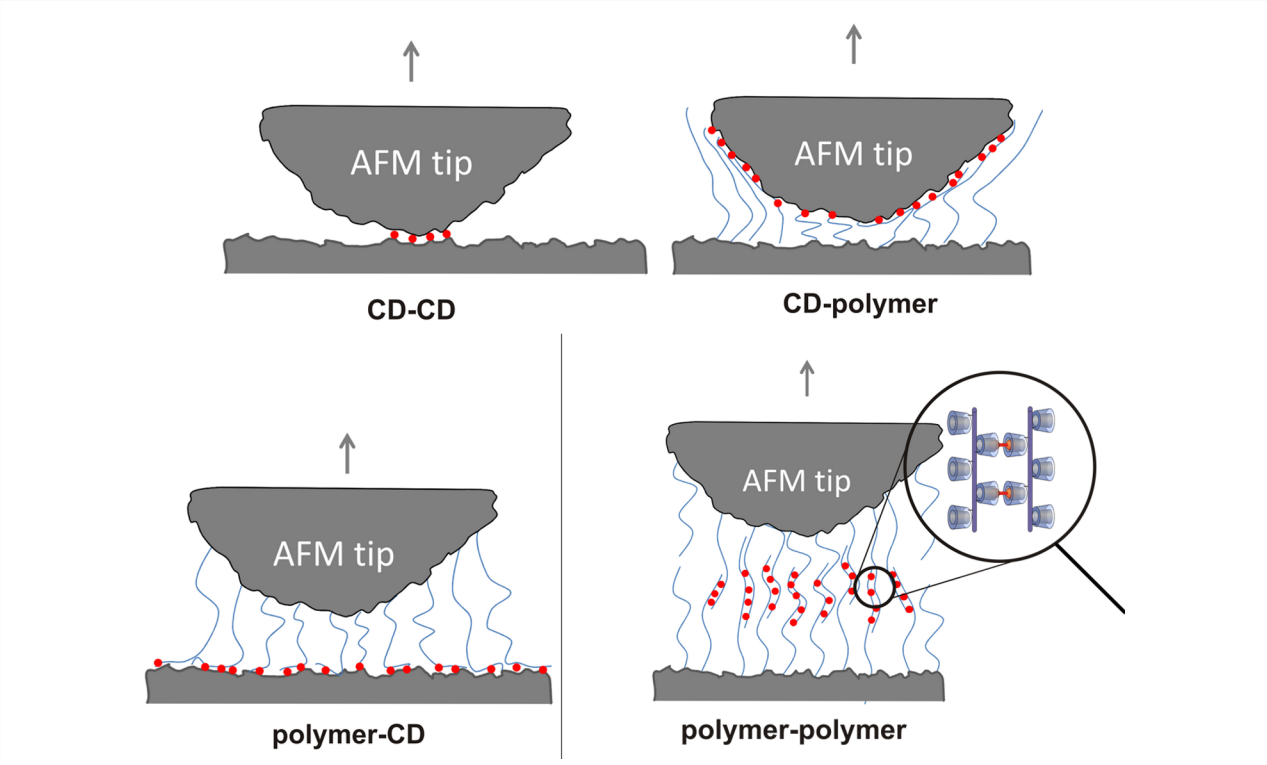

Figure 2: Schematic representation of tip and surface modifications realized in this study (bottom). Blue lines symbolize the CD polymers, red circles the complexed ditopic linkers.

[50,51], which was esterified to **3** with *tert*-butanol catalyzed by H_2SO_4 (Scheme 1). The TMS-protected diacetylene derivative **4** was prepared by Sonogashira reaction of **3** with trimethylsilylacetylene. Subsequent deprotection of the TMS groups using tetra-*n*-butylammonium fluoride and saponification of the *tert*-butyl ester with trifluoroacetic acid resulted in the corresponding benzoic acid **6**. The latter was coupled to 6-monoamino-6-deoxy-β-CD [52] using *N,N'*-dicyclohexylcarbodiimide (DCC) and 1-hydroxybenzotriazole (HOBt) applying a procedure known for terephthalic acid [53]. The resulting product, monomer **7**, was easily isolated due to its low solubility in water which was attributed to self-inclusion between hydrophobic phenyl moieties and β-CD rings leading to daisy chains [54].

The polymerization of **7** was performed through Glaser coupling in pyridine catalyzed by Cu(I)/Cu(II). After removal of low molecular weight material by ultrafiltration polymer **8** was isolated as a light orange solid in 91% yield. Polyrotaxane formation, which might prevent the accessibility of the CD-moieties located on the polymer backbone, was avoided by the presence of pyridine as a non-polar solvent. Both NOESY NMR experiments and circular dichroism (results not shown) do not indicate any significant interaction of the CDs and the aromatic backbone. Compared to monomer **7**, peak broadening and the disappearance of the ^{1}H NMR signals of the acetylene protons at 4.54 and 4.36 ppm indicate the formation of polymer **8**. The presence of the conjugated backbone was confirmed by UV–vis and fluorescence measurements in water. Compared to **7**, a characteristic bathochromic shift could be observed both in the absorption and emission spectra of polymer **8** (Figure 3) showing the presence of the extended polyconjugated π-system.

Quantitative information about the molecular weight distribution of **8** was obtained by MALDI–TOF measurements using an ionic liquid matrix (HABA/TMG_2) [55]. A representative MALDI spectrum, shown in Figure 4, exhibits a wide range of broad signals starting from the signal of the dimer at

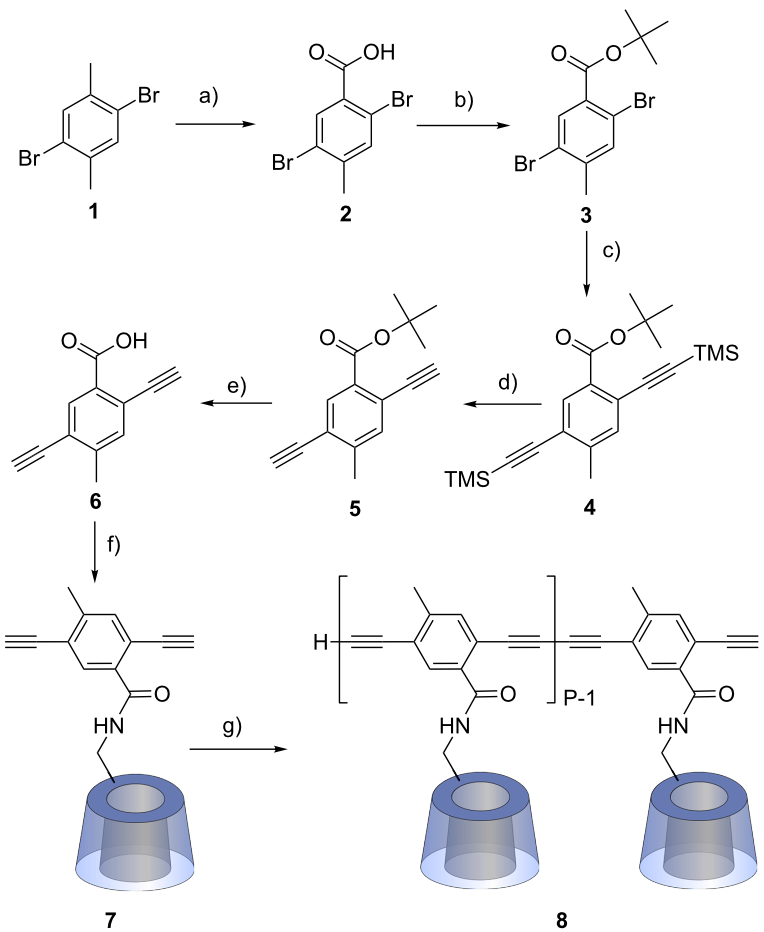

Scheme 1: Synthesis of the CD polymer. a) conc. HNO_3, reflux, 6 d; b) *tert*-butanol, cat. H_2SO_4, $MgSO_4$, CH_2Cl_2, rt, sealed vessel, 4 d; c) TMSA, $PdCl_2$ (10 mol %), CuI (5 mol %), PPh_3 (0.5 equiv), Et_3N, 80 °C, 48 h; d) TBAF, THF, −20 °C, 30 min; e) TFA, CH_2Cl_2, rt, 18 h; f) 6-monoamino-6-deoxy-ß-CD, DCC, HOBt, DMF, rt, 8 d; g) cat. CuCl, cat. $Cu(OAc)_2$, pyridine, 60 °C, 24 h.

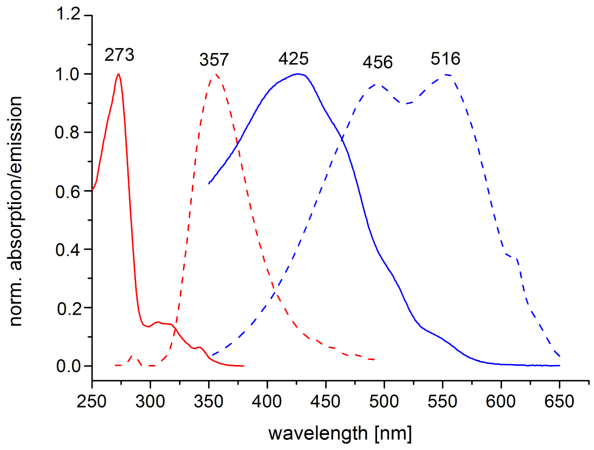

Figure 3: Absorption spectra of monomer **7** (solid red line) and polymer **8** (solid blue line) in water. Emission spectra of monomer **7** (dotted red line) and polymer **8** (dotted blue line) in water excited at 290 nm and 335 nm, respectively.

m/*z* 2,621.33 Da detected as $[M + Na]^+$ and ending at the 38mer at *m*/*z* 48,196.23 Da for a S/N ratio ≥3, with an average 1297.4 mass units shift corresponding to one additional repeating unit. Among each discrete envelope, one to three supplementary ions, have been detected with a constant 165.2 mass unit shift, revealing the presence of small quantities of the repeat unit originating from unmodified benzoic acid derivative **6**, e.g., at 2,621.33 and 2,786.52 Da (Figure 4). The MS analysis reveals the high structural perfection of the polymer **8** where at most one CD entity per polymer molecule is missing. Integration of the relative distribution of the most intense ions of each population allowed to estimate both the number average molecular weight, M_n, and the mass average molecular weight, M_w, of 8,765.77 Da, and 22,023.56 Da, respectively. These values result in a polydispersity index PDI = M_w/M_n of 2.59 typical for normal distributions. From the value of M_w an average contour length L = 17 nm of the macromolecule was calculated. A more detailed analysis of the MS data is provided in Supporting Information File 1.

SANS and SAXS measurements of the CD polymer

Structural characteristics of the CD polymer **8** have been investigated by small-angle neutron and X-ray scattering experiments (SANS/SAXS). SANS data (KWS-1, JCNS at Heinz Maier-Leibnitz Zentrum [56]) for a polymer concentration range from 0.005 to 0.03 g/cm^3 are presented in Figure 5. SANS intensities are normalized to polymer concentration and therefore scattering intensities depend on polymer chain mass (or mass of chain aggregates), square of scattering contrast, conformation of polymer chain, and interaction between the

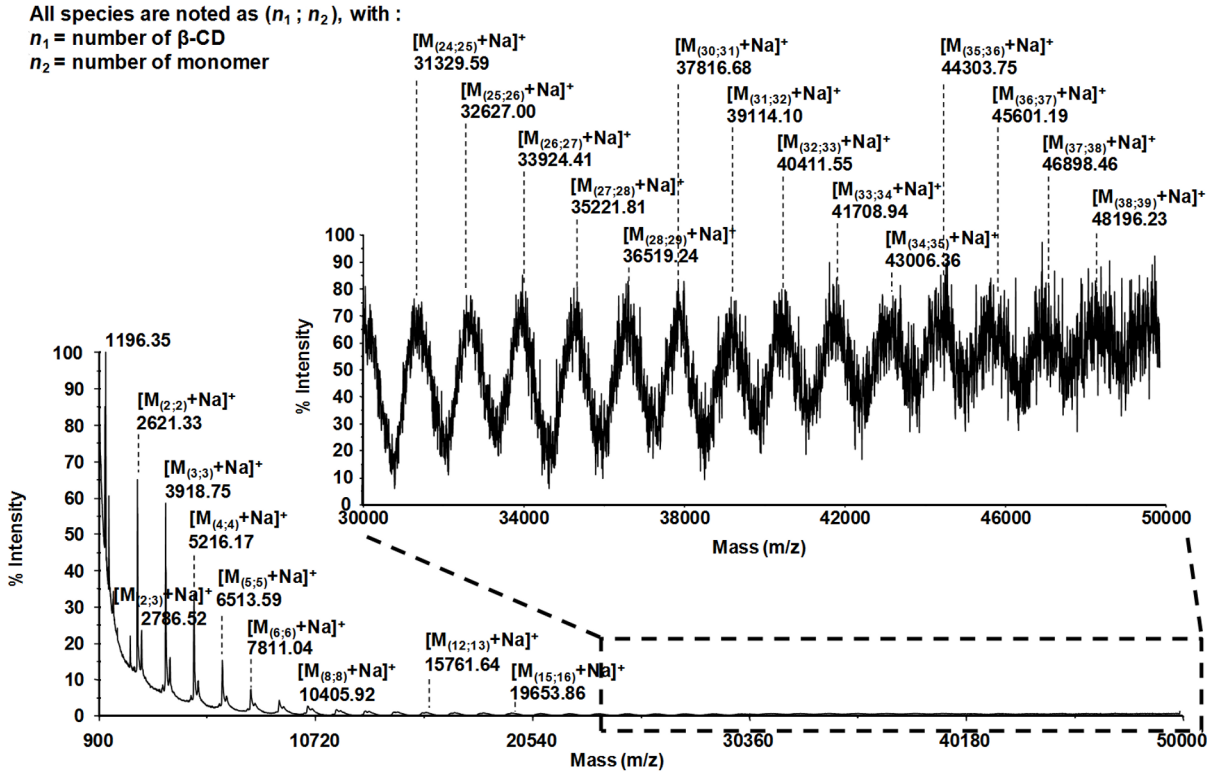

Figure 4: Positive linear MALDI–TOF spectrum of polymer **8** using HABA/TMG$_2$ matrix.

chains (aggregates). There are only minor differences in scattering for concentrations up to 0.02 g/cm^3 indicating no significant aggregation between polymer chains with increasing concentration which would lead to highly ordered polymer species. The decrease of scattering intensity for the highest concentration of 0.03 g/cm^3 can be attributed to interaction of polymer chains. The SAXS curve measured at 0.03 g/mL shows a similar shape as the neutron data (Supporting Information File 1, Figure S1).

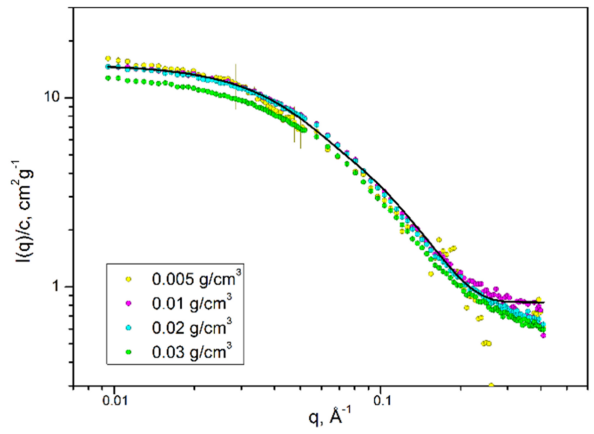

Figure 5: SANS data for polymer **8** and fit by cylindrical model (solid line).

The low-q range of scattering data has been analyzed with a Debye function. The apparent radius of gyration $R_{g,app}$ and the scattering at "zero angle", $I(0)$, were obtained by fitting the scattering data for $q < 0.02$ Å^{-1} [57]:

$$f_{\text{Debye}}(x) = 2\left(e^{-x} - 1 + x\right)/x^2, \quad (1)$$

where $x = q^2 R_{g,app}{}^2$. The scattering intensity is given by

$$I(q)/c = I(0) f_{\text{Debye}}(x) = M_{app} Dr^2{}_m f_{\text{Debye}}(x), \quad (2)$$

where the apparent molar weight, M_{app}, is connected with the real molar weight, M, via a structure factor $S(0)$ (interaction among polymer chains) as $M \times S(0) = M_{app}$ and $\Delta\rho_m$ is the difference in neutron scattering length density between polymer and solvent normalized to the density of polymer. The local structure of the polymer cylindrical cross-section was extracted by applying indirect Fourier transformation (IFT) [58] to the experimental data from the high-q range. Detailed information applying this method is presented in Supporting Information File 1. The resulting parameters for the concentration dependence of $I(0)$, scattering at "zero angle" of a cylindrical cross-section of polymer $I_{CS}(0)$, radius of gyration $R_{g,app}$, and radius of gyration of a cylindrical cross-section $R_{g,CS}$ are presented in Table 1. The ratio between $I(0)$ and $I_{CS}(0)$ provides the apparent contour length of the polymer chain. SAXS and SANS indicate a contour length of 130–160 Å, i.e., 15 monomer units with the length of one unit of L_{mon} = 9.2 Å and the chemical composition $C_{54}H_{75}NO_{35}$ (molecular weight 1298.17 g/mol). $R_{g,CS}$ has been used to calculate the cross-section diameter of the homogeneous cylinder to be 30 Å.

Scattering intensities do not change significantly with concentration indicating that the value of $S(0)$ is close to 1. We consider the values for L_{app} and M_{app} as lower limits. They are probably affected by the inexact determination of the scattering contrast.

The apparent mass and contour length of polymer **8** with values of about 18 kDa and 130–160 Å are in the same range as those obtained by MALDI measurements (M_w = 22 kDa, L = 170 Å) and confirm the structural characteristics of the stiff CD polymer.

The flexibility of chains of polymer **8** was determined by means of a Holtzer plot [59]. Detailed information and the corresponding data are presented in Supporting Information File 1. The absence of a characteristic inflection point, where the scattering intensity changes from q^{-1} as for rigid cylinder to q^{-2} (or to $q^{-5/3}$ when self-avoidance is important) as for flexible chains,

Table 1: Structural parameters of polymer **8** (apparent radius of gyration, scattering at zero angle, radius of gyration of polymer cross-section, scattering at zero angle of polymer cross-section, apparent contour length obtained from the ratio between $I(0)$ and $I_{CS}(0)$, and calculated apparent mass of polymer **8**, obtained from the length of monomer unit $M_{app} = M_{mon} \times L_{app}/L_{mon}$).

Conc, g/mL	$R_{g,app}$, Å	$I(0)$, cm^2·g^{-1}	$R_{g,CS}$, Å	$I_{CS}(0)$, Å^{-1}·cm^2·g^{-1}	L_{app}, Å	M_{app}, kDa
0.03 (SAXS)	38.0 ± 1.5	680 ± 10 a.u.	10.2 ± 0.5	5.23 ± 0.05 a.u.	130	18
0.005	37.4 ± 3.5	16.2 ± 0.3	9.8 ± 0.5	0.099 ± 0.002	164	23
0.01	31.6 ± 2.5	15.0 ± 0.2	9.7 ± 0.5	0.119 ± 0.002	126	18
0.02	32.7 ± 1.6	14.9 ± 0.2	9.5 ± 0.5	0.117 ± 0.002	127	18
0.03	34.6 ± 1.5	13.0 ± 0.1	9.4 ± 0.5	0.100 ± 0.002	130	18

indicates that polymer chains are short and rigid, i.e., that the persistence length is of the same order as the contour length of the polymer.

The SAXS data has been analyzed by models representing the expected shape of polymers. It was assumed that there is no interaction between aggregates, which means that the scattering intensities depend only on the size and shape of the aggregates [60]. Details are shown in Supporting Information File 1.

The scattering data could be described (Figure 5 above and Figure S1 in Supporting Information File 1) by a population of rigid cylinders of length 110 ± 5 Å and radius of cross-section of 12 ± 2 Å. Neglecting the interaction between polymer chains in the model leads to the slightly lower length values.

Complexation of monotopic and ditopic guests

In contrast to monomer **7**, polymer **8** was soluble in water up to a concentration of 0.15 mM (based on the repeating unit). This allows the investigation of the complexation of ditopic and monotopic guests, **9** and **10**, respectively. The solubility of the host polymer **8** as a function of the concentration of both guests **9** and **10** (Scheme 2) was determined by UV−vis spectroscopy using the extinction coefficient ε of **8** (14,800 M^{-1} cm^{-1}) at 425 nm. A more detailed description of the solubility measurements is presented in Supporting Information File 1.

Addition of hydrophilic guest **10** caused an increase in solubility of host polymer **8** in water (Figure 6). The surprisingly steep initial slope of the phase solubility diagram, m = 1.4 (repeating unit/guest) could be well represented by a model where every second CD moiety has to be complexed by the hydrophilic guest to significantly improve the solubility in water. Binding constants of about 40,000 M^{-1}, which were in the same range as literature values for the incorporation of adamantane derivatives into β-CD, [61] were obtained using ITC measurements considering a two-step sequential complexation with guest **10**. Further information is provided in Supporting Information File 1. Incomplete complexation with cationic guest molecules is indicated by a significant lower binding constant of 670 M^{-1} for the second binding complexation step, which is strongly inhibited as a result of the electronic repulsion of charged guest molecules in close proximity to each other. In contrast, a pronounced reduction of the solubility of CD polymer **8** was observed in the presence of ditopic guest **9**, which was attributed to the interconnection of polymer chains through the complexation of the ditopic guest. The very low concentration of connector **9** necessary for the almost complete precipitation of the host polymer **8** can be explained by the high integrability of the host–guest system based on the shape-persistence of the polyconjugated polymer backbone of **8**.

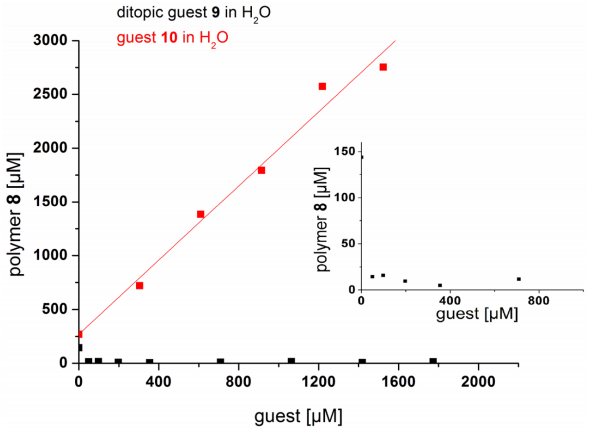

Figure 6: Solubility of polymer **8** in the presence of ditopic connector **9** (black graph) and 1-aminoadamantane hydrochloride **10** (red graph), respectively in water at 25 °C.

Attachment of polymer 8 to silicon surfaces

Planar silicon wafers, as well as the silicon AFM tip, were first functionalized by a polysiloxane monolayer bearing isothio-

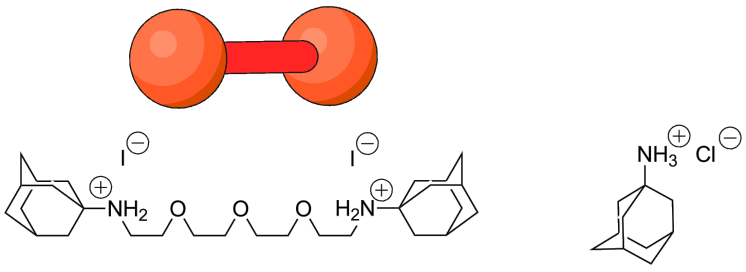

9 **10**

Scheme 2: Ditopic and monotopic guest molecules.

cyanate groups, which smoothly react with amines forming stable thiourea links [48]. Monolayers of β-CD or β-CD-polymer were obtained by attachment of monoamino β-CD or amino-modified CD polymer **12**, synthesized from polymer **8** (Scheme 3) through Cu(I)-catalyzed azide–alkyne cycloaddition (CuAAC) with the triethylene glycol linker **11** (N_3-TEG-NH_2) which had been prepared in a five-step procedure [62,63].

Probing multivalent interactions by AFM

The adhesive forces of **12**, due to supramolecular interactions with ditopic guest **9**, between a planar silicon surface and an AFM tip both modified with the CD polymer **12** or 6-monoamino-6-deoxy-β-CD were systematically investigated by AFM. While adhesion was very weak in pure water, significant adhesion took place over a wide range of distances in a 10 μM solution of ditopic guest **9** (Figure 7a–d). For comparison, we also investigated the adhesion forces between CD and **12**, **12** and CD, and CD and CD at the tip and the planar surface, respectively, caused by the adamantane connector **9**. Adhesive forces were recorded as function of the tip–surface distance upon retracting of the tip from the surface for all four configurations. The pull-off force required to detach the tip from the surface in the presence of connector molecules was of the order of 500 pN for the CD–CD configuration and about 1 nN for all configurations involving CD polymers (**12**). These values are significantly higher than the pull-off forces of about 250 pN measured in control experiments for all configurations. The graphical summary in Figure 7a suggests that the pull-off forces for the **12**–**12** configuration are slightly higher than for the **12**–CD and for the CD–**12** configuration.

While the pull-off force is similar, the overall appearance of the force curves differs for the three polymer configurations. The interaction distance varies significantly for the different configurations. The CD–CD configuration has the shortest and the polymer–polymer configuration the longest range of interactions. The interaction range can be quantified by the tip–surface distance at which the last rupture occurs, referred to as maximum rupture length. The histograms of the maximum rupture length for all four configurations are presented in Figure 7. For the CD–CD configuration, the most probable maximum rupture length of 5 nm corresponds to the combined height of the monolayers on tip and surface, each of about 2.5 nm. The typical rupture length for the CD–**12** configuration is 10 nm, while it is 29 nm for the **12**–CD configuration. The difference in maximum rupture length indicates a difference in the detachment mechanism. In the CD–**12** configuration, the polymers bind to the sloped facets of the asperity of the AFM tip. Upon pulling, the polymers are sheared from the tip apex by rupturing all bonds simultaneously leading to one large rupture peak at a small tip–surface distance. For the **12**–CD configuration, a force plateau observed in the force-distance curve in Figure 7c reveals the peeling of a polymer chain from the CD-coated surface resulting in a rupture length similar to the length of the polymer chains.

For the **12**–**12** configuration, many additional small detachment events lead to a broadening of the pull-off curve and reveal the rupture of bonds for tip–surface distances as large as 110 nm in Figure 7d. The broad distribution of rupture length, which extends to roughly the double of that of the **12**–CD configura-

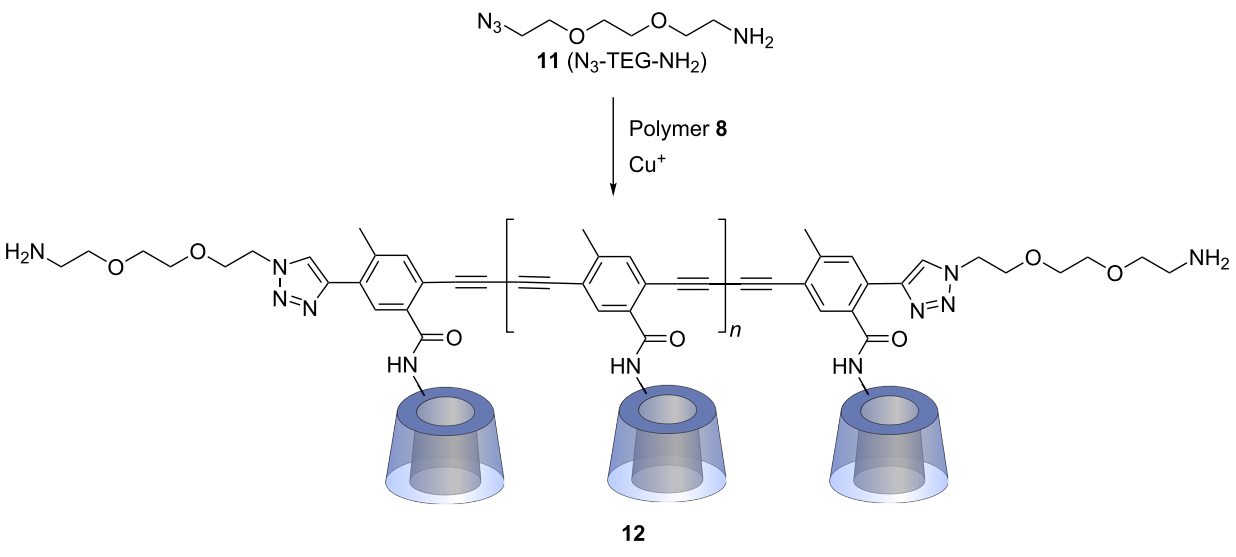

Scheme 3: Synthesis of amino functionalized polymer **12**.

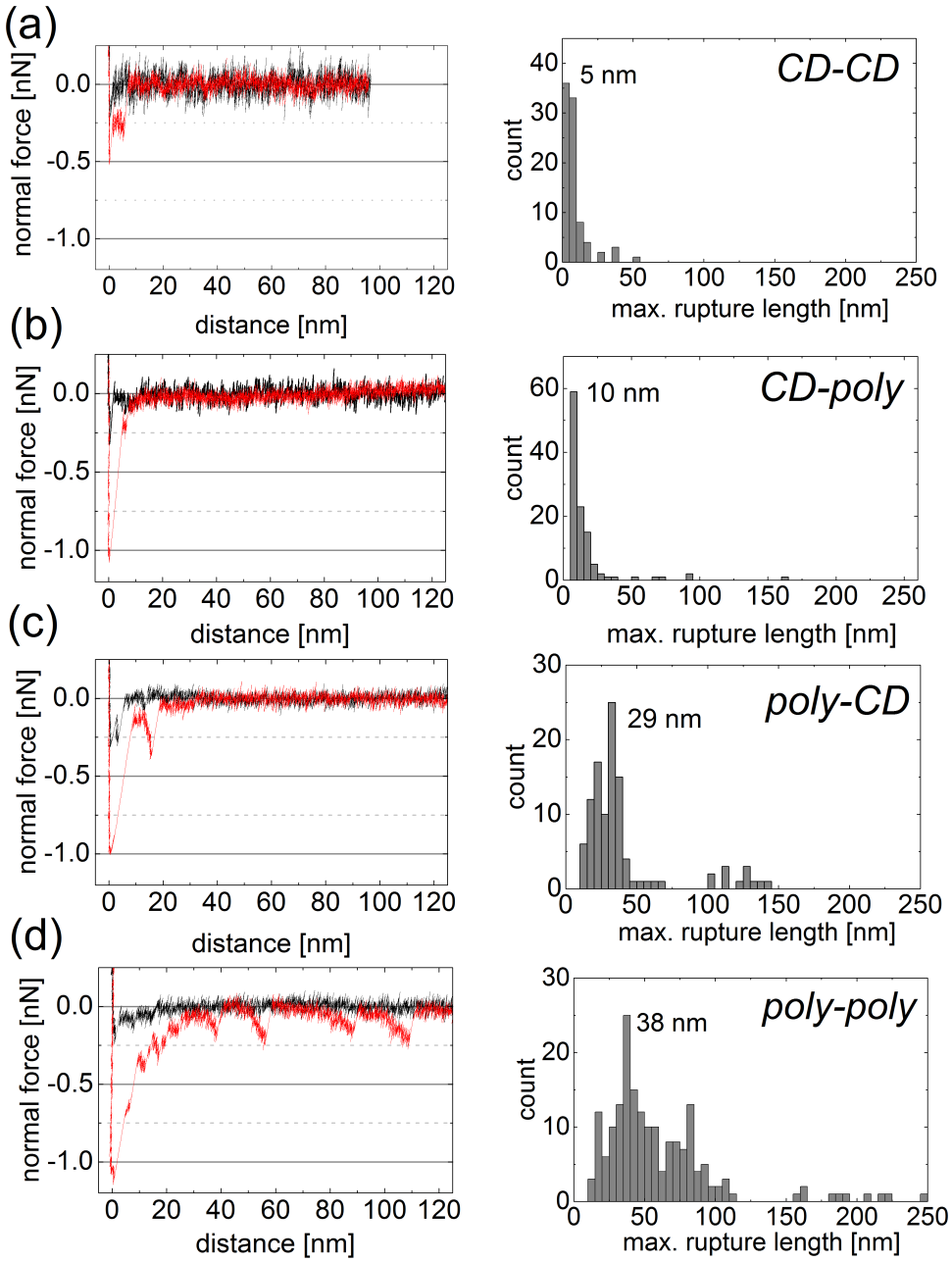

Figure 7: Characteristic force curves recorded during retraction of the AFM tip from the surface. Four functionalizations are compared: (a) cyclodextrin (CD) layers on tip and surface, (b) CD layer on the tip and polymers (**12**) on the surface, (c) polymers (**12**) on the tip and CD layer on the surface, and (d) polymers (**12**) on tip and surface. Black curves represent control experiments in pure water, red curves experiments in solution containing ditopic connector **9**. The maximum negative force is referred to as the pull-off force. The histograms summarize the distribution of maximum rupture length for every configuration.

tion, indicates that individual long polymer chains interlock, explaining also the characteristic stretching events in the force-distance curve. The most probable maximum rupture length for the **12**–**12** system is 38 nm, which is double of the average polymer length of 17 nm predicted from the MALDI–TOF and SANS/SAXS results. The agreement confirms the picture that the maximum rupture length reflects the final detachment of supramolecular bonds at the end of stretched polymer chains attached to AFM tip and surface.

The higher sensitivity of our AFM set up compared to the MALDI–TOF instrument allowed us to even detect single rup-

ture events at a distance up to 250 nm, which proved that some individual chains had a length of at least 125 nm. Compared to MALDI–TOF measurements in which the small number of high molecular weight polymer chains are hardly detectable, AFM experiments overemphasize the few longest polymer chains probing the interactions of the regularly spaced CDs in CD polymer **12** and ditopic connector molecules. Due to this observation AFM is an excellent detection tool for analysing cooperative effects in ordered supramolecular systems.

The differences between the four configurations of functionalization can be further quantified by integration of the force curves, resulting in the work of separation which has been employed before as a suitable parameter for the quantification of polymer detachment [45]. In line with the characteristic shape of the example force curves, the work of separation increased significantly in the order CD–CD, CD–**12**, **12**–CD and **12**–**12** configuration (Figure 8). The relative increase in the work of adhesion from control experiments to measurements of the specific interactions caused by the connector molecule **9** was even higher than the respective increase in pull-off force due to the very short range of the non-specific adhesive interactions.

The significant difference in the interaction range and thus in the work of separation between CD–**12** and **12**–CD configuration can be explained by the asymmetry between curved tip and flat surface and the resulting difference in the detachment mechanism. Polymers attached to the surface bind to the side faces of the tip with its nanometer-scale apex radius. Upon retraction, the force acts along the polymer and shears the polymer off the tip, with all bonds rupturing more or less simultaneously. In contrast, polymers attached to the tip bind to the flat surface such that upon retraction the polymer is peeled from the surface by the orthogonal force, one bond breaking after another. The different detachment scenarios are depicted in the schematic drawings in Figure 2. The shearing configuration (CD–**12**) leads to simultaneous rupture of all bonds, while the peeling configuration (**12**–CD) involves bending of the polymer and consecutive rupture. The strongest adhesion is offered by the supramolecular interlocking of polymers attached to tip and surface. Supramolecular interconnection between two CD polymer **12** molecules through the ditopic guest **9** is expected to be superior to the one between CD polymer **12** and CD because of the higher regularity of the CD spacing at the polymer compared to the spacing within the CD monolayer. We conclude that the regularity of the CD polymer **12** allows to establish a much higher number of supramolecular bonds with the connector **9** giving rise to about a fivefold enhancement of the work of separation.

Many force curves exhibit a well-defined last rupture event. A representative example is shown in Figure 9a, where the force drops from around 63 pN to zero at a distance of 110 nm. The distribution of rupture forces for the last rupture events, shown in Figure 9b, has a clear maximum at 63 pN, determined by a Gaussian fit to the distribution, and a weak second maximum at about double this value.

We conclude that 63 ± 10 pN is the rupture force for a single bond between our supramolecular polymers **12** established by the ditopic guest **9**. The value agrees with rupture force measured for adamantane–CD complexes with CD molecules in the surface layers when the stiffness of the AFM cantilever is taken into account [64].

Force curves like those shown in Figure 7 can be repeated on the same spot of one sample many times with very similar results. The repeatability confirms the reversibility of the underlying interactions. It is difficult to estimate the number of supramolecular bonds contributing to pull-off forces of 1 nN in

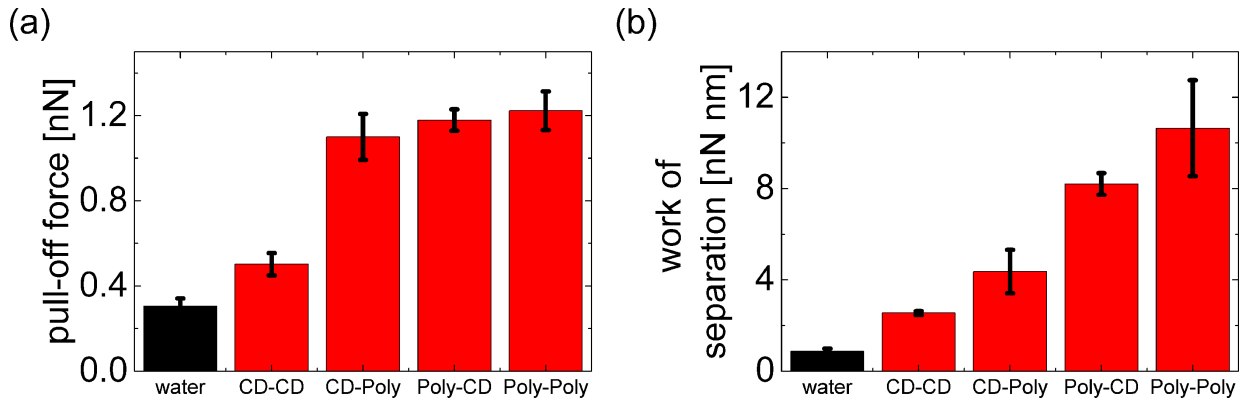

Figure 8: Graphical summary of experimental results for the four configurations of CD attachment introduced in Figure 2: (a) pull-off forces, (b) work of separation. The error bars indicate standard deviations for averages over different lateral positions on the functionalized surface.

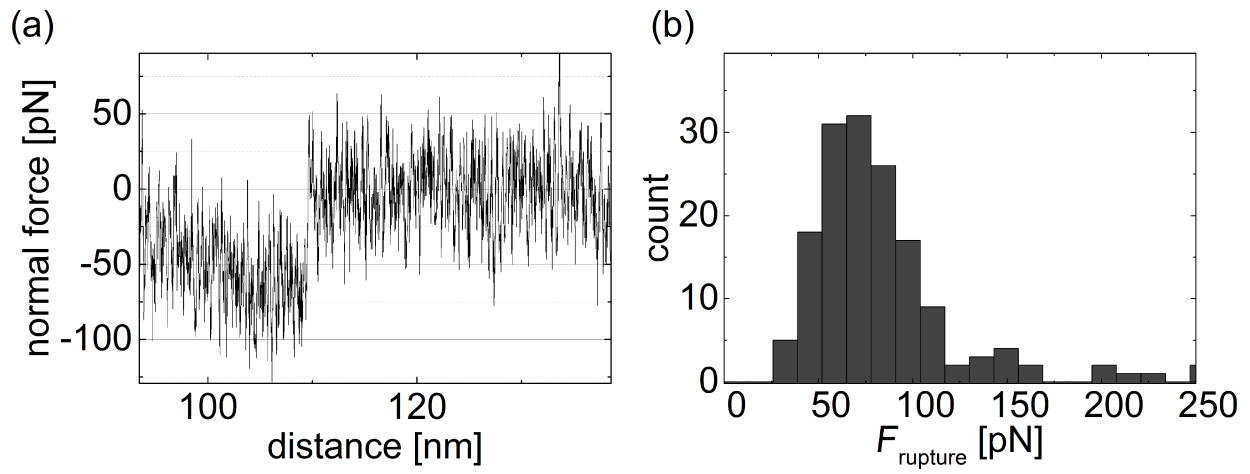

Figure 9: (a) Detail of the end of a force curve for a polymer-functionalized tip retracted from a polymer-functionalized surface. This is the last unbinding event which occurs at a tip–surface distance of about 110 nm, indicating the possible range of interaction for polymer functionalization of tip and surface. (b) Distribution of force drops for the last unbinding event with a maximum at 63 pN and a possible second maximum at about double this value.

Figure 7. Based on the single bond rupture force one could assume contributions by 16 supramolecular bonds or even more since it is unlikely that all bonds are loaded to their rupture force. As long as we have no experimental means to exactly determine the number of polymers molecules involved we cannot evaluate the number of interconnections per polymer. Since a significant number of single rupture events at large tip–surface distances require forces of around 200–250 pN (Figure 7d) up to four bonds per polymer pair appear reasonable.

Probing multivalent interactions by friction AFM

Finally, friction force experiments have been performed for the **12**–CD configuration. The tip of the AFM slides in contact across the surface, where polymers attached to the tip may interact with the CD layer on the surface. A characteristic result is presented in Figure 10. The average friction force increases by a factor of 2.5 due to the supramolecular interactions in comparison with control experiments in water. The friction force curve exhibit peculiar spikes when adamantane connector molecules are present. These spikes represent an irregular stick-slip motion of the tip. When one or several polymers are bound to the surface, the tip is stuck and the increasing force leads to torsion of the cantilever until the force is large enough to detach the polymers and drag them further across the surface. The highest friction force spikes of the **12**–CD configuration exhibit a force drop of 2 nN, similar to the highest pull-off forces for the same system. Shearing of a series of bonds, as described for adhesion in the CD–**12** configuration, is also the mechanism underlying friction in the **12**–CD configuration. Stick spike forces of 2 nN are enhanced by at least a factor of 3 compared to the one for the CD–CD system previously described [48]. This spike force may be enhanced by the multivalency effects discussed above, but its strength indicates that more than one polymer molecule might be involved.

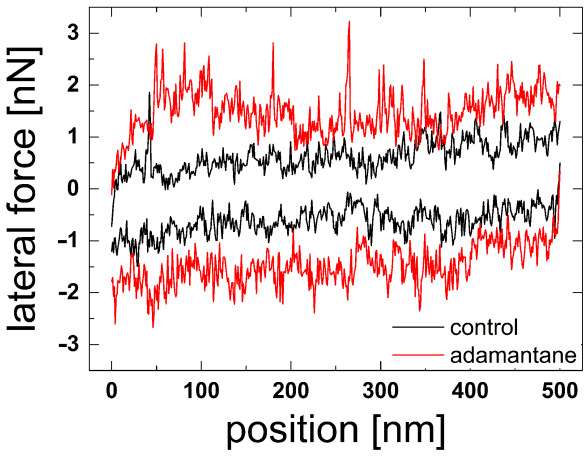

Figure 10: Characteristic result of a friction experiment for a polymer-functionalized tip sliding on a surface carrying a CD layer. Lateral forces are plotted as a function of lateral tip position when sliding 500 nm back and forth with a velocity of 45 nm/s.

Conclusion

In conclusion, regular water-soluble shape-persistent CD polymers based on poly(phenylene butadiynylene) were prepared by a straightforward Glaser coupling/click chemistry approach, which can be attached to planar silicon surfaces as well as AFM tips. Structural perfection of the resulted polymers was con-

firmed by MALDI–TOF measurements revealing the presence of high molecular weight materials with up to 38 repeat units. High integrability of the scaffold was proven by UV–vis supported solubility measurements upon addition of ditopic adamantane connectors. Small-angle neutron scattering and X-ray experiments reveal the presence of stiff cylindrical polymer chains with contour lengths of about 13–16 nm, which corresponds to the values obtained by MALDI and AFM measurements. Hard substrates with the shape-persistent polymers and interconnected by ditopic guest molecules require about five times higher separation energies than those functionalized with conventional CD monolayers. This significant enhancement of adhesion can be attributed to a strong cooperative effect favored by the rigidity of the polymer backbone and the regular spacing of the CD moieties. The range of adhesive interactions could be extended from 5 to 38 nm, which will also allow the interconnection of surfaces with higher roughness. The stiff polymers exhibit a clear contrast between shearing and peeling mechanisms, depending on the geometrical configuration of attachment. The distribution of the maximum rupture lengths in the force microscopy experiments confirms the molecular weight distribution of the CD polymers estimated by MALDI–TOF and the average contour length determined by SANS/SAXS. In addition, force microscopy experiments emphasize the longest polymer chains and their maximum length.

Supporting Information

Supporting Information File 1

Experimental procedures, MALDI–TOF spectra, details on SANS/SAXS instrumentation and analysis, surface preparation protocols and other instrumentation parameters.
[http://www.beilstein-journals.org/bjoc/content/supplementary/1860-5397-13-95-S1.pdf]

Acknowledgements

The authors thank Annegret Engelke and Blandine Bossmann for performing UV and fluorescence measurements. Devid Hero is gratefully acknowledged for the synthetic support preparing the modified CD starting materials. Neutron scattering experiments performed at the KWS-1 instrument operated by the Jülich Centre for Neutron Science (JCNS) at the Heinz Maier-Leibnitz Zentrum (MLZ), Garching, Germany. The support of Clement Blanchet (EMBL) is kindly acknowledged. This work benefited from the use of the SasView application, originally developed under NSF award DMR-0520547.

This work was supported by the Volkswagen Foundation through the program Integration of Molecular Components in Functional Macroscopic Systems.

References

1. Wegner, G. *Macromol. Symp.* **2003,** *201,* 1–9. doi:10.1002/masy.200351101
2. Höger, S. *Chem. – Eur. J.* **2004,** *10,* 1320–1329. doi:10.1002/chem.200305496
3. Schweez, C.; Shushkov, P.; Grimme, S.; Höger, S. *Angew. Chem., Int. Ed.* **2016,** *55,* 3328–3333. doi:10.1002/anie.201509702 *Angew. Chem.* **2016,** *128,* 3389–3394. doi:10.1002/ange.201509702
4. Zhang, G.; Mastalerz, M. *Chem. Soc. Rev.* **2014,** *43,* 1934–1947. doi:10.1039/C3CS60358J
5. Yang, J.-S.; Swager, T. M. *J. Am. Chem. Soc.* **1998,** *120,* 5321–5322. doi:10.1021/ja9742996
6. Aida, T.; Mejer, E. W.; Stupp, S. I. *Science* **2012,** *335,* 813–817. doi:10.1126/science.1205962
7. Facchetti, A. *Chem. Mater.* **2011,** *23,* 733–758. doi:10.1021/cm102419z
8. Fasting, C.; Schalley, C. A.; Weber, M.; Seitz, O.; Hecht, S.; Koksch, B.; Dernedde, J.; Graf, C.; Knapp, E.-W.; Haag, R. *Angew. Chem.* **2012,** *124,* 10622–10650. doi:10.1002/ange.201201114 *Angew. Chem. Int. Ed.* **2012,** *51,* 10472–10498. doi:10.1002/anie.201201114
9. Choudhury, P. K.; Bagchi, D.; Menon, R. *J. Phys.: Condens. Matter* **2009,** *21,* 195801. doi:10.1088/0953-8984/21/19/195801
10. Jeschke, G.; Sajid, M.; Schulte, M.; Ramezanian, N.; Volkov, A.; Zimmermann, H.; Godt, A. *J. Am. Chem. Soc.* **2010,** *132,* 10107–10117. doi:10.1021/ja102983b
11. Harre, K.; Wegner, G. *Polymer* **2006,** *47,* 7312–7317. doi:10.1016/j.polymer.2006.05.067
12. Ahn, Y.; Jang, Y.; Selvapalam, N.; Yun, G.; Kim, K. *Angew. Chem., Int. Ed.* **2013,** *52,* 3140–3144. doi:10.1002/anie.201209382
13. Anderson, C. A.; Jones, A. R.; Briggs, E. M.; Novitsky, E. J.; Kuykendall, D. W.; Sottos, N. R.; Zimmerman, S. C. *J. Am. Chem. Soc.* **2013,** *135,* 7288–7295. doi:10.1021/ja4005283
14. Reczek, J. J.; Kennedy, A. A.; Halbert, B. T.; Urbach, A. R. *J. Am. Chem. Soc.* **2009,** *131,* 2408–2415. doi:10.1021/ja808936y
15. Harada, A.; Takashima, Y.; Nakahata, M. *Acc. Chem. Res.* **2014,** *47,* 2128–2140. doi:10.1021/ar500109h
16. Mei, J.; Leung, N. L. C.; Kwok, R. T. K.; Lam, J. W. Y.; Tang, B. Z. *Chem. Rev.* **2015,** *115,* 11718–11940. doi:10.1021/acs.chemrev.5b00263
17. Wenz, G. *Angew. Chem., Int. Ed.* **1994,** *33,* 803–822. doi:10.1002/anie.199408031
18. Wenz, G. *Adv. Polym. Sci.* **2009,** *222,* 204–254. doi:10.1007/12_2008_13
19. Yang, L.; Tan, X.; Wang, Z.; Zhang, X. *Chem. Rev.* **2015,** *115,* 7196–7239. doi:10.1021/cr500633b
20. Du, X.; Zhou, J.; Shi, J.; Xu, B. *Chem. Rev.* **2015,** *115,* 13165–13307. doi:10.1021/acs.chemrev.5b00299
21. Krieg, E.; Bastings, M. M. C.; Besenius, P.; Rybtchinski, B. *Chem. Rev.* **2016,** *116,* 2414–2472. doi:10.1021/acs.chemrev.5b00369
22. Weickenmeier, M.; Wenz, G.; Huff, J. *Macromol. Rapid Commun.* **1997,** *18,* 1117–1123. doi:10.1002/marc.1997.030181216
23. Nakahata, M.; Takashima, Y.; Harada, A. *Macromol. Rapid Commun.* **2016,** *37,* 86–92. doi:10.1002/marc.201500473
24. Ludden, M. J. W.; Reinhoudt, D. N.; Huskens, J. *Chem. Soc. Rev.* **2006,** *35,* 1122–1134. doi:10.1039/b600093m

25. Ludden, M. J. W.; Ling, X. Y.; Gang, T.; Bula, W. P.; Gardeniers, H. J. G. E.; Reinhoudt, D. N.; Huskens, J. *Chem. – Eur. J.* **2008,** *14,* 136–142. doi:10.1002/chem.200701250
26. Hsu, S.-H.; Yilmaz, M. D.; Reinhoudt, D. N.; Velders, A. H.; Huskens, J. *Angew. Chem.* **2013,** *125,* 742–747. doi:10.1002/ange.201207647 *Angew. Chem. Int. Ed.* **2013,** *52,* 714–719. doi:10.1002/anie.201207647
27. Perl, A.; Gomez-Casado, A.; Thompson, D.; Dam, H. H.; Jonkheijm, P.; Reinhoudt, D. N.; Huskens, J. *Nat. Chem.* **2011,** *3,* 317–322. doi:10.1038/nchem.1005
28. Ludden, M. J. W.; Mulder, A.; Tampé, R.; Reinhoudt, D. N.; Huskens, J. *Angew. Chem.* **2007,** *119,* 4182–4185. doi:10.1002/ange.200605104 *Angew. Chem. Int. Ed.* **2007,** *46*, 4104–4107. doi:10.1002/anie.200605104
29. Terao, J.; Homma, K.; Konoshima, Y.; Imoto, R.; Masai, H.; Matsuda, W.; Seki, S.; Fujihara, T.; Tsuji, Y. *Chem. Commun.* **2014,** *50,* 658–660. doi:10.1039/C3CC47105E
30. Terao, J. *Chem. Rec.* **2011,** *11,* 269–283. doi:10.1002/tcr.201100009
31. Terao, J.; Tsuda, S.; Tanaka, Y.; Okoshi, K.; Fujihara, T.; Tsuji, Y.; Kambe, N. *J. Am. Chem. Soc.* **2008,** *131,* 16004–16005. doi:10.1021/ja9074437
32. Masai, H.; Terao, J.; Makuta, S.; Tachibana, Y.; Fujihara, T.; Tsuji, Y. *J. Am. Chem. Soc.* **2014,** *136,* 14714–14717. doi:10.1021/ja508636z
33. Masai, H.; Terao, J.; Seki, S.; Nakashima, S.; Kiguchi, M.; Okoshi, K.; Fujihara, T.; Tsuji, Y. *J. Am. Chem. Soc.* **2014,** *136,* 1742–1745. doi:10.1021/ja411665k
34. Terao, J.; Tanaka, Y.; Tsuda, S.; Kambe, N.; Taniguchi, M.; Kawai, T.; Saeki, A.; Seki, S. *J. Am. Chem. Soc.* **2009,** *131,* 18046–18047. doi:10.1021/ja908783f
35. Terao, J.; Kimura, K.; Seki, S.; Fujihara, T.; Tsuji, Y. *Chem. Commun.* **2012,** *48,* 1577–1579. doi:10.1039/C1CC13012A
36. Ogoshi, T.; Takashima, Y.; Yamaguchi, H.; Harada, A. *Chem. Commun.* **2006,** 3702–3704. doi:10.1039/b605804c
37. Rief, M.; Clausen-Schaumann, H.; Gaub, H. E. *Nat. Struct. Biol.* **1999,** *6,* 346–349. doi:10.1038/7582
38. Kufer, S. K.; Puchner, E. M.; Gumpp, H.; Liedl, T.; Gaub, H. E. *Science* **2008,** *319,* 594–596. doi:10.1126/science.1151424
39. Piner, R. D.; Zhu, J.; Xu, F.; Hong, S.; Mirkin, C. A. *Science* **1999,** *283,* 661–663. doi:10.1126/science.283.5402.661
40. Bacharouche, J.; Degardin, M.; Jierry, L.; Carteret, C.; Lavalle, P.; Hemmerlé, J.; Senger, B.; Auzély-Velty, R.; Boulmedais, F.; Boturyn, D.; Coche-Guérente, L.; Schaaf, P.; Francius, G. *J. Mater. Chem. B* **2015,** *3,* 1801–1812. doi:10.1039/C4TB01261E
41. Kaftan, O.; Tumbiolo, S.; Dubreuil, F.; Auzély-Velty, R.; Fery, A.; Papastavrou, G. *J. Phys. Chem. B* **2011,** *115,* 7726–7735. doi:10.1021/jp110939c
42. Han, X.; Qin, M.; Pan, H.; Cao, Y.; Wang, W. *Langmuir* **2012,** *28,* 10020–10025. doi:10.1021/la301903z
43. Pussak, D.; Ponader, D.; Mosca, S.; Pompe, T.; Hartmann, L.; Schmidt, S. *Langmuir* **2014,** *30,* 6142–6150. doi:10.1021/la5010006
44. Zhang, Y.; Yu, Y.; Jiang, Z.; Xu, H.; Wang, Z.; Zhang, X.; Oda, M.; Ishizuka, T.; Jiang, D.; Chi, L.; Fuchs, H. *Langmuir* **2009,** *25,* 6627–6632. doi:10.1021/la901360c
45. Ratto, T. V.; Rudd, R. E.; Langry, K. C.; Balhorn, R. L.; McElfresh, M. C. *Langmuir* **2006,** *22,* 1749–1757. doi:10.1021/la052087d
46. Gomez-Casado, A.; Dam, H. H.; Yilmaz, M. D.; Florea, D.; Jonkheijm, P.; Huskens, J. *J. Am. Chem. Soc.* **2011,** *133,* 10849–10857. doi:10.1021/ja2016125
47. Bozna, B. L.; Blass, J.; Albrecht, M.; Hausen, F.; Wenz, G.; Bennewitz, R. *Langmuir* **2015,** *31,* 10708–10716. doi:10.1021/acs.langmuir.5b03026
48. Blass, J.; Albrecht, M.; Bozna, B. L.; Wenz, G.; Bennewitz, R. *Nanoscale* **2015,** *7,* 7674–7681. doi:10.1039/C5NR00329F
49. Blass, J.; Bozna, B. L.; Albrecht, M.; Krings, J. A.; Ravoo, B. J.; Wenz, G.; Bennewitz, R. *Chem. Commun.* **2015,** *51,* 1830–1833. doi:10.1039/C4CC09204J
50. Bonifacio, M. C.; Robertson, C. R.; Jung, J.-Y.; King, B. T. *J. Org. Chem.* **2005,** *70,* 8522–8526. doi:10.1021/jo051418o
51. Cocherel, N.; Poriel, C.; Rault-Berthelot, C.; Barrière, F.; Audebrand, N.; Slawin, A. M. Z.; Vignau, L. *Chem. – Eur. J.* **2008,** *14,* 11328–11342. doi:10.1002/chem.200801428
52. Wenz, G.; Strassnig, C.; Thiele, C.; Engelke, A.; Morgenstern, B.; Hegetschweiler, K. *Chem. – Eur. J.* **2008,** *14,* 7202–7211. doi:10.1002/chem.200800295
53. Kretschmann, O.; Choi, S. W.; Miyauchi, M.; Tomatsu, I.; Harada, A.; Ritter, H. *Angew. Chem.* **2006,** *118,* 4468–4472. doi:10.1002/ange.200504539 Angew. Chem. Int. Ed. 2006, 45, 4361-4365. doi:10.1002/anie.200504539
54. Wenz, G.; Han, B.-H.; Müller, A. *Chem. Rev.* **2006,** *106,* 782–817. doi:10.1021/cr970027+
55. Przybylski, C.; Blin, F.; Jarroux, N. *Macromolecules* **2011,** *44,* 1821–1830. doi:10.1021/ma102641q
56. Feoktystov, A. V.; Frielinghaus, H.; Di, Z.; Jaksch, S.; Pipich, V.; Appavou, M.-S.; Babcock, E.; Hanslik, R.; Engels, R.; Kemmerling, G.; Kleines, H.; Ioffe, A.; Richter, D.; Brückel, T. *J. Appl. Crystallogr.* **2015,** *48,* 61–70. doi:10.1107/S1600576714025977
57. Debye, P. *J. Phys. Colloid Chem.* **1947,** *51,* 18–32. doi:10.1021/j150451a002
58. Glatter, O. *J. Appl. Crystallogr.* **1977,** *10,* 415–421. doi:10.1107/S0021889877013879
59. Denkinger, P.; Burchard, W. *J. Polym. Sci., Part B: Polym. Phys.* **1991,** *29,* 589–600. doi:10.1002/polb.1991.090290508
60. Pedersen, J. S. *Adv. Colloid Interface Sci.* **1997,** *70,* 171–210. doi:10.1016/S0001-8686(97)00312-6
61. Rekharsky, M. V.; Inoue, Y. *Chem. Rev.* **1998,** *98,* 1875–1918. doi:10.1021/cr970015o
62. Deng, L.; Norberg, O.; Uppalapat, S.; Yan, M.; Ramström, O. *Org. Biomol. Chem.* **2011,** *9,* 3188–3198. doi:10.1039/c1ob05040k
63. Schmidt, G.; Timm, C.; Grube, A.; Volk, C. A.; Köck, M. *Chem. – Eur. J.* **2012,** *18,* 8180–8189. doi:10.1002/chem.201101362
64. Blass, J.; Albrecht, M.; Wenz, G.; Zang, Y. N.; Bennewitz, R. *Phys. Chem. Chem. Phys.* **2017,** *19,* 5239–5245. doi:10.1039/C6CP07532K

License and Terms

BEILSTEIN JOURNAL OF ORGANIC CHEMISTRY

One-pot synthesis of block-copolyrotaxanes through controlled *rotaxa*-polymerization

Jessica Hilschmann, Gerhard Wenz and Gergely Kali*

Full Research Paper

Open Access

Address:
Organic Macromolecular Chemistry, Saarland University, Campus C4.2, 66123 Saarbrücken, Germany

Email:
Gergely Kali* - gergely.kali@uni-saarland.de

* Corresponding author

Keywords:
block copolymer; cyclodextrin; polyisoprene; polyrotaxane; RAFT polymerization

Beilstein J. Org. Chem. **2017,** *13,* 1310–1315.
doi:10.3762/bjoc.13.127

Received: 24 February 2017
Accepted: 14 June 2017
Published: 03 July 2017

This article is part of the Thematic Series "Spatial effects in polymer chemistry".

Guest Editor: H. Ritter

Abstract

The aqueous reversible addition fragmentation chain-transfer (RAFT) copolymerization of isoprene and bulky comonomers, an acrylate and an acrylamide in the presence of methylated β-cyclodextrin was employed for the first time to synthesize block-copolyrotaxanes. RAFT polymerizations started from a symmetrical bifunctional trithiocarbonate and gave rise to triblock-copolymers where the outer polyacrylate/polyacrylamide blocks act as stoppers for the cyclodextrin rings threaded onto the inner polyisoprene block. Statistical copolyrotaxanes were synthesized by RAFT polymerization as well. RAFT polymerization conditions allow control of the composition as well as the sequence of the constituents of the polymer backbone which further effects the CD content and the aqueous solubility of the polyrotaxane.

Introduction

Polymer necklaces, i.e., polyrotaxanes and pseudopolyrotaxanes, are supramolecular assemblies comprising polymeric axes with macrocycles threaded on them [1-4]. In the case of polyrotaxanes, the dethreading of the macrocycles is prevented by bulky stopper groups placed along the chain or at the chain ends. The importance of these supramolecules lies in the possibility to modify the properties, or even cross-link polymers without chemical modification of the backbone. Through polyrotaxane formation solubility [2-5], as well as mechanical [1-3,6-9] and electrical properties [10], can be improved. Cross-linking of threaded macrocycles gives rise to so-called slide-ring gels with unique mechanical properties [6,11-13]. One of the most important class of important macrocycles, applied in polyrotaxane chemistry, are cyclodextrins (CDs) because they are nontoxic, biodegradable and available in industrial scale. Furthermore, CDs can be simply functionalized by modification of the hydroxy groups [14].

There are several CD-based polyrotaxanes known with homo- and block-copolymer axes, mostly based on poly(ethylene

oxide), poly(propylene oxide) or their copolymers [15-21], since these polymers can form sufficiently stable complexes with CDs. The application potential of these polyrotaxanes was already investigated in the fields of biomedicine, as drug [22] or gene [23] delivery vehicles, or in materials sciences, as slide ring gels [6]. Polyrotaxanes are mostly synthesized by a threading approach [2], a multistep method starting from pre-synthesized (co)polymers. Due to the hydrophobic interaction, as the driving force of complex formation, the threading of the CDs is only achievable in aqueous solution, but the hydrogen bonds between the hydroxy groups impede the water solubility of the products. Thus, the stoppering reaction is mostly limited to organic solutes, in which dethreading already takes place. This multistep reaction methodology hinders the large-scale production and broad application of these materials.

Recently our group has developed a method for a simple and environmentally friendly synthesis of polyrotaxanes. This, so called *rotaxa*-polymerization, is an aqueous, free radical copolymerization of a hydrophobic monomer, complexed in a host, with a stopper comonomer [24,25]. This latter has to be large enough to prevent the dissociation of the growing axis and the host, as it happens in the case of aqueous CD assisted homopolymerizations of hydrophobic monomers [26-28] including dienes [29]. This approach drastically widens the range of suitable hydrophobic polymeric axes, to all monomers being complexed in CD or hydrophilic CD derivatives. Up to now, *rotaxa*-polymerization was only performed via free radical reaction without control of the polymer chain length as well as statistical distribution of stopper groups along the axis. Herein, we report for the first time a simple one-pot synthesis of polyrotaxanes with control of length and sequence of the polymer axis through RAFT *rotaxa*-polymerization of isoprene in water. RAFT polymerization was indeed already started from a PEG α-CD pseudopolyrotaxane, but unthreading of α-CD was found to be a severe problem during polymerization, which could only be overcome by elaborate attachment of "molecular hooks" to both chain ends [30]. Furthermore, polyisoprene is advantageous for biomedical applications because of its high biocompatibility and biodegradability [31-33]. Here should be noted that polyisoprene was already subjected to pseudopolyrotaxane formation, with limited success, i.e., with β-CD only oligoisoprenes (degree of polymerization < 9) could form complexes with low coverage (3.0%) [34].

RAFT polymerization is a useful tool to form well-defined block-copolymers starting from a chain transfer agent (CTA) that drastically reduces the actual radical concentration in a fast equilibrium reaction [35-37]. This controlled polymerization should be advantageous for this work, compared to other polymerization techniques, such as atom transfer radical polymerization, because of the lack of toxic metal additives, and because of good control exerted in aqueous solution. The water-soluble bifunctional CTA *S*,*S*′-bis(α,α′-dimethyl-α″-acetic acid)trithiocarbonate (DMATC) was selected because it allows synthesis of symmetrical triblock-copolymers in two steps. Other benefits of trithiocarbonate CTAs are the good hydrolytic stability [38], as well as their approved application in controlled isoprene polymerization [39,40]. Randomly methylated β-CD (RAMEB) was chosen as the CD derivative for this polyrotaxane synthesis since it is highly water-soluble and provides a sufficiently high binding constant for isoprene [24,25].

Results and Discussion

In a first trial, statistical RAFT copolymerization of isoprene complexed in RAMEB was performed with water-soluble bulky comonomers, namely *N*-[tris(hydroxymethyl)methyl]acrylamide (TRIS-AAm) or 2-hydroxyethyl methacrylate (HEMA), shown in Scheme 1. The role of these bulky comonomers was to prevent the unthreading of RAMEB rings from the polymeric axis during and after polymerization. The resulting statistical copolymers were clearly soluble in water thus they could be purified by ultrafiltration. Besides water, the polyrotaxanes were also soluble in DMSO and less polar solvents, such as THF and chloroform. The weight fraction of RAMEB (Table 1) in the product was quantified from the optical rotation of a solution of the polymer (for the detailed description see Supporting Information File 1). The eventual content of free RAMEB in the product was checked by isothermal calorimetry (ITC) and was around 3 wt %. The conversion of the monomers was calculated from the yield of polyrotaxane minus the total RAMEB content. In both cases, the monomer conversions were around 60 wt % and the amount of threaded CD ranged between 47 and 65 wt %. These compositions were also supported by the integrals of the ^{1}H NMR spectra (Supporting Information File 1).

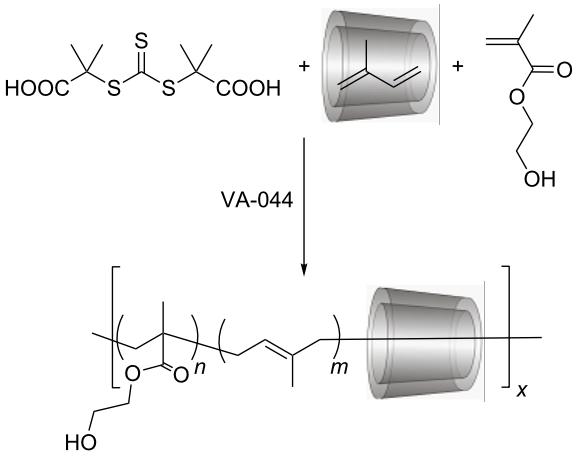

Scheme 1: Synthesis route of RAMEB based statistical polyrotaxane.

Table 1: Yields, CD contents and weight average molar masses (M_{prx}), degrees of polymerization (P_w) and isoprene/stopper ratios (*i*/*st*) and dispersities (*Đ*) of the produced RAMEB based polyisoprene polyrotaxanes.

Polymer no.	comonomer	Yield (wt %)	RAMEB content (wt %)	M_{prx}[a] (kDa)	P_w	*i*/*st*[b]	*Đ*
1	TRIS-AAm	67	47	40.5	270	8.5	1.8
2	HEMA	58	60	41.0	205	4.6	2.2

[a]Molar mass calculated from the molar mass of the acetylated polyrotaxanes measured by GPC; [b]*i*/*st*: molar ratio of isoprene/stopper in the polymer as calculated from ^{1}H NMR.

The restricted mobility of the threaded macrocycles should lead to peak broadening in the ^{1}H NMR spectra of the polyrotaxanes [41]. This peak broadening was indeed observed in the ^{1}H NMR spectra of both polymers (Figure 1b and Supporting Information File 1) and was regarded as the first indication for a polyrotaxane structure. In addition, the agreement of the diffusion coefficients *D* for all proton NMR signals of the polymeric axis, RAMEB and the stopper in the diffusion-ordered NMR spectrum (DOSY, Figure 1b) further proved the existence of the polyrotaxane [42]. The *D* values of 1.0×10^{-10} and 4.1×10^{-11} m^2/s were found for TRIS-AAm, and HEMA stoppered polyrotaxanes, respectively. The weight average molar mass M_w determined by GPC was in both cases around 40 kDa, which means that the choice of the stopper was not critical for the composition and the size of the polyrotaxane. The amount of stopper integrated into the polyrotaxane was indeed difficult to quantify because of superposition of the ^{1}H NMR signals with the ones of RAMEB, but the molar ratio isoprene/stopper (*i*/*st*) in the polymer could be estimated based on the integral values from the ^{1}H NMR spectrum, using the region A (0.5–2.5 ppm) of the polymer backbone and the corresponding peaks of the stopper comonomers (Supporting Information File 1). Based on this calculation the estimated *i*/*st* values 8.5 and 4.6 were obtained for polyrotaxanes **1** and **2**, respectively. Also, the C=O vibrations of the polyacrylate units in the IR spectra of the polyrotaxanes were indicative for the integration of the stopper units into the polymer (see Supporting Information File 1).

The molar masses of polyrotaxanes **1** and **2** were determined after complete acetylation by GPC in THF (for results see Table 1). From the molar ratio *i*/*st*, the average molar mass per monomer repeat was derived $\overline{M_{mon}} = 79$ Da for both polyrotaxanes **1** and **2**, which allows to calculate the degree of polymerization P_w of the polymer backbone according to $P_w = (1 - w_{CD})M_{prx} / \overline{M_{mon}}$ the values of P_w were in reasonable agreement with the molar ratio of the related monomer vs CTA (175), which was indicative for a significant control of the radical polymerization by the CTA. The observed polydispersity indices M_w/M_n = 1.8–2.2 being higher than for regular RAFT polymerizations was attributed to a broad distribution of the number of methylated CD rings threaded on the polymer chains and the additional distribution of the number of methyl groups in the randomly methylated β-CD.

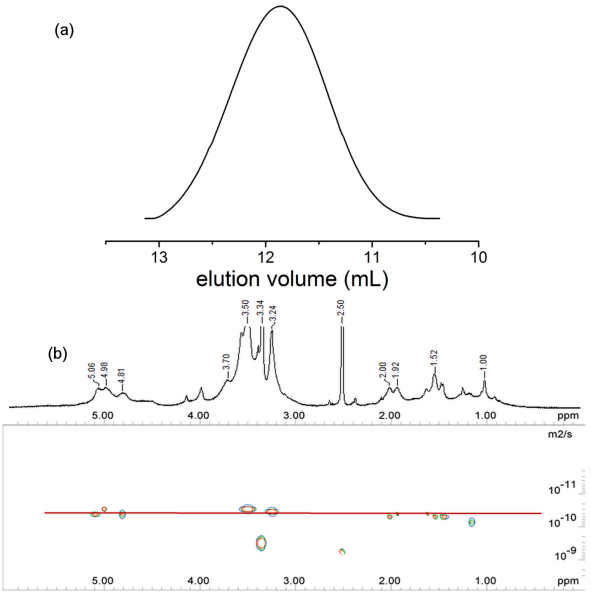

Figure 1: (a) GPC trace of the polyHEMA-*co*-polyisoprene polyrotaxane **1** and (b) 500 MHz ^{1}H NMR and DOSY spectra of poly(TRIS-AAm)-*co*-polyisoprene polyrotaxane **2** in DMSO-d_6.

After the success of a *rotaxa*-RAFT polymerization, we investigated the synthesis of ABA triblock-copolyrotaxanes from the same building blocks in a two-step process as displayed in Scheme 2. First, one of the stopper monomers was homopolymerized by RAFT process starting from the bifunctional CTA, DMATC. In the second step, isoprene, complexed in RAMEB, was further polymerized utilizing the homopolymeric polyHEMA or polyTRIS-AAm as macro CTAs in water. Since the resulting block-copolyrotaxanes were nearly insoluble in water, they could be isolated through simple heat filtration, i.e., were heated up to 80 °C and filtered off at this temperature. Since the polymers were soluble in DMSO, the composition could be investigated by polarimetry and ^{1}H NMR spectroscopy (see Table 2) as described in the first part.

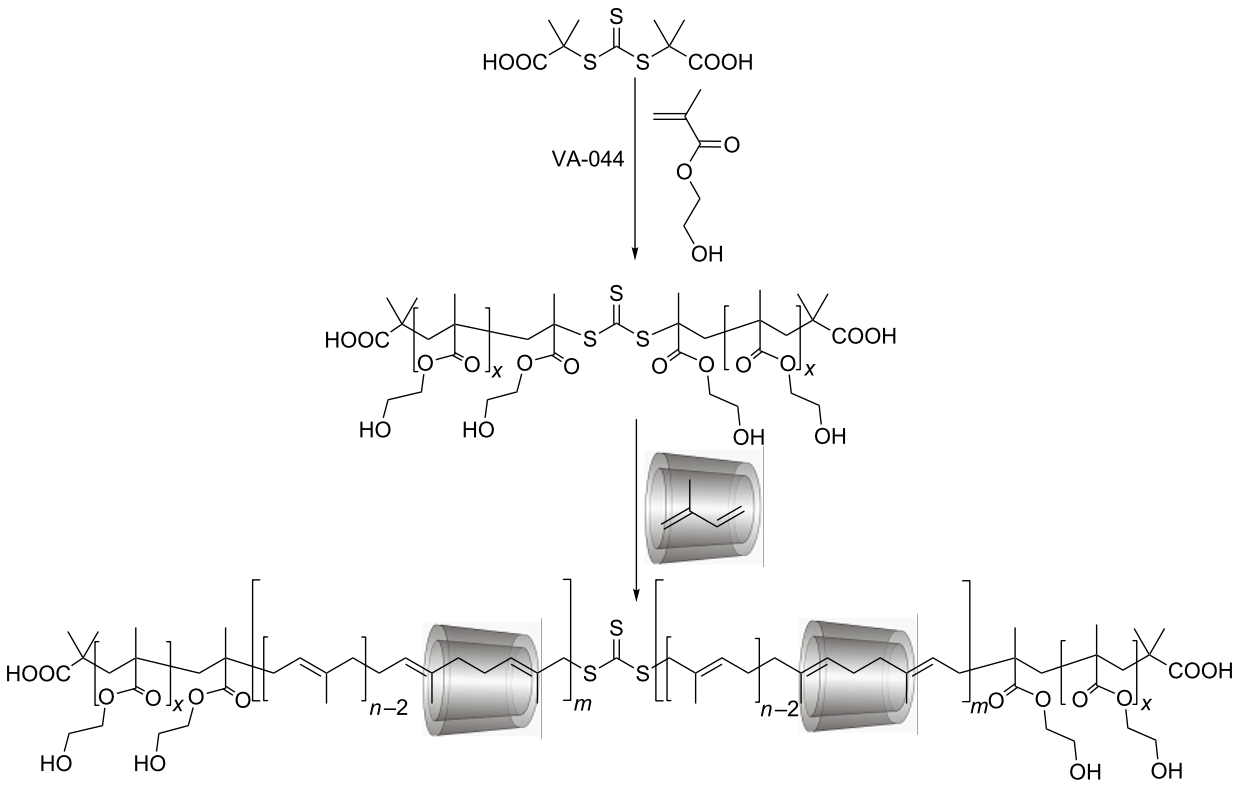

Scheme 2: Schematic representation of the synthetic procedure for the preparation of randomly methylated β-CD based block-copolymeric polyrotaxane.

Table 2: Yields, RAMEB content and weight average molar masses (M_{prx}) and degrees of polymerization (P_w) of the polymers obtained by RAFT polymerization.

Polymer no.	CTA	Monomer	Molar ratio monomer/CTA	Yield (wt %)	RAMEB (wt %)	M_{prx}[a] (kDa)	$Đ$	P_w of new block[b]
3	DMATC	HEMA	16	95	0	9	2.5	21
4	**3**	isoprene	77	48	49	47	2.8	62
5	DMATC	TRIS-AAm	16	90	0	4	1.8	29
6	**5**	isoprene	80	51	65	45	1.9	77

[a]Molar mass calculated from the molar mass of the acetylated polyrotaxanes measured by GPC; [b]P_w of the new polyisoprene block was calculated from ^{1}H NMR.

The ^{1}H NMR spectrum (Figure 2b) of the polymer **4** shows the signals of all RAMEB constituents at 3.0–4.1 and 4.5–5.0 ppm, polyisoprene at 1.0–2.3 and 5.0 ppm and of polyHEMA at 0.7–2.1 and 3.3–4.0 ppm. The noticeable peak broadening again is indicative of the formation of ABA triblock-copolyrotaxane. The DOSY measurements were carried out for the block-copolymer polyrotaxanes in DMSO. The same diffusion coefficients were detected for all components, such as RAMEB, isoprene, and stopper segments, verifying the polyrotaxane formation, as presented in Figure 2b. Diffusion coefficients of both block-polyrotaxanes were around 3.0×10^{-11} m^2/s, due to the similar molar masses for both polyrotaxanes after block-copolymerization.

The molar masses of polyrotaxanes **3**–**6** were determined after complete acetylation by GPC in THF (Table 2). First, after homopolymerization, the molar masses were 9 and 4 kDa for the polyHEMA and polyTRIS-AAm stoppers blocks, respectively. After block copolymerization with isoprene complexed in RAMEB, the corresponding molar masses increased significantly to 50 and 45 kDa, indicating further polymerization and coinciding polyrotaxane formation. Starting from both poly-

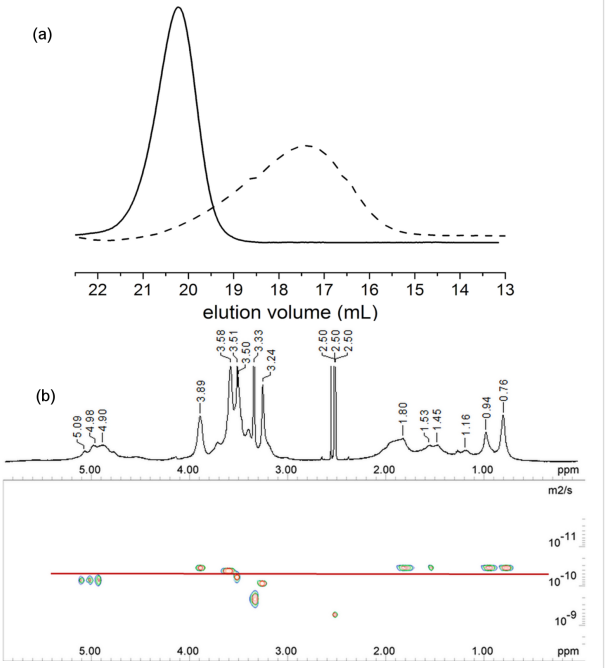

Figure 2: (a) GPC traces of the macroCTA **5** (solid line) and the poly(TRIS-AAm)-*b*-polyisoprene-*b*-poly(TRIS-AAm) polyrotaxane **6** (dashed line), and (b) 500 MHz, ^{1}H NMR and DOSY spectra of poly-HEMA-*b*-polyisoprene-*b*-polyHEMA polyrotaxane **4** in DMSO-d_6.

HEMA and polyTRIS-AAm CTAs, monomer conversions were around 50%. For these block-copolymers with polyrotaxane middle blocks, the CD contents were 49 and 65 wt % of RAMEB. For the polyHEMA based polyrotaxane **4**, this coverage was a bit lower than for the statistical copolymerization and also the obtained polyisoprene block length P_w was slightly lower than the theoretical value. These deviations are most likely explained by the limited aqueous solubility and the high molar mass (9 kDa) of the polyHEMA CTA **3**. In contrast to HEMA-based block-copolyrotaxane, the coverage of polyTRIS-AAm-based block-copolyrotaxane **6** was higher than that of for the statistical one, while the molar mass remained the same, and the polyisoprene block length P_w being close to the theoretical value (77 instead of 80). This indicates a good control of the CTA over the polymerization. The composition of the backbone *i*/*st* can be easily calculated from the molar masses of the blocks to the polymeric axes. These *i*/*st* ratios were 4.70 and 8.75 for polyrotaxanes **4** and **6**, respectively. The corresponding *i*/*st* values, estimated from the ^{1}H NMR spectra were 3.00 and 8.30. The too low value obtained for the HEMA stoppered polyrotaxane was attributed to the superposition of the signals of –CH_2-OH from HEMA and of RAMEB which hinders the accurate determination of the polymer composition. The polydispersity indices were again slightly higher than that of for regular RAFT polymerizations, 2.8 and 1.9 for polyrotaxanes **4** and **6**, respectively. This increased PDI is connected to the statistical threading of the cyclodextrin rings, which also have some mass distribution. The higher PDI 2.8 of the polyHEMA block-copolyrotaxane **4** was attributed to the low aqueous solubility of the polyHEMA CTA.

Conclusion

The above-described procedure is the first controlled *rotaxa*-polymerization resulting in well-defined statistical and block-copolymeric polyrotaxanes. The method is versatile and should work for many monomers and CD derivatives. The resulting triblock-copolyrotaxanes might be good stocks for the synthesis of highly elastic slide-ring gels and hydrogels. Due to the biocompatibility of the constituents and the ability of the polyrotaxanes to self-assemble, these materials might also be applicable for drug delivery or tissue engineering.

Supporting Information

Supporting Information File 1

General methods, experimental procedures, and characterization of compounds **1**–**6**.
[http://www.beilstein-journals.org/bjoc/content/supplementary/1860-5397-13-127-S1.pdf]

Acknowledgements

This work was funded by the Federal Ministry of Research and Technology (BMBF), Project No. 03VP01051. Thanks to Devid Hero for his synthetic work, and Blandine Boßmann for GPC measurements.

References

1. Wenz, G.; Keller, B. *Angew. Chem., Int. Ed. Engl.* **1992,** *31,* 197–199. doi:10.1002/anie.199201971
2. Wenz, G.; Han, B.-H.; Müller, A. *Chem. Rev.* **2006,** *106,* 782–817. doi:10.1021/cr970027+
3. Arunachalam, M.; Gibson, H. W. *Prog. Polym. Sci.* **2014,** *39,* 1043–1073. doi:10.1016/j.progpolymsci.2013.11.005
4. Harada, A.; Li, J.; Kamachi, M. *Nature* **1992,** *356,* 325–327. doi:10.1038/356325a0
5. Gibson, H. W.; Liu, S.; Lecavalier, P.; Wu, C.; Shen, Y. X. *J. Am. Chem. Soc.* **1995,** *117,* 852–874. doi:10.1021/ja00108a002
6. Mayumi, K.; Ito, K.; Kato, K. *Polyrotaxane and Slide-Ring Materials;* Royal Society of Chemistry, 2016.
7. Gong, C.; Ji, Q.; Subramaniam, C.; Gibson, H. W. *Macromolecules* **1998,** *31,* 1814–1818. doi:10.1021/ma9713116
8. Gibson, H. W.; Shen, Y. X.; Bheda, M. C.; Gong, C. *Polymer* **2014,** *55,* 3202–3211. doi:10.1016/j.polymer.2014.05.007
9. Harada, A.; Takashima, Y.; Nakahata, M. *Acc. Chem. Res.* **2014,** *47,* 2128–2140. doi:10.1021/ar500109h
10. Lee, M.; Choi, U. H.; Colby, R. H.; Gibson, H. W. *Macromol. Chem. Phys.* **2015,** *216,* 344–349. doi:10.1002/macp.201400426

11. Kato, K.; Inoue, K.; Kidowaki, M.; Ito, K. *Macromolecules* **2009,** *42,* 7129–7136. doi:10.1021/ma9011895
12. Kato, K.; Yasuda, T.; Ito, K. *Macromolecules* **2013,** *46,* 310–316. doi:10.1021/ma3021135
13. Noda, Y.; Hayashi, Y.; Ito, K. *J. Appl. Polym. Sci.* **2014,** *131,* No. 40509. doi:10.1002/app.40509
14. Wenz, G. *Angew. Chem., Int. Ed. Engl.* **1994,** *33,* 803–822. doi:10.1002/anie.199408031
15. Mayer, B.; Klein, C. T.; Topchieva, I. N.; Köhler, G. *J. Comput.-Aided Mol. Des.* **1999,** *13,* 373–383. doi:10.1023/A:1008095501870
16. Topchieva, I. N.; Kolmonikova, E. L.; Banatskaya, M. I.; Kabanov, V. A. *Vysokomol. Soedin., Ser. A Ser. B* **1993,** *35,* 395–398.
17. Tsai, C.-C.; Zhang, W.-B.; Wang, C.-L.; Van Horn, R. M.; Graham, M. J.; Huang, J.; Chen, Y.; Guo, M.; Cheng, S. Z. D. *J. Chem. Phys.* **2010,** *132,* 204903. doi:10.1063/1.3428769
18. Mondjinou, Y. A.; Hyun, S.-H.; Xiong, M.; Collins, C. J.; Thong, P. L.; Thompson, D. H. *ACS Appl. Mater. Interfaces* **2015,** *7,* 23831–23836. doi:10.1021/acsami.5b01016
19. Badwaik, V.; Mondjinou, Y.; Kulkarni, A.; Liu, L.; Demoret, A.; Thompson, D. H. *Macromol. Biosci.* **2016,** *16,* 63–73. doi:10.1002/mabi.201500220
20. Zhang, X.; Zhu, X.; Ke, F.; Ye, L.; Chen, E.-r.; Zhang, A.-y.; Feng, Z.-g. *Polymer* **2009,** *50,* 4343–4351. doi:10.1016/j.polymer.2009.07.006
21. Kong, T.; Lin, J.; Ye, L.; Zhang, A.-y.; Feng, Z.-g. *Polym. Chem.* **2015,** *6,* 5832–5837. doi:10.1039/C5PY00674K
22. Kang, Y.; Zhang, X.-M.; Zhang, S.; Ding, L.-S.; Li, B.-J. *Polym. Chem.* **2015,** *6,* 2098–2107. doi:10.1039/C4PY01431F
23. Wen, C.; Hu, Y.; Xu, C.; Xu, F.-J. *Acta Biomater.* **2015,** *32,* 110–119. doi:10.1016/j.actbio.2015.12.033
24. Kali, G.; Eisenbarth, H.; Wenz, G. *Macromol. Rapid Commun.* **2016,** *37,* 67–72. doi:10.1002/marc.201500548
25. Hilschmann, J.; Kali, G.; Wenz, G. *Macromolecules* **2017,** *50,* 1312–1318. doi:10.1021/acs.macromol.6b02640
26. Glöckner, P.; Ritter, H. *Macromol. Rapid Commun.* **1999,** *20,* 602–605. doi:10.1002/(SICI)1521-3927(19991101)20:11<602::AID-MARC602>3.0.CO;2-K
27. Choi, S.; Amajjahe, S.; Ritter, H. *Adv. Polym. Sci.* **2009,** *222,* 79–113. doi:10.1007/12_2008_6
28. Ritter, H.; Tabatabai, M. *Prog. Polym. Sci.* **2002,** *27,* 1713–1720. doi:10.1016/S0079-6700(02)00022-9
29. Groenendaal, L.; Ritter, H.; Storsberg, J. Method for Producing Polymers on the Basis of 1,3 Dienes. WO Patent WO 2001038408 A2, May 31, 2001.
30. Tamura, A.; Tanaka, H.; Yui, N. *Polym. Chem.* **2014,** *5,* 4511–4520. doi:10.1039/c4py00379a
31. Shah, A. A.; Hasan, F.; Shah, Z.; Kanwal, N.; Zeb, S. *Int. Biodeterior. Biodegrad.* **2013,** *83,* 145–157. doi:10.1016/j.ibiod.2013.05.004
32. Baruch-Teblum, E.; Mastai, Y.; Landfester, K. *Eur. Polym. J.* **2010,** *46,* 1671–1678. doi:10.1016/j.eurpolymj.2010.05.007
33. Uhrich, K. E.; Cannizzaro, S. M.; Langer, R. S.; Shakesheff, K. M. *Chem. Rev.* **1999,** *99,* 3181–3198. doi:10.1021/cr940351u
34. Michishita, T.; Takashima, Y.; Harada, A. *Macromol. Rapid Commun.* **2004,** *25,* 1159–1162. doi:10.1002/marc.200400108
35. Barner-Kowollik, C., Ed. *Handbook of RAFT Polymerization;* Wiley-VCH Verlag GmbH. & Co. KGaA: Weinheim, 2008.
36. Köllisch, H.; Barner-Kowollik, C.; Ritter, H. *Macromol. Rapid Commun.* **2006,** *27,* 848–853. doi:10.1002/marc.200600067
37. Köllisch, H. S.; Barner-Kowollik, C.; Ritter, H. *Chem. Commun.* **2009,** *9,* 1097–1099. doi:10.1039/b818897a
38. Convertine, A. J.; Lokitz, B. S.; Lowe, A. B.; Scales, C. W.; Myrick, L. J.; McCormick, C. L. *Macromol. Rapid Commun.* **2005,** *26,* 791–795. doi:10.1002/marc.200500042
39. Jitchum, V.; Perrier, S. *Macromolecules* **2007,** *40,* 1408–1412. doi:10.1021/ma061889s
40. Germack, D. S.; Wooley, K. L. *J. Polym. Sci., Part A: Polym. Chem.* **2007,** *45,* 4100–4108. doi:10.1002/pola.22226
41. Zhao, T.; Beckham, H. W. *Macromolecules* **2003,** *36,* 9859–9865. doi:10.1021/ma035513f
42. Johnson, C. S., Jr. *Prog. Nucl. Magn. Reson. Spectrosc.* **1999,** *34,* 203–256. doi:10.1016/S0079-6565(99)00003-5

License and Terms

BEILSTEIN JOURNAL OF ORGANIC CHEMISTRY

Detection of therapeutic radiation in three-dimensions

John A. Adamovics

Review

Open Access

Address:
Department of Chemistry, Biochemistry and Physics, Rider University, 2083 Lawrenceville Road, Lawrenceville, NJ 08648-3099, USA

Email:
John A. Adamovics - jadamovics@rider.edu

Keywords:
dosimeters; leuco dyes; polymers; radiation; triarylmethane synthesis

Beilstein J. Org. Chem. **2017,** *13,* 1325–1331.
doi:10.3762/bjoc.13.129

Received: 02 March 2017
Accepted: 14 June 2017
Published: 05 July 2017

This article is part of the Thematic Series "Spatial effects in polymer chemistry".

Guest Editor: H. Ritter

Abstract

For over the last twenty years there has been a multitude of sophisticated three-dimensional radiation delivery procedures developed which requires a corresponding verification of the impact on patients. This article reviews the state of the art in the development of chemical detectors used to characterize the three-dimensional shape of therapeutic radiation. These detectors are composed of polyurethane, radical initiator and a leuco dye, which is radiolytically oxidized to a dye absorbing at 630 nm.

Introduction

Radiotherapy treatment is a complex 3D process, which is the principle treatment modality for most cancers [1]. The two main types of radiation therapy are external beam and internal beam. External beam radiation can be sorted into 2 main types of ionizing radiation: photon (X-rays and gamma rays) and particle radiation (electron, protons, neutrons, and carbon ions) [1]. Internal radiation therapy can be delivered by either a solid radioactive source (brachytherapy), or a liquid radiation source placed near or inside the cancerous area.

In the last decade the sophistication and complexity of radiation therapy treatment has increased dramatically. Advances have been so swift that an imbalance has arisen with verification technologies (dosimeters) with sufficient capability to verify complex treatments and ensure accurate, safe implementation [2]. There have been reports of high failure rates for complex radiation treatments [3,4]. These concerns and others have led many to recognize an urgent need to strengthen the foundations of quality assurance (QA) in radiation therapy [3,4]. One of the most frequently used dosimetric tools is two-dimensional radiochromic film where a color is formed upon reaction with ionizing radiation [5].

A ferrous sulfate solution (Fricke solution) where ferrous (Fe^{2+}) ions are oxidized to ferric ions (Fe^{3+}) was the first chemical approach to quantifying ionizing radiation [6]. During irradiation water is decomposed to reactive HO· and H· radicals which further react with oxygen to produce the hydroperoxy radical which oxidizes the ferrous ions (Scheme 1) [7,8]. The ferric ion generates a blue color that is quantified spectrophotometrically.

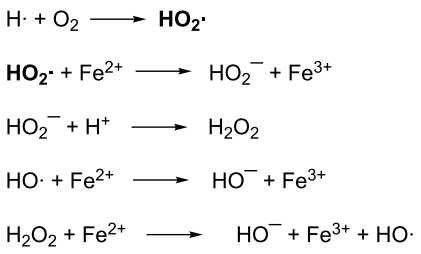

Scheme 1: Ionizing radiation reactions in the Fricke dosimeter.

In order to stabilize the geometric dose information in the Fricke solution aqueous based gel matrices containing the chelator xylenol orange were reported [9-11] with the molecular structure shown in Figure 1. When analyzed spectrophotometrically, a non-irradiated ferrous/agarose/xylenol orange (FAX) gel shows visible-light absorption at 440 nm; after exposure to ionizing radiation, there is an increase in absorption at 585 nm. Even though diffusion has been diminished it continues to be an issue [12].

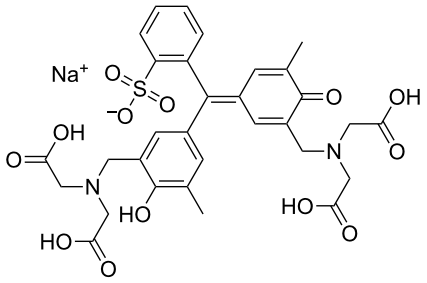

Figure 1: Structure of xylenol orange.

These diffusion limitations were overcome in a gel matrix by the polymerization of acrylamide with *N*,*N*'-methylenebisacrylamide and various monomers to yield a cloud like precipitate in the aqueous gel [13]. Due to the nature of their radical chemistry, polymer gel dosimeters have several limitations. They are susceptible to atmospheric oxygen inhibiting the polymerization processes. Irradiated dosimeters scatter light during optical scanning. The solutions are toxic, require 24 hours to equilibrate, and require a container to maintain the dosimeter shape [13].

Interest in a 3D dosimeter made of a transparent plastic was initially reported in 1961 [14]. The ideal dosimeter would be firm in structure and tissue equivalent [14]. This review describes such a 3D dosimeter, which we have been studying since 2004, composed primarily of the polymer polyurethane containing a radiochromic leuco dye and a radical initiator [15].

Review

Leuco dyes and radical initiators

Our initial studies focused on a broad class of compounds referred to as leuco dyes which switch between two chemical forms of which one is colorless. The transformations are caused by the in put of energy either from heat, light or change in pH [16]. The leuco dyes by themselves are not oxidized at clinical radiation doses. Consequently, radical initiators were necessary to promote the transformation. A variety of leuco dyes and radical initiators were screened for response to ionizing radiation. Initially the most promising leuco dye was leucomalachite green (LMG) which is a *N*,*N*-dimethyl-substituted triarylmethane (DTM) [17].

Triarylmethanes (TAMs) have wide ranging commercial, technological and medical applications [17]. In mechanistic chemistry, a triarylmethane demonstrated the first observable organic radical species [18]. TAMs were first synthesized using the Baeyer condensation in 1877 where one equivalent of aryl aldehyde is reacted with 2 equivalents of an electron-rich aromatic compound such as *N*,*N*-dimethylaniline [19] (Scheme 2). This reaction is usually carried out in the presence of various acids [16,20-35]. Microwave radiation procedures have also been reported [36,37].

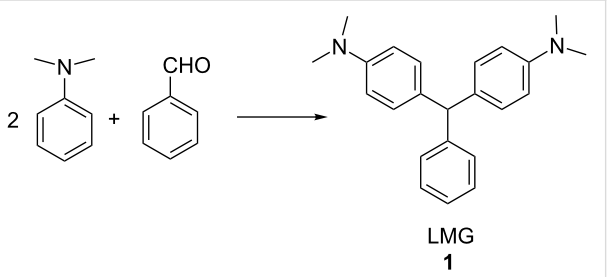

Scheme 2: Sulfuric acid/urea promoted synthesis of LMG.

We prepared several DTMs (Table 1) and measured their respective sensitivities to radiation [38-40] and confirmed structures by ^{1}H and ^{13}C NMR [20-36]. Progress of the reaction to form the DTMs was conveniently achieved by monitoring the ^{1}H NMR spectra, in which the representative CHO proton singlet of the starting aryl aldehyde (ca. 11 ppm) diminishes as the characteristic singlet of the methine DTM product (ca. 5.5 ppm) grows during the course of the reaction. The conformational structure of a DTM has been experimentally determined by computational modeling and vibrational spectra to be twisted much like a three-bladed propeller [20]. We found that numerous other aromatic aldehydes gave good results while highly hindered aryl aldehydes, such as pentamethylbenzaldehyde, 2-fluorenecarboxaldehyde, 9-anthracenecarboxaldehyde, and 1-pyrenecarboxaldehyde, yielded no detectable DTM prod-

Table 1: Synthesized DTBs and their LMG (**1**) relative radiation dose sensitivity.

DTB	Relative dose sensitivity	DTB	Relative dose sensitivity
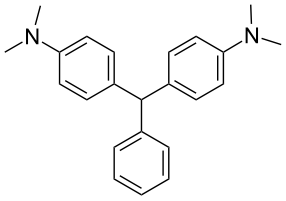 **1**	100	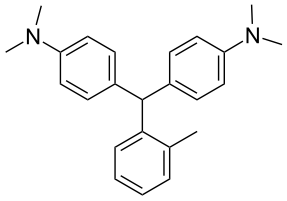 **5**	400
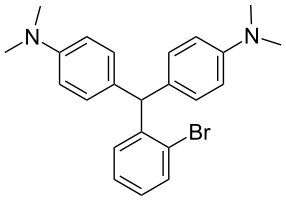 **2**	450	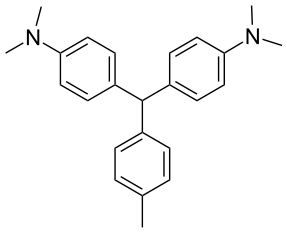 **6**	200
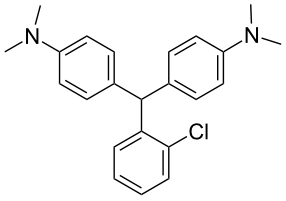 **3**	340	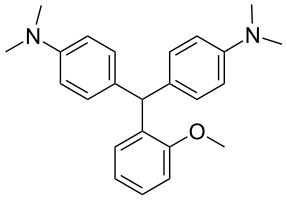 **7**	200
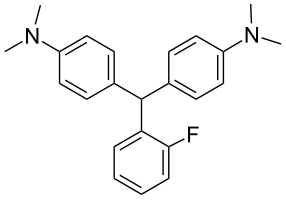 **4**	60	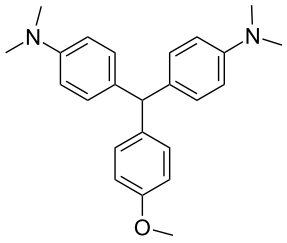 **8**	350

ucts. *N*,*N*,*N*-trialkyl-substituted triarylmethanes (e.g., leuco crystal violet) were also synthesized using the above synthetic procedures (e.g., 4-dimethylaminobenzaldehyde as starting aryl aldehyde) but these were too easily oxidized during fabrication of the dosimeters to be useful. Other *N*,*N*-dialkylaniline derviatives, (diethyl, dipropyl and dibutyl) provided the corresponding DTMs. However, only the *N*,*N*-diethyl derivatives proved to be useful as leuco dyes in our dosimeters.

Radical initiators

In order for the dosimeter to be reactive to a clinical radiation dose a radical initiator is required. The most effective class of initiators are halocarbons while azo- and peroxide-based initiators were unstable to the temperatures generated during the manufacture of the dosimeters [17,41]. The dose sensitivity was found to be consistent with the bond energy of the carbon–halogen bond. The observed sensitivity was in the order $R_3C–I > R_3C–Br > R_3C–Cl$ [42-44]. Due to the high electron density of radical initiators containing iodine even at relatively low concentrations (100 mM) result in dosimeters that are not tissue equivalent [43-45].

Polyurethane

Acrylic, epoxy, polycarbonate, polyester, polystyrene, polyurethane, polyvinyl chloride and silicone were the common transparent plastics that were evaluated as potential 3D dosimeter matrices [17]. Polyvinyl chlorides and silicones were not further considered since their effective atomic number is not tissue equivalent. Acrylates, polyesters, polystyrenes and polycarbonates were also eliminated due to the relatively high

exotherms created (>100 °C) during polymerization which prematurely oxidize the leuco dyes and rendered the dosimeter product unusable due to high background color. Epoxy resins, which use basic curatives, oxidize leuco dyes making them inappropriate for use as dosimetric matrices. This left the polyurethanes as the most viable option.

Transparent polyurethane starting materials are commercially available in two parts where part A is typically a mixture of dicyclohexylmethane-4,4'-diisocyanate (HMDI, Figure 2) and it's polyether prepolymer (CAS 531-70-03-9). While part B is a polyether or polyester polyol mixture which is proprietary [46]. Other aliphatic diisocyanate also used are 1,6-hexamethylene diisocyanate (HDI) and isophorone diisocyanate (IPDI) [47]. The polymerization reaction is exothermic and the rate of curing is dependent on the temperature, concentration of reactive groups, total volume of the reactants and type and concentration of metal catalyst. A number of metals have been studied in the polymer reaction but the most frequently used are dibutyltin dilaurate and phenyl mercuric acetate [48,49]. Besides catalyzing the polyurethane reaction metals (such as Bi, Sn, and Zn) at 1–3 mM have also have demonstrated an effect on the dose sensitivity of the dosimeter [50].

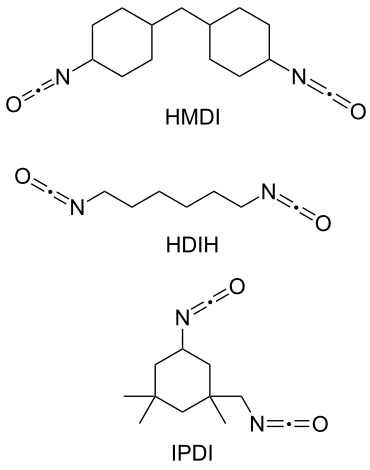

Figure 2: Aliphatic diisocyantes HMDI, HDI, IPDI.

The formulation procedure involves solubilizing the reactants, introducing the resulting solution into a mold; then allowing the polymer to cure at ambient temperature (>20 °C) in a pressure tank (30–60 psi). Performance of the reaction under pressure eliminates formation bubbles of carbon dioxide which is formed as a byproduct of the reaction of adventitious moisture with the diisocyanate. The degree of hardness of the dosimeter can be contolled by the type of polyol and catalyst utilized. Hardness ranging from rigid to tissue-like can be achieved [46]. The urethane reaction also tolerates up to relatively high addition (50%) of various solvents such as butyl acetate and most phthalates.

Dosimeter radiolysis

The initial radiolytic reaction is the dissociation of the radical initiator and subsequent reaction with LMG to create a radical which absorbs at ca 425 nm followed by the formation of the malachite green cation absorbing at 630 nm [51,52] (Figure 3).

The density of the radical is primarily on the central carbon with some charge distribution to the nitrogen substituents [51-53]. Radical stability is largely due to steric protection [53] of the central carbon which is consistent with what is observed for the radiation dose sensitivities of the eight DTMs which varied from 4.5 times greater than LMG for the most sterically hindered bromide derivative **2** to the least for the *ortho*-fluoride **4** with 0.6 less dose sensitivity than LMG (Table 1). This is also consistent for the *ortho*-methyl derivative **5** being more dose sensitive than it's *para*-methyl derivative **6**. There are electronic contributions of the *para*-methyl **6** in stabilizing the radical relative to **1** which has no *para*-substituent. For the *ortho*- and *para*-methoxy derivatives, **7** and **8**, respectively, the interpretation of the steric and electronic contributions is not as straight forward since **8** is more dose sensitive than **7** and almost that of **5**. The addition of polar aprotic solvents such as DMSO also enhances the dose sensitivity [52].

The other important characteristic is the post-irradiation color stability where in general those DTMs with the greatest steric hindrance near the methine carbon provide the greatest color stability. In contrast the *para*-substituent DTBs have demonstrated the most facile color fading [39]. A combination of singlet oxygen and light is thought to be the cause of bleaching of DTBs [54] even though for these dosimeters the effect is minimal [55].

Dosimeters

Due to the versatile nature of the dosimeter system described above virtually any shaped dosimeter can be fabricated as illustrated below (Figure 4).

Optical computed tomography (OCT) scanning

In order to create a 3D image of the irradiated dosimeter, it is placed inside a tank of refractive index matching solvent and on one side of the tank there is a collimated light source that shines through the dosimeter, a stepper motor rotates the dosimeter 360 degrees as the C-mount camera /lens [56] captures images at 1 degree increments (Figure 5). The 360 2D images are reassembled to give a full 3D image of the color density within the dosimeter [56].

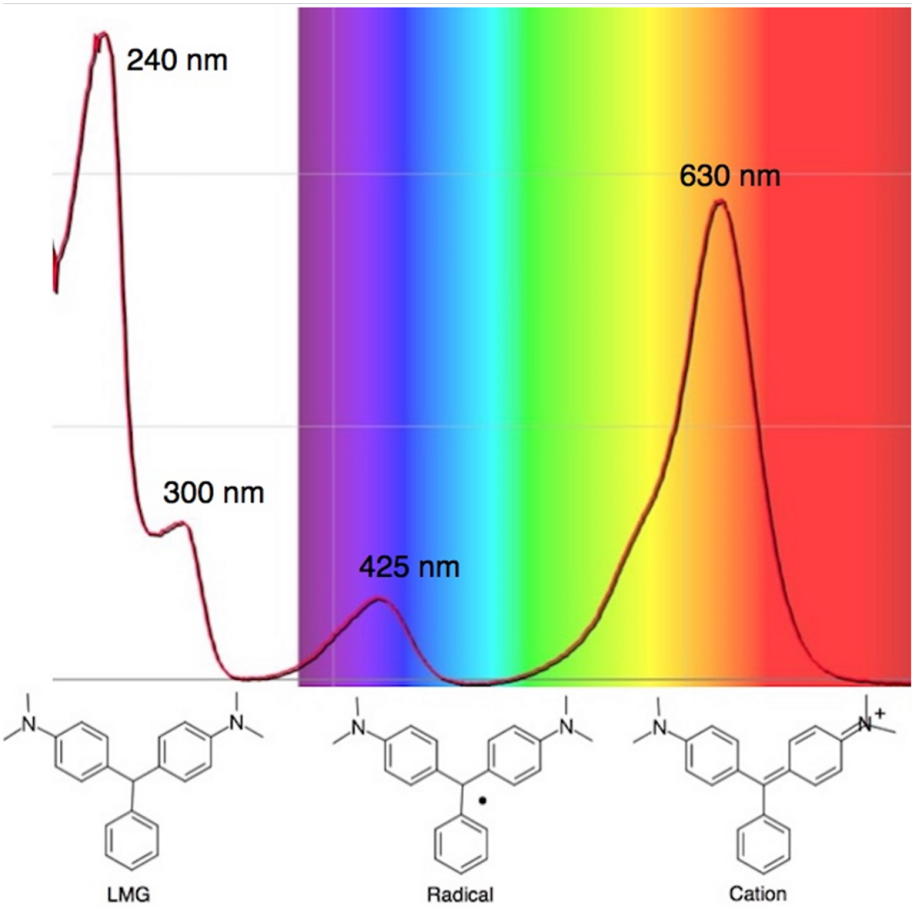

Figure 3: Absorption spectrum of irradiated leucomalachite green.

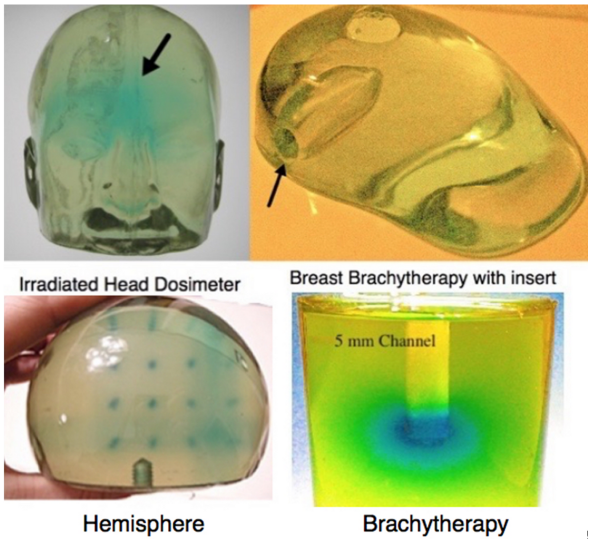

Figure 4: 3D dosimeters fabricated in our lab for a variety of radiation therapies. Top left a head dosimeter (12 kg); on the right a breast dosimeter with an inset for brachytherapy; bottom left an irradiated hemisphere; bottom right a cylindrical brachytherapy dosimeter with 5 mm channel for insert the radiation seed.

Overview

Due to the DTMs that differ in their physiochemical properties and polyurethanes that are commercially available a wide array of clinical related radiation treatment applications have been demonstrated. These include internally delivered radiation in which a cavity is created in the dosimeter for placement of radioactive seeds, deformable dosimetry in which the elastic properties of the dosimeter are manipulated to mimic those of human tissue, and reusable dosimetry [39,43,44]. Clinical research dosimeter adaptions have also made possible the study of alternative treatment approaches such as the addition of nanoparticles containing metals to the dosimeter to evaluate enhanced radiation effects [57] and utilizing mice in evaluating radiation treatment plans [58].

Conclusion

Over the last twelve years there has been significant progress made in developing chemical-based three-dimensional radiation detection systems but as of this review these dosimeters are primarily used in clinical research settings. This is partially due to the lack of a viable commercially available OCT scanner and

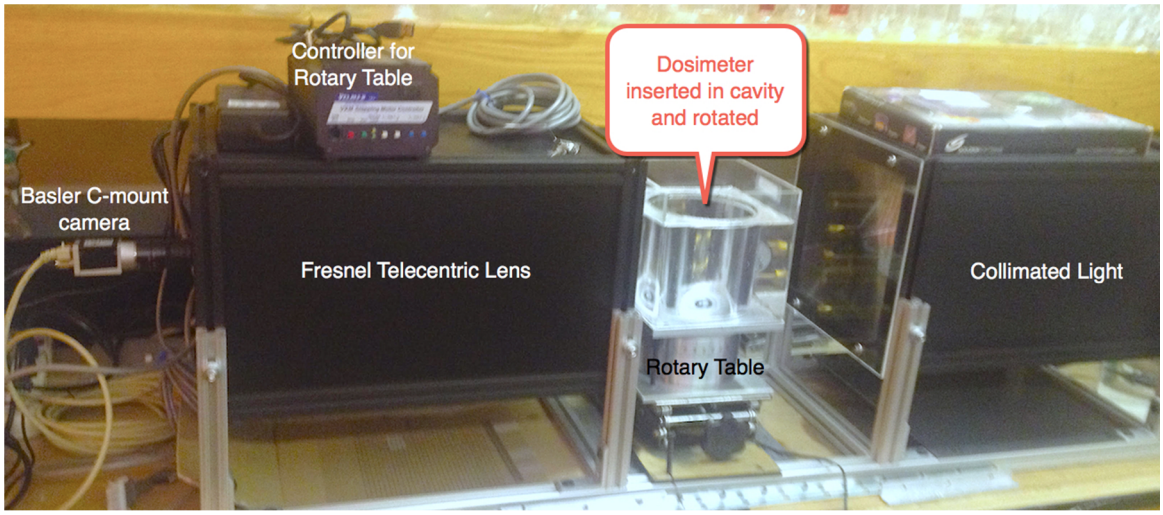

Figure 5: OCT scanner used in our lab to create 3D images.

availability of alternative semi-3D radiation measuring systems that interpolate 3D radiation dose distributions based on a sparse array of point detectors [59] which does not measure true 3D.

Acknowledgements

J. A. is grateful to the numerous students who have worked on this project and to Dr. Richard Wood for his review of this manuscript.

References

1. National Cancer Institute, Radiation Therapy for Cancer. https://www.cancer.gov/about-cancer/treatment/types/radiation-therapy (accessed Feb 1, 2017).
2. Molineu, A.; Hernandez, N.; Nguyen, T.; Ibbott, G.; Followill, D. *Med. Phys.* **2013,** *40,* No. 022101. doi:10.1118/1.4773309
3. Starkschall, G. *J. Appl. Clin. Med. Phys.* **2010,** *11,* 1. doi:10.1120/jacmp.v11i2.3328
4. Herman, M., *Medical Radiation: an Overview of the Issues.* On behalf of the American Association of Physicists in Medicine (AAPM), 2011.
5. Soares, C. G. *Radiat. Meas.* **2006,** *41* (Suppl. 1), S100–S116. doi:10.1016/j.radmeas.2007.01.007
6. Fricke, H.; Morse, S. *Am. J. Roentgenol., Radium Ther. Nucl. Med.* **1927,** *18,* 430–432.
7. Fricke, F. S.; Hart, E. J. Chemical Dosimetry. In *Radiation Dosimetry,* 2nd ed.; Attix, F. H.; Roesch, W. C., Eds.; Academic Press: New York, 1966; Vol. 2, p 167.
8. Schreiner, L. J. *J. Phys.: Conf. Ser.* **2004,** 9–21. doi:10.1088/1742-6596/3/1/003
9. Gore, J. C.; Yang, Y. S. *Phys. Med. Biol.* **1984,** *29,* 1189–1197. doi:10.1088/0031-9155/29/10/002
10. Bero, M. A.; Gilboy, W. B.; Glover, P. M.; Keddie, J. L. *Nucl. Instrum. Methods Phys. Res., Sect. A* **1999,** *422,* 617–620. doi:10.1016/S0168-9002(98)00970-X
11. Baldock, C.; Harris, P. J.; Piercy, A. R.; Healy, B. *Australas. Phys. Eng. Sci. Med.* **2001,** *24,* No. 19. doi:10.1007/BF03178282
12. Maryanski, M. J.; Gore, J. C.; Kennan, R. P.; Schulz, R. J. *Magn. Reson. Imaging* **1993,** *11,* 253–258. doi:10.1016/0730-725X(93)90030-H
13. Doran, S. J. *Appl. Radiat. Isot.* **2009,** *67,* 393–398. doi:10.1016/j.apradiso.2008.06.026
14. Potsaid, M. S.; Irie, G. *Radiology (Oak Brook, IL, U. S.)* **1961,** *77,* 61–65. doi:10.1148/77.1.61
15. Adamovics, J.; Maryanski, M. J. *Radiat. Prot. Dosim.* **2006,** *120,* 107–112. doi:10.1093/rpd/nci555
16. Muthyala, R., Ed. *Chemistry and applications of leuco dyes;* Plenum Press: New York, 1997.
17. Adamovics, J.; Jordan, K.; Dietrick, J. *J. Phys.: Conf. Ser.* **2006,** *56,* 172. doi:10.1088/1742-6596/56/1/020
18. Gomberg, M. *J. Am. Chem. Soc.* **1900,** *22,* 757–771. doi:10.1021/ja02049a006
19. Fischer, O. *Ber. Dtsch. Chem. Ges.* **1877,** *10,* 1624.
20. Bardajee, G. R. *Beilstein J. Org. Chem.* **2011,** *31,* 135–144. doi:10.3762/bjoc.7.19
21. Halimehjani, A. Z.; Shamiri, E. V.; Hooshmand, S. E. *J. Appl. Chem. Res.* **2016,** *10,* 79–85.
22. Muthyala, R.; Katritzky, A. R.; Lan, X. *Dyes Pigm.* **1994,** *25,* 303–324. doi:10.1016/0143-7208(94)87017-9
23. Ritchie, C. D.; Sager, W. F.; Lewis, E. S. *J. Am. Chem. Soc.* **1962,** *84,* 2349–2356. doi:10.1021/ja00871a016
24. Alvaro, M.; Garcia, H.; Sanjuán, A.; Esplá, M. *Appl. Catal., A* **1998,** *175,* 105–112. doi:10.1016/S0926-860X(98)00213-0
25. Chalk, A. J.; Halpern, J.; Harkness, A. C. *J. Am. Chem. Soc.* **1959,** *81,* 5854–5857. doi:10.1021/ja01531a004
26. Zhang, Z.-H.; Yang, F.; Li, T.-S.; Fu, C.-G. *Synth. Commun.* **1997,** *27,* 3823–3828. doi:10.1080/00397919708007307
27. An, L.-T.; Ding, F.-Q.; Zou, J.-P. *Dyes Pigm.* **2008,** *77,* 478–480. doi:10.1016/j.dyepig.2007.06.004
28. Bardajee, G. R.; Jafarpour, F. *Cent. Eur. J. Chem.* **2009,** *7,* No. 138. doi:10.2478/s11532-008-0100-x

29. Jafarpour, F.; Bardajee, G. R.; Pirelahi, H.; Oroojpour, V.; Dehnamaki, H.; Rahmdel, S. *Chin. J. Chem.* **2009,** *27,* 1415–1419. doi:10.1002/cjoc.200990238
30. Rao, H. S. P.; Rao, A. V. B. *Beilstein J. Org. Chem.* **2016,** *11,* 496–504. doi:10.3762/bjoc.12.49
31. Nambo, M.; Crudden, C. M. *ACS Catal.* **2015,** *5,* 4734–4742. doi:10.1021/acscatal.5b00909
32. Nair, V.; Thomas, S.; Mathew, S. C.; Abhilash, K. G. *Tetrahedron* **2006,** *62,* 6731–6747. doi:10.1016/j.tet.2006.04.081
33. Li, Z.; Duan, Z.; Kang, J.; Wang, H.; Yu, L.; Wu, Y. *Tetrahedron* **2008,** *64,* 1924–1930. doi:10.1016/j.tet.2007.11.080
34. Guzmán-Lucero, D.; Guzmán, J.; Likhatchev, D.; Martinez-Palou, R. *Tetrahedron Lett.* **2005,** *46,* 1119–1122. doi:10.1016/j.tetlet.2004.12.091
35. Malpert, J. H.; Grinevich, O.; Strehmel, B.; Jarikov, V.; Mejiritski, A.; Neckers, D. C. *Tetrahedron* **2001,** *57,* 967–974. doi:10.1016/S0040-4020(00)01088-7
36. Khosropour, A. R.; Esmaeilpoor, K.; Moradie, A. *J. Iran. Chem. Soc.* **2006,** *3,* 81–84. doi:10.1007/BF03245794
37. Reddy, C. S.; Nagaraj, A.; Srinivas, A.; Reddy, G. P. *Indian J. Chem., Sect. B* **2009,** *48,* 248–254.
38. Alqathami, M.; Adamovics, J.; Benning, R.; Qiao, G.; Geso, M.; Blencowe, A. *Radiat. Phys. Chem.* **2013,** *85,* 204–209. doi:10.1016/j.radphyschem.2012.11.006
39. Juang, T. Clinical and Research Applications of 3D Dosimetry. Ph.D. Thesis, Duke University, Durham, North Carolina, USA, 2015.
40. Adamovics, J. Three-dimensional shaped solid dosimeter and method of use. U.S. Pat. Appl. US20070020793 A1, Jan 25, 2007.
41. Miyaji, T.; Tokita, S.; Tachikawa, T.; Azuma, C. *J. Photopolym. Sci. Technol.* **2001,** *14,* 225–226. doi:10.2494/photopolymer.14.225
42. Denisov, E. T.; Denisova, T. G.; Pokidova, T. S. *Handbook of free radical initiators;* John Wiley & Sons, Inc.: New York, 2005.
43. Alqathami, M.; Blencowe, A.; Qiao, G.; Butler, D.; Geso, M. *Radiat. Phys. Chem.* **2012,** *81,* 867–873. doi:10.1016/j.radphyschem.2012.03.022
44. Alqathami, M. Novel 3D radiochromic dosimeters for advanced radiotherapy techniques. Ph.D. Thesis, RMIT University, Australia, 2013.
45. Singh, V. P.; Badiger, N. M. *J. Med. Phys.* **2014,** *39,* 24–31. doi:10.4103/0971-6203.125489
46. BJB Enterprises. https://bjbenterprises.com/index.php/polyurethanes/castable/ (accessed Feb 1, 2017).
47. Delebecq, E.; Pascault, J.-P.; Boutevin, B.; Ganachaud, F. *Chem. Rev.* **2013,** *113,* 80–118. doi:10.1021/cr300195n
48. Saunders, K. J. Polyurethanes. *Organic Polymer Chemistry;* Springer Netherlands: Dordrecht, 1988; pp 358–387. doi:10.1007/978-94-009-1195-6_16
49. de Lima, V.; da Silva Pelissoli, N.; Dullius, J.; Ligabue, R.; Einloft, S. *J. Appl. Polym. Sci.* **2010,** *115,* 1797–1802. doi:10.1002/app.31298
50. Alqathami, M.; Blencowe, A.; Qiao, G.; Adamovics, J.; Geso, M. *Radiat. Phys. Chem.* **2012,** *81,* 1688–1695. doi:10.1016/j.radphyschem.2012.06.004
51. Ayyangar, N. R.; Tilak, B. D. Basic Dyes. In *The Chemistry of Synthetic Dyes;* Venkataraman, K., Ed.; Academic Press: New York, 1971; Vol. IV, pp 103–160. doi:10.1016/B978-0-12-717004-6.50010-2
52. Bobrowski, K.; Dzierzkowska, G.; Grodkowski, J.; Stuglik, Z.; Zagorski, Z. P.; McLaughlin, W. L. *J. Phys. Chem.* **1985,** *89,* 4358–4366. doi:10.1021/j100266a041
53. Hicks, R. G. *Org. Biomol. Chem.* **2007,** *5,* 1321–1338. doi:10.1039/b617142g
54. Oda, H. *Dyes Pigm.* **2005,** *66,* 103–108. doi:10.1016/j.dyepig.2004.09.009
55. Alqathami, M.; Blencowe, A.; Ibbott, G. *Phys. Med. Biol.* **2016,** *61,* 813–824. doi:10.1088/0031-9155/61/2/813
56. Thomas, A.; Newton, J.; Adamovics, J.; Oldham, M. *Med. Phys.* **2011,** *38,* 4846–4857. doi:10.1118/1.3611042
57. Alqathami, M.; Blencowe, A.; Yeo, U. J.; Doran, S. J.; Qiao, G.; Geso, M. *Int. J. Radiat. Oncol., Biol., Phys.* **2012,** *84,* e549–e555. doi:10.1016/j.ijrobp.2012.05.029
58. Bache, S. T.; Juang, T.; Belley, M. D.; Koontz, B. F.; Adamovics, J.; Yishizumi, T. T.; Kirsch, D. G.; Oldham, M. *Med. Phys.* **2015,** *42,* 846–855. doi:10.1118/1.4905489
59. Feygelman, V.; Zhang, G.; Stevens, C.; Nelms, B. E. *J. Appl. Clin. Med. Phys.* **2011,** *12,* 146–168. doi:10.1120/jacmp.v12i2.3346

License and Terms

BEILSTEIN JOURNAL OF ORGANIC CHEMISTRY

Block copolymers from ionic liquids for the preparation of thin carbonaceous shells

Sadaf Hanif, Bernd Oschmann, Dmitri Spetter, Muhammad Nawaz Tahir, Wolfgang Tremel and Rudolf Zentel*

Full Research Paper

Open Access

Address:
Institute for Organic Chemistry, University of Mainz, Duesbergweg 10-14, 55128 Mainz, Germany

Email:
Rudolf Zentel* - zentel@uni-mainz.de

* Corresponding author

Keywords:
block copolymer; carbon; ionic liquid; polymeric ionic liquid; RAFT polymerization

Beilstein J. Org. Chem. **2017,** *13,* 1693–1701.
doi:10.3762/bjoc.13.163

Received: 11 May 2017
Accepted: 02 August 2017
Published: 16 August 2017

This article is part of the Thematic Series "Spatial effects in polymer chemistry".

Guest Editor: H. Ritter

Abstract

This paper describes the controlled radical polymerization of an ionic-liquid monomer by RAFT polymerization. This allows the control over the molecular weight of ionic liquid blocks in the range of 8000 and 22000 and of the block-copolymer synthesis. In this work we focus on block copolymers with an anchor block. They can be used to control the formation of TiO_2 nanoparticles, which are functionalized thereafter with a block of ionic-liquid polymer. Pyrolysis of these polymer functionalized inorganic nanoparticles leads to TiO_2 nanoparticles coated with a thin carbonaceous shell. Such materials may, e.g., be interesting as battery materials.

Introduction

Ionic liquids (ILs) are organic salts. Most of them have a melting point below 100 °C [1,2]. These organic salts do not have the same structure like inorganic salts. This is due to the structure of the ion pairs. They are built of organic asymmetric cations, like imidazolium, pyridinium or alkylammonium and inorganic anions, such as halides, mineral acid anions, or polyatomic inorganic anions (PF_6^-, BF_4^-) [3]. Because of the steric hindrance, they are not able to build a strong lattice like inorganic salts. Therefore, not much energy is needed to overcome the lattice energy and melt the salt. Ion liquids are also called “green solvents”, because of their low vapor pressure, fire resistance and thermal stability [4]. Beside this, they have a high ionic conductivity, large heat capacity and good thermal and chemical stability [5]. Properties, like solubility can be varied easily by exchanging the anion. Ionic liquids are often used as an electrolyte or organic solvent. Furthermore, they are also used in catalysis or in organic synthesis. Due to their selective solubility for ions [6-8], they can be used to predetermine the

presence of ions on surfaces, a property which is very important for electrochemical conversions or the uptake of ions into the crystal lattice [9].

Polymeric ionic liquids (PILs) are made of ionic liquids with a polymerizable group, like a vinyl or acrylate group. They build a new class of macromolecules with unique properties. Alternatively, it is possible to coordinate low molar mass ionic liquids to polymers by complexation of their anions to cyclodextrin side chains. This can have an influence on their lower critical solution temperature (LCST) [10,11]. Beside their use as organic solvent, they are applied as catalytic membranes, thermotropic liquid crystals [12], polymer electrolytes, ionic conductive materials, CO_2 absorbing materials, microwave absorbing materials and porous materials [4]. Most of these polymers were synthesized by free radical polymerization. There are just few reports about controlled/living radical polymerization, like nitroxide-mediated polymerization (NMP), atom transfer radical polymerization (ATRP) and reversible addition–fragmentation chain transfer polymerization (RAFT) [2]. In general, by controlled radical polymerization techniques it is possible to prepare polymers with narrow polydispersity, controlled molecular weight and also well-defined block copolymers. Such block copolymers with ionic liquid blocks might enable to control the properties of PILs spatially. An interesting aspect of this might be (i) a reduction of the dimension of the ion conductivity in PIL block copolymers due to their demixed morphology or (ii) the control of ion conduction near surfaces, if PIL brushes are fixed to a surface [13]. This last example of a spatially restricted access of ions to a surface can be very interesting in combination with redox reactions [14,15], a case in which the accessibility of special ions to the surface is crucial. Another aspect where spatial control gets crucial is the locally directed formation of thin carbonaceous shells. As demonstrated by Yuan et al., PILs are suitable carbon precursors with high carbon yields and good electric conductivity [16]. There are many different morphologies of carbon achievable, like hallow carbon spheres [17], nanotubes, membranes and fibers [18]. Due to their charged nature the PILs show a low vapor pressure and are non-volatile, leading to high carbon yields [19]. Furthermore, PILs offer the possibility of selective doping of the carbon by the choice of the counter ion. Heteroatoms like nitrogen and phosphor can be incorporated into the carbonaceous shell to improve or enhance properties like catalytic and electronic conductivity [18,20,21].

Independently from the work on polymeric ionic liquids, thin shells of carbonaceous materials around inorganic nanoparticles have been intensively investigated recently [22-25]. This interest is related to the search for improved battery materials for the reversible storage of electricity. To further improve batteries in terms of energy and power density, current research activities are directed, for example, towards new electrode active materials like TiO_2, ZnO, Si or $LiFePO_4$ [26]. However, both electronic and ionic conductivity of these materials are typically rather low. To overcome this issue, the combination of nanostructuring and the incorporation of conductive carbon was shown to be a successful strategy [27]. While nanostructuring of inorganic particles increases the electrode/electrolyte contact area and allows an easier diffusion of the cations, the incorporation of electronic transport pathways allows an improved charging of the nanoparticles [27]. In this context carbonaceous secondary structures and coatings [27,28] can be applied to increase electronic conductivity. In addition, the surface reactivity of the nanosized particles in contact with the electrolyte is reduced. Recently, it could be shown that block copolymers with an anchor group could bind to inorganic nanoparticle surfaces, where a second polymer block could be converted into a conductive carbon shell, improving the properties of nanoparticles like TiO_2 or ZnO with respect to the reversible storage of lithium or sodium ions [22-25]. Using a block copolymer with an anchor group to bind on the nanoparticle surface allows the formation of a homogenous and thin coating. So far, polyacrylonitrile has been used as a carbonizable block, but polymeric ionic liquids are attractive as well.

An approach to coat nanoparticles with either (i) a thin film of PILs or (ii) a homogeneous carbonaceous layer derived from ionic liquids requires – at first – a synthetic route to block copolymers, which possess besides an anchor block [29], a block of polymerized ionic liquid monomers. Such a route will be presented here.

Results and Discussion

The schematic synthesis route to carbon-coated TiO_2 nanoparticles using block copolymers is displayed in Figure 1a. The block copolymers containing an anchoring block and a carbonizable block should function – at first – as a ligand for the nanoparticle synthesis to produce polymer functionalized nanoparticles. The heat treatment at 650 °C of the hybrid material enables the conversion of the polymer shell into a carbon shell. The required block copolymers containing the carbonizable block and the anchoring block, which can bind onto the nanoparticle surface, was synthesized by RAFT polymerization as described in Figure 1b.

In a first step the PIL block is synthesized using 1-vinyl-3-cyanomethylimidazolium bromide (**1**) as an IL monomer, which was prepared following a literature procedure [16]. During this process the nitrogen atom in the imidazole ring in position 3 is quaternized. Monomer **1** was polymerized with 2-dodecylsulfanylthiocarbonylsulfanyl-2-methylpropionic acid (DMP, **2**)

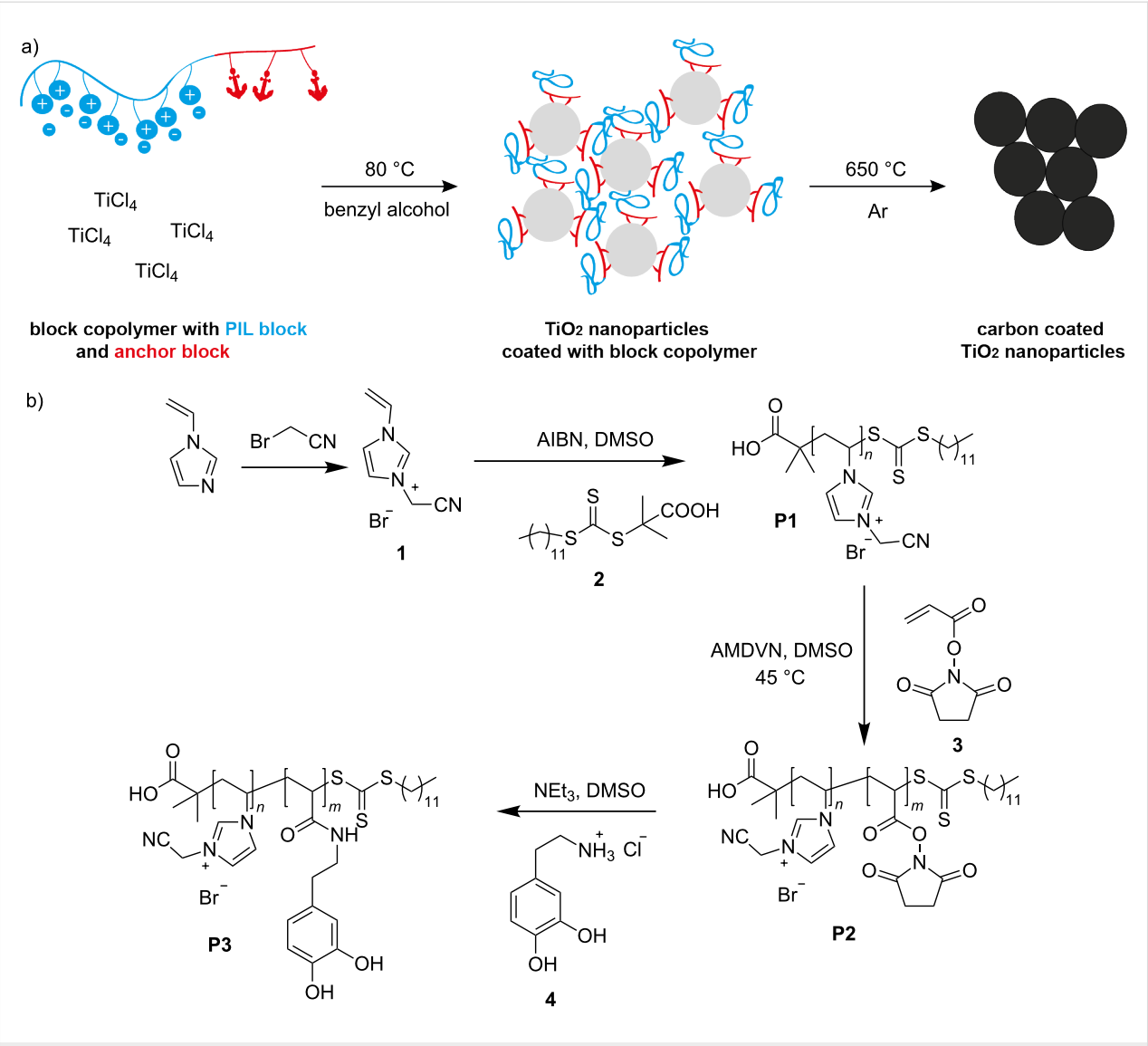

Figure 1: (a) Schematic illustration of the synthesis route of carbon coated TiO_2 nanoparticles. (Left) in situ synthesis of the TiO_2 nanoparticles with the block copolymer as a ligand on the surface followed by the pyrolysis of the particles resulting in homogenously coated nanoparticles. (b) Synthesis route for the preparation of the block copolymer, beginning from the monomer synthesis to the block copolymer and finally the post-polymerization modification step.

[30] as a chain transfer agent (CTA) and α,α'-azoisobutyronitrile (AIBN) as the initiator in the RAFT polymerization. Even though the synthesis of PILs by applying a controlled process has been reported to be difficult [1], we could obtain PILs in a controlled way by using a high ratio of initiator to CTA (1:2). Following this procedure we could vary the molecular weight of the PIL by variation of the CTA:monomer ratio and synthesize different block copolymers (see Table 1). The obtained polymers were characterized by size-exclusion chromatography (SEC), the elugrams are shown in Figure 2 and Figure S4 (Supporting Information File 1). The polymers described in our work have a narrow polydispersity index (PDI) varying from 1.11 (for the PIL block) up to 1.23 for the block copolymer. In order to show how controllable the polymerization of IL by RAFT polymerization is, we synthesized three block copolymers with different chain lengths for both the PIL block and the anchor block. For the PIL block we could synthesize short blocks, containing only 22 repeating units, as well as longer chain lengths consisting of 38 or 72 monomer units (as estimated by ^{1}H NMR). The corresponding SEC elugrams (Figure 2 and Figure S4, Supporting Information File 1) reveal that the dispersity of the first block is quite narrow in all cases (PDI < 1.20). All the data regarding molecular weight and polydispersity are listed in Table 1. The average block length of the anchor group was kept constant with 20 repeating units (estimated by ^{1}H NMR spectroscopy).

Table 1: Molecular weight and polydispersity of all synthesized polymers. **P1A–C** represents the PIL block. **P2A–C** represent the block copolymer and **P3A–C** the polymer after post-polymerization.

P1	M_n (g mol^{-1})	PDI	P2	M_n (g mol^{-1})	PDI	P3	M_n (g mol^{-1})	PDI
P1A	8 400	1.12	**P2A**	12 501	1.25	**P3A**	13 660	1.31
P1B	15 930	1.11	**P2B**	22 718	1.17	**P3B**	23 922	1.23
P1C	21 926	1.20	**P2C**	27 205	1.26	**P3C**	29 459	1.54

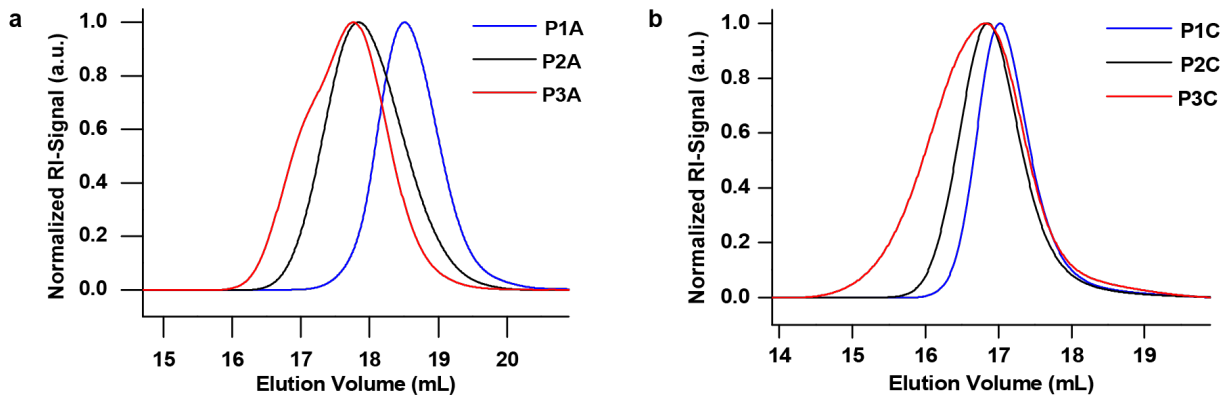

Figure 2: a) Size-exclusion chromatography of **P1A** (blue), **P2A** (black) and **P3A** (red) and b) size-exclusion chromatography of **P1C** (blue), **P2C** (black) and **P3C** (red) in hexafluoroisopropanol (HFIP). As expected, **P2** shows a shift towards higher molecular weight, which confirms the successful synthesis of the block copolymer. **P3** shows no further shift but a broader distribution, due to the dopamine group which interacts with the column material.

All synthesized polymers were characterized by ^{1}H NMR spectroscopy, which is shown in Figure 3. For the PIL block the spectrum is shown in blue. The resonance signals which occur at higher chemical shifts (7.8–9.8 ppm) belong to the protons in the imidazolium ring. The chemical shifts at 0.8 ppm and 1.2 ppm belong to the alkyl chain of the CTA, while the remaining signals are attributed to the polymer. The DOSY NMR spectrum (Figure S3 in Supporting Information File 1) proves that there is only one polymeric species. This excludes a mixture of homopolymers and demonstrates that block copolymers are obtained. The anchor block was thereby introduced in two synthetic steps. First, a block copolymerization using a reactive ester monomer was performed. Subsequently, the reactive ester block was aminolyzed to introduce dopamine (**4**) as the anchoring unit. Dopamine has been proven to coordinate well on transition metal oxide surfaces [29,31,32]. This route was chosen because dopamine cannot be polymerized in a radical process due to its phenolic structure that would act as an inhibitor. Hence we use the reactive ester chemistry by first introducing an active ester block, which can be easily substituted afterwards in a post-polymerization modification process. *N*-Acryloxysuccinimide (NAS, **3**) was chosen as a reactive ester because of its tolerance towards trace amounts of water present in DMSO, which is required for the block copolymerization as a polar solvent to solubilize the PIL macro-CTA. Optimized reaction conditions using 2,2-azobis(4-methoxy-2,4-dimethylvaleronitrile) (AMDVN) as an initiator, resulted in the successful block copolymerization. This was confirmed by ^{1}H NMR spectroscopy after stirring for 20 hours at 45 °C. The broad signal which is typical for the NAS block can be observed at 2.8 ppm as shown in Figure 3. Another proof for the formation of a reactive ester block was given by IR spectroscopy. A new band can be observed at 1732 cm^{-1} and is assigned to the carbonyl group of the reactive ester (see Figure S5, Supporting Information File 1). In the last step the aminolysis of the reactive ester block with dopamine was performed, which leads also to a partial removal of the thioester end group. For this purpose a large excess of dopamine was applied. The ^{1}H NMR spectrum in Figure 3 proves the successful conversion of the reactive ester to the corresponding amide. The NAS shift at 2.8 ppm vanished, while new shifts appeared at 6.5 ppm and in the range of 8.5–8.8 ppm corresponding to the aromatic ring of dopamine. This can be further confirmed by IR spectroscopy (Figure S6, Supporting Information File 1), where the NAS band disappeared, whereas a new band at 1647 cm^{-1} appears, which is assigned to the newly formed amide bond.

The block copolymers **P1C**–**P3C** were used for the in situ synthesis of TiO_2 particles [33,34]. Here, the block copolymer has several functions. It acts as a ligand during the nanoparticle syn-

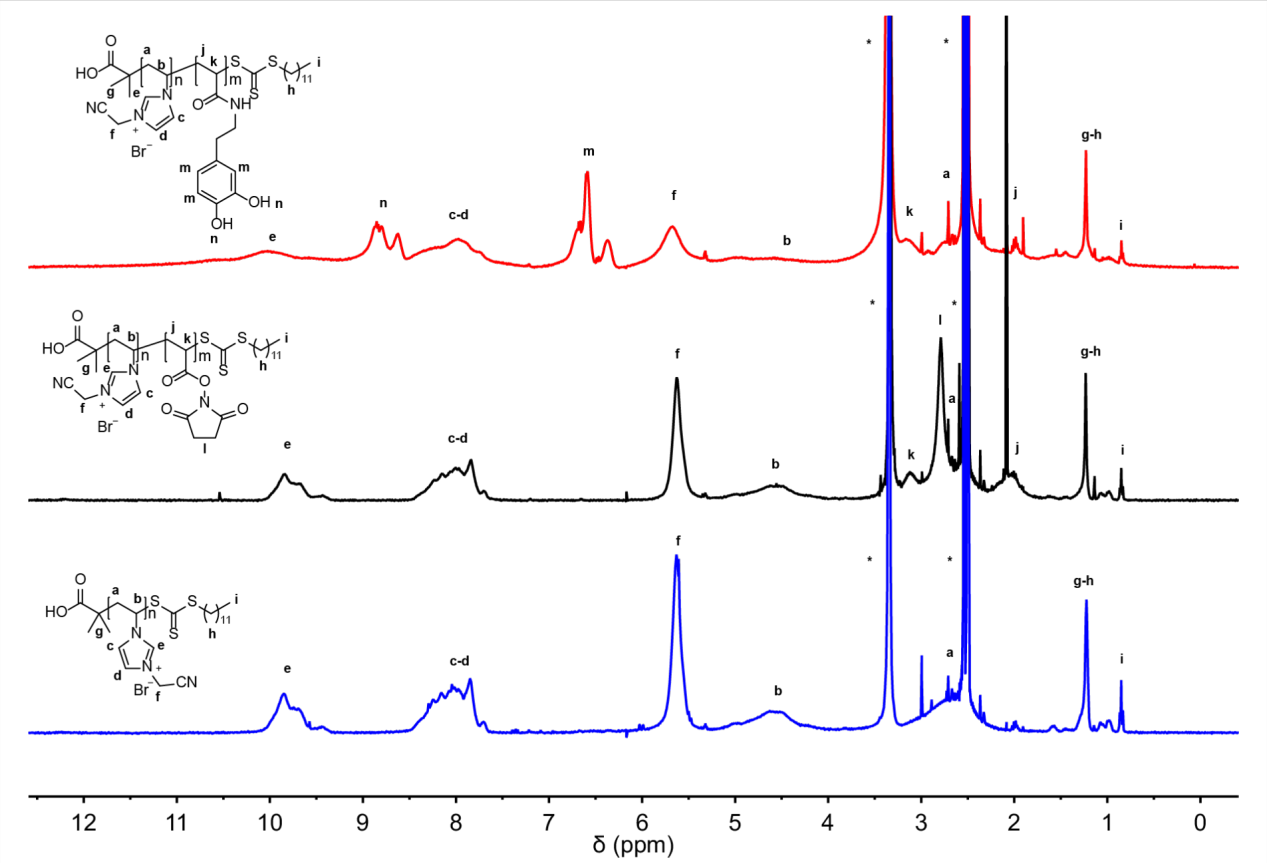

Figure 3: ^{1}H NMR spectrum of **P1**, **P2** and **P3**, all measured in DMSO-d_6. In blue the spectrum of the PIL block is shown. The black spectrum belongs to the block copolymer with the reactive ester block. At 2.8 ppm a new shift can be seen, which is dedicated to the succinimide group in the reactive ester. The spectrum in red shows the polymer after the post-polymerization step. The shift at 2.8 ppm from the reactive ester disappeared. At 6.5 ppm and 8.8 ppm the chemical shifts from the dopamine group are shown.

thesis avoiding the aggregation of nanoparticles, which would lower the surface area and increases the diffusion distances in the final particles for Na or Li ions. For the in situ nanoparticle synthesis $TiCl_4$ was dissolved in benzyl alcohol and the block copolymer was added and stirred at 80 °C for 72 hours. The resulting brown suspension was precipitated using chloroform and hexane (1:3) and the precipitated product was centrifuged. The process was repeated three times to remove solvent and unbound ligand. The product was dried under vacuum at room temperature. To examine the content of ligands on the surface, thermogravimetric analysis was performed (TGA) after several centrifugation steps, as shown in Figure 4a. A total weight loss of 20% was determined. Although the particles were dried proper in high vacuum a shoulder around 200 °C shows up. This shoulder belongs to benzyl alcohol, which was used as a solvent for the synthesis. As a rough estimate for the weight loss of the coordinated polymer only the weight loss above 240 °C is considered to 20%. For the carbonization process the hybrid material was pyrolyzed in argon atmosphere and heated up to 650 °C. The application of higher temperatures (above 700 °C) is not advisable. Due to the use of TiO_2, phase transitions of the anatase TiO_2 might occur, which leads to a mixture of anatase and rutile TiO_2. XRD measurements (Figure 5) show that under the applied conditions, the pyrolyzed nanoparticles still contain TiO_2.

In addition, a macroscopic color change of the hybrid material can be observed. As-synthesized TiO_2 nanoparticles coated with the block copolymer looks brown due to the bound catechol. However, the color turns black after the pyrolysis (Figure 4d) indicating the presence of carbon material. This was proven by Raman spectroscopy revealing typical carbonaceous bands, such as the G-band at 1584 cm^{-1} and the D-band at 1355 cm^{-1}, which is shown in Figure 4c. Furthermore, the residual carbonaceous content was determined by TGA, where the weight loss decreases from 20% (for the block copolymer coated particles) to 10% for the carbon coated particles (Figure 4a).

The resulting particles were also characterized by transmission electron microscopy (TEM), and corresponding images are shown in Figure 6a and 6b. The average particle diameter is ≈8 nm. Figure 6b shows nanoparticles sheathed and

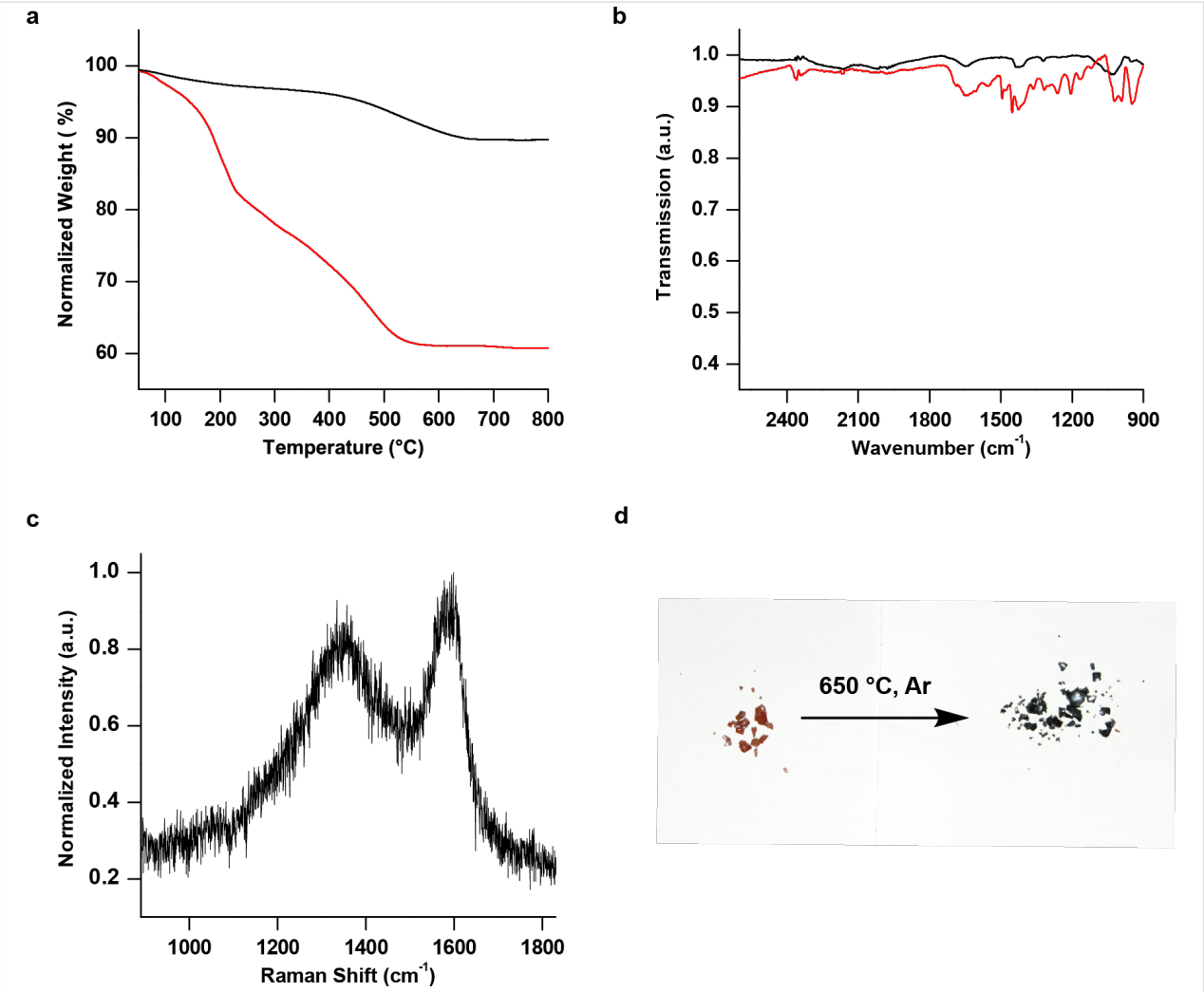

Figure 4: a) TGA measurement of the particles coated with block copolymer and particles coated with carbon, measured under oxygen atmosphere with a heating rate of 5 °C/min. In red the functionalized particles before pyrolysis. The weight loss up to 200 °C indicates the presence of the solvent (benzyl alcohol) which was used for the preparation of the particles. A mass loss of 20% can be observed. The black curve shows the functionalized particles after pyrolysis. b) IR spectrum of pure TiO_2 particles (black) and the functionalized particles with the block copolymer on the surface (red). New bands are visible from 1685 cm^{-1} to 1166 cm^{-1} attributed to the block copolymer, showing their presence on the surface. c) Raman spectrum of pyrolyzed particles, showing the D-Band (1355 cm^{-1}) and G-band (1584 cm^{-1}), which proves the carbonaceous structure. d) Picture of the functionalized particles before (brown) and after pyrolysis (black).

connected through lattices which might also help to provide longer paths for electrons to travel within the electrode. Summarizing, the Raman spectrum, the TGA measurements and the TEM images proves the success of the formation of a thin coating around the TiO_2 particles. Currently, we are investigating the application of the hybrid material in batteries.

Conclusion

In conclusion, we were able to synthesize well-defined block copolymers containing a PIL block and a reactive ester block. Besides, we showed the post-polymerization modification of these polymers, while remaining the block copolymer structure and simultaneously introducing an anchor group. Afterwards, we showed the successful in situ synthesis of TiO_2 particles with the block copolymer as a ligand on the surface. Raman spectroscopy and TEM images show that PILs are suitable carbon precursors and the herein introduced materials can be further applied as anode material in lithium or sodium ion batteries.

Experimental

All chemicals were acquired from commercial sources (Acros or Sigma-Aldrich) and used without further purification. Synthesis and structural characterization: NMR spectroscopy was applied with a Bruker ARX 400 spectrometer. Fourier-transform infrared (FTIR) spectroscopy was conducted on a Jasco FT/IR 4100 spectrometer with an attenuated total reflectance

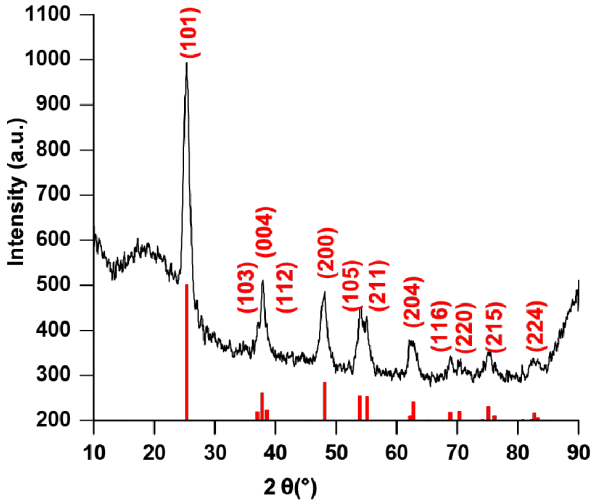

Figure 5: PXRD pattern of carbon-coated TiO_2 particles.

(ATR) unit. The SEC measurements were carried out at 40 °C with a solution of HFIP with 3 g L^{-1} K^+TFA^- as eluent. Modified silica was used as stationary phase and a refractive index detector, JASCO G1362A RID, was used. Poly(methyl methacrylate) (PMMA) was used as calibration standard. TGA was performed with a Perkin Elmer Pyris 6 instrument with an oxygen flow. Raman spectroscopy was conducted with Horiba Jobin Y LabRAM HR spectrometer with a frequency doubled neodymium-doped yttrium aluminum garnet (Nd:YAG) laser. X-ray diffraction was performed on a Siemens D 5000 diffractometer equipped with Cu Kα radiation source (wavelength of 1.54056 Å) for both as synthesized as well as carbon coated TiO_2 nanoparticles. TEM samples were prepared by dispersing the sample in ethanol and drop casting on 300 mesh carbon coated copper grids. The images were captured with a transmission electron microscope, a Tecnai G2 Spirit with an acceleration voltage of 120 kV.

Synthesis of PIL: The IL and also DMP which was used as chain transfer agent, were synthesized as already described in the literature [16,30]. For the RAFT polymerization the IL monomer (1 equiv), DMP (0.05 equiv for **P1A**, 0.02 equiv for **P1B**, 0.013 equiv for **P1C**) and the initiator AIBN (0.025 equiv for **P1A**, 0.01 equiv for **P1B**, $6.5 \cdot 10^{-3}$ equiv for **P1C**) were mixed together and dissolved in DMSO, followed by three freeze-pump-thaw cycles. The reaction mixture was stirred for 20 h at 70 °C. Afterwards the mixture was purified by precipitation in acetone. ^{1}H NMR (400 MHz, DMSO-d_6) δ (ppm) 9.85 (m, C-2 of imidazolium ring), 8.01 (m, C-4 and C-5 of imidazolium ring), 5.63 (s, CH_2CN), 4.62 (br, polymer backbone), 2.91 (m, polymer backbone), 1.23 (m, CTA dodecyl chain), 0.85 (t, dodecyl-CH_3 of CTA); FTIR ν: 2973 (w), 2255 (w), 1626 (m), 1553 (s), 1425 (m), 1159 (s), 1019 (m), 748 cm^{-1} (w).

Synthesis of P (IL-*b*-NAS): PIL was used as macro-CTA. Together with NAS (20 equiv) and 2,2-azobis(4-methoxy-2,4-dimethylvaleronitrile) (0.2 equiv) PIL was dissolved in DMSO. After three freeze-pump-thaw cycles the mixture was stirred at 40 °C for 20 h. Afterwards the polymer was worked up by precipitation in acetone. ^{1}H NMR (400 MHz, DMSO-d_6) δ (ppm) 9.85 (m, C-2 of imidazolium ring), 7.85 (m, C-4 and C-5 of imidazolium ring), 5.64 (s, CH_2CN), 4.51 (br, polymer backbone), 2.91 (m, polymer backbone), 2.80 (s, CH_2-CH_2 of

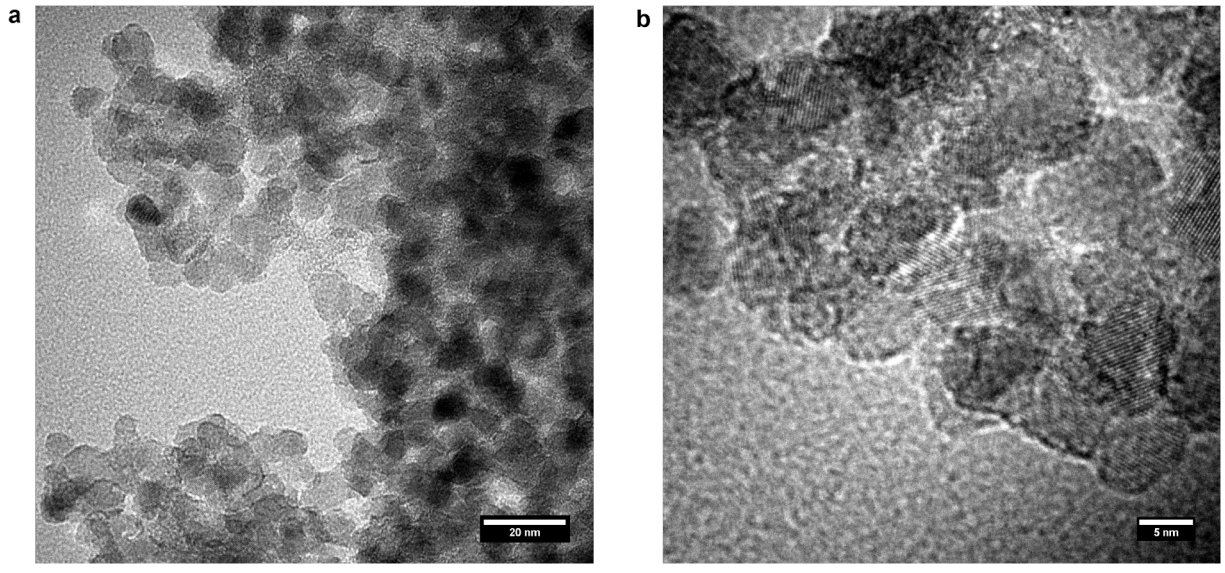

Figure 6: TEM images of the carbon coated TiO_2 nanoparticles.

NAS), 1.23 (m, CTA dodecyl chain), 0.85 (t, dodecyl-CH_3 of CTA); FTIR ν: 2969 (w), 2255 (w), 1808 (m), 1732 (s, C=O, reactive ester), 1553 (s), 1204 (m), 1161 cm^{-1} (m); SEC (eluent: HFIP): 23 098 g mol^{-1}, PDI = 1.17.

Synthesis of P (IL-*b*-DAAM): P (IL-*b*-NAS) (1 equiv) and lithium bromide (50 equiv) were dissolved in DMSO in a Schlenk flask. Dopamine hydrochloride (50 equiv) and triethylamine (50 equiv) were also dissolved in DMSO. The two solutions were combined and stirred overnight at 50 °C. For work-up, the polymer was precipitated in acetone. ^{1}H NMR (400 MHz, DMSO-d_6) δ (ppm) 9.97 (m, C-2 of imidazolium ring), 8.85 (br, OH of dopamine), 7.94 (m, C-4 and C-5 of imidazolium ring), 6.58–6.36 (br, ArH of dopamine), 5.66 (s, CH_2CN), 4.58 (br, polymer backbone), 3.15 (br, polymer backbone), 2.91 (m, polymer backbone), 1.23 (m, CTA dodecyl chain), 0.85 (t, dodecyl-CH_3 of CTA); FTIR ν: 2969 (w), 2255 (w), 1691 (m), 1645 (m, C=O, amide of dopamine), 1553 (s), 1434 (m), 1160 (m), 1020 cm^{-1} (m); SEC (eluent: HFIP): 23 180 g mol^{-1}, PDI = 1.22.

Synthesis of in situ functionalized TiO_2 nanoparticles: 400 mg of catechol containing polymeric ligand was dissolved in 10 mL of DMSO (Sigma-Aldrich) and added to 70 mL of benzyl alcohol (Acros). The content of the flask was heated to 80 °C. The solution was degassed and filled with argon using a Schlenk line. The process was repeated three times. To this argon filled solution 3.2 mL of $TiCl_4$ was slowly injected under vigorous stirring. The dark red solution was kept at 80 °C for 72 hours while constantly stirring at 750 rpm. The resulting brown suspension was precipitated using $CHCl_3$ and hexane (1:3) and the precipitated product was centrifuged. The process was repeated three times to remove the solvent and unbound ligand. The product was dried under vacuum at room temperature.

Pyrolization of as-functionalized TiO_2 nanoparticles: All samples were pyrolyzed using the same conditions. 40 mg of the as-functionalized TiO_2 nanoparticles were filled in a corundum boat, which was placed in a tube furnace. The heating rate was 5 °C/min up to a temperature of 650 °C, which was held for 1 h under a constant flow of argon. After that, the samples were cooled down naturally.

Supporting Information

Supporting Information File 1

Additional spectra.
[http://www.beilstein-journals.org/bjoc/content/supplementary/1860-5397-13-163-S1.pdf]

References

1. Yuan, J.; Schlaad, H.; Giordano, C.; Antonietti, M. *Eur. Polym. J.* **2011,** *47,* 772–781. doi:10.1016/j.eurpolymj.2010.09.030
2. Yuan, J.; Mecerreyes, D.; Antonietti, M. *Prog. Polym. Sci.* **2013,** *38,* 1009–1036. doi:10.1016/j.progpolymsci.2013.04.002
3. Yuan, J.; Antonietti, M. *Polymer* **2011,** *52,* 1469–1482. doi:10.1016/j.polymer.2011.01.043
4. Vijayakrishna, K.; Jewrajka, S. K.; Ruiz, A.; Marcilla, R.; Pomposo, J. A.; Mecerreyes, D.; Taton, D.; Gnanou, Y. *Macromolecules* **2008,** *41,* 6299–6308. doi:10.1021/ma800677h
5. Mori, H.; Yahagi, M.; Endo, T. *Macromolecules* **2009,** *42,* 8082–8092. doi:10.1021/ma901180j
6. Su, Y.-Z.; Fu, Y.-C.; Wei, Y.-M.; Yan, J.-W.; Mao, B.-W. *ChemPhysChem* **2010,** *11,* 2764–2778. doi:10.1002/cphc.201000278
7. Whitehead, J. A.; Lawrance, G. A.; McCluskey, A. *Green Chem.* **2004,** *6,* 313–315. doi:10.1039/B406148A
8. Abbott, A. P.; Capper, G.; Davies, D. L.; Rasheed, R. K.; Shikotra, P. *Inorg. Chem.* **2005,** *44,* 6497–6499. doi:10.1021/ic0505450
9. Kim, T. Y.; Lee, H. W.; Stoller, M.; Dreyer, D. R.; Bielawski, C. W.; Ruoff, R. S.; Suh, K. S. *ACS Nano* **2011,** *5,* 436–442. doi:10.1021/nn101968p
10. Amajjahe, S.; Choi, S.; Munteanu, M.; Ritter, H. *Angew. Chem., Int. Ed.* **2008,** *47,* 3435–3437. doi:10.1002/anie.200704995
11. Amajjahe, S.; Ritter, H. *Macromolecules* **2008,** *41,* 3250–3253. doi:10.1021/ma702593s
12. Jazkewitsch, O.; Ritter, H. *Macromol. Rapid Commun.* **2009,** *30,* 1554–1558. doi:10.1002/marc.200900187
13. Barpanda, P.; Chotard, J.-N.; Delacourt, C.; Reynaud, M.; Filinchuk, Y.; Armand, M.; Deschamps, M.; Tarascon, J.-M. *Angew. Chem., Int. Ed.* **2011,** *50,* 2526–2531. doi:10.1002/anie.201006331
14. Edinger, C.; Waldvogel, S. R. *Eur. J. Org. Chem.* **2014,** 5144–5148. doi:10.1002/ejoc.201402714
15. Herold, S.; Waldvogel, S. R.; Little, R. D.; Yoo, S. J. *Electrochim. Acta* **2016,** *196,* 735–740. doi:10.1016/j.electacta.2016.03.006
16. Yuan, J.; Giordano, C.; Antonietti, M. *Chem. Mater.* **2010,** *22,* 5003–5012. doi:10.1021/cm1012729
17. Soll, S.; Fellinger, T.-P.; Wang, X.; Zhao, Q.; Antonietti, M.; Yuan, J. *Small* **2013,** *9,* 4135–4141. doi:10.1002/smll.201300680
18. Gong, J.; Lin, H.; Antonietti, M.; Yuan, J. *J. Mater. Chem. A* **2016,** *4,* 7313–7321. doi:10.1039/C6TA01945E
19. Fellinger, T.-P.; Thomas, A.; Yuan, J.; Antonietti, M. *Adv. Mater.* **2013,** *25,* 5838–5855. doi:10.1002/adma.201301975
20. Paraknowitsch, J. P.; Zhang, J.; Su, D.; Thomas, A.; Antonietti, M. *Adv. Mater.* **2010,** *22,* 87–92. doi:10.1002/adma.200900965
21. Yuan, J.; Márquez, A. G.; Reinacher, J.; Giordano, C.; Janek, J.; Antonietti, M. *Polym. Chem.* **2011,** *2,* 1654–1657. doi:10.1039/c1py00196e
22. Oschmann, B.; Bresser, D.; Tahir, M. N.; Fischer, K.; Tremel, W.; Passerini, S.; Zentel, R. *Macromol. Rapid Commun.* **2013,** *34,* 1693–1700. doi:10.1002/marc.201300531
23. Bresser, D.; Oschmann, B.; Tahir, M. N.; Mueller, F.; Lieberwirth, I.; Tremel, W.; Zentel, R.; Passerini, S. *J. Electrochem. Soc.* **2015,** *162,* A3013–A3020. doi:10.1149/2.0031502jes
24. Oschmann, B.; Tahir, M. N.; Mueller, F.; Bresser, D.; Lieberwirth, I.; Tremel, W.; Passerini, S.; Zentel, R. *Macromol. Rapid Commun.* **2015,** *36,* 1075–1082. doi:10.1002/marc.201400647
25. Tahir, M. N.; Oschmann, B.; Buchholz, D.; Dou, X.; Lieberwirth, I.; Panthöfer, M.; Tremel, W.; Zentel, R.; Passerini, S. *Adv. Energy Mater.* **2016,** *6,* No. 1501489. doi:10.1002/aenm.201501489

26. Wagemaker, M.; Mulder, F. M. *Acc. Chem. Res.* **2013,** *46,* 1206–1215. doi:10.1021/ar2001793
27. Bruce, P. G.; Scrosati, B.; Tarascon, J.-M. *Angew. Chem., Int. Ed.* **2008,** *47,* 2930–2946. doi:10.1002/anie.200702505
28. Aricò, A. S.; Bruce, P.; Scrosati, B.; Tarascon, J.-M.; van Schalkwijk, W. *Nat. Mater.* **2005,** *4,* 366–377. doi:10.1038/nmat1368
29. Zorn, M.; Zentel, R. *Macromol. Rapid Commun.* **2008,** *29,* 922–927. doi:10.1002/marc.200800165
30. Lai, J. T.; Filla, D.; Shea, R. *Macromolecules* **2002,** *35,* 6754–6756. doi:10.1021/ma020362m
31. Tahir, M. N.; Zink, N.; Eberhardt, M.; Therese, H. A.; Faiss, S.; Janshoff, A.; Kolb, U.; Theato, P.; Tremel, W. *Small* **2007,** *3,* 829–834. doi:10.1002/smll.200600663
32. Shukoor, M. I.; Natalio, F.; Ksenofontov, V.; Tahir, M. N.; Eberhardt, M.; Theato, P.; Schröder, H. C.; Müller, W. E. G.; Tremel, W. *Small* **2007,** *3,* 1374–1378. doi:10.1002/smll.200600664
33. Tahir, M. N.; Eberhardt, M.; Theato, P.; Faiß, S.; Janshoff, A.; Gorelik, T.; Kolb, U.; Tremel, W. *Angew. Chem., Int. Ed.* **2006,** *45,* 908–912. doi:10.1002/anie.200502517
34. Niederberger, M.; Bartl, M. H.; Stucky, G. D. *J. Am. Chem. Soc.* **2002,** *124,* 13642–13643. doi:10.1021/ja027115i

License and Terms